Pathology of the Deep Cerebellar Nuclei in EAE and Implications for Monitoring Early MS

Submitted by

Dain Maxwell

Bachelor of Science

Master of Bioinformatics and Technology (Coursework)

A thesis submitted in total fulfilment of the degree of Masters of Philosophy

School of Science, Health and Engineering

La Trobe University

Victoria, Australia

April 2021

Statement of Authorship

Except where reference is made in the text of the thesis, this thesis contains no material published elsewhere or extracted in whole or in part from a thesis submitted for the award of any other degree or diploma.

No other person's work has been used without due acknowledgement in the main text of the thesis.

This thesis has not been submitted for the award of any degree or diploma in any other tertiary institution.

Signed: Dain Luke Maxwell   Date: 14/04/2021

Table of Contents

Table of Figures

List of Abbreviations

BBB	Blood brain barrier
CFA	Complete Freund's adjuvant
CNS	Central nervous system
CP	Chronic progressive
CR	Chronic remitting
CS	Clinical score
DAPI	6-diamidino-2-phenylindole
DCN	Deep cerebellar nuclei
DPI	Days post injection
DPX	Dibutyl phthalate polystyrene xylene
EAE	Experimental autoimmune encephalomyelitis
GFAP	Glial fibrillary acidic protein
GL	Granular layer
GM	Grey matter
HAMS	Highly active multiple sclerosis
H&E	Haematoxylin and eosin
IFN-γ	Interferon γ
IHC	Immunohistochemistry
IP	Intraperitoneal
LARTF	La Trobe animal research and training facility
MAG	Myelin associated glycoprotein
ML	Molecular layer
MOG	Myelin oligodendrocyte glycoprotein
MRI	Magnetic resonance imaging
MBP	Myelin basic protein
MS	Multiple sclerosis
NAWM	Normal appearing white matter
NHMRC	National health and medical research council
OCT	Optimum Cutting Temperature
PBS	Phosphate buffered saline

PL	Purkinje layer
PLP	Proteolipid protein
PdMS	Paediatric-onset multiple sclerosis
PPMS	Primary progressive multiple sclerosis
RPM	Revolutions per minute
RRMS	Relapsing-remitting multiple sclerosis
SPMS	Secondary progressive multiple sclerosis
TH_1	T-helper cells
TMEV	Theiler's murine encephalomyelitis virus
TNF-α	Tumour necrosis factor alpha
VO	Vehicle only
WM	White matter

Abstract

Multiple sclerosis (MS) is an autoimmune disorder targeting the central nervous system, manifesting principally in young adults. With over 2.8 million affected individuals worldwide, this disease is a major health care burden. While a growing number of MS therapeutics significantly improve symptoms, almost all are directed against the inflammatory component of the disease and have little to no impact on neurodegeneration and progressive disability. Neurodegeneration is an early and major pathological process in the cerebral and cerebellar cortices and deep grey matter (GM) structures. However, cerebellar disease in particular has been understudied in both MS and its experimental model experimental autoimmune encephalomyelitis (EAE).

The aim of this theses is first to identify facets of cerebellar pathology in EAE that may be representative of MS pathology and second, to determine whether cerebellar deficits could be used as early indicators of candidate drug efficacy. In a time course experiment ranging from pre-clinical to severe disease, the cerebellum was investigated via histology, immunohistochemistry and performance on the rotarod. Immunopathological approaches showed classical white matter inflammatory lesions from the early clinical stage surrounding but not entering the deep cerebellar nuclei (DCN). On the other hand, disseminated T cells/apoptotic cells, extensive reactive microglia and neuronal loss were observed throughout the DCN. To estimate cerebellar deficits several rotarod protocols were investigated. However, none showed any significant drop in performance prior to clinical onset suggesting that for EAE the rotarod may not be a sufficiently sensitive test for early cerebellar dysfunction.

These studies demonstrate that the DCN in EAE exhibits pathological hallmarks reminiscent of those demonstrated in deep GM nuclei in MS. They suggest that the DCN is a relevant region to investigate mechanisms underlying progression in MS. However,

more sensitive approaches will need to be developed to use cerebellar deficits in evaluation

of candidate drug efficacy.

Chapter 1 Cerebellar disease in MS and EAE

Multiple sclerosis (MS) has the dubious honour of being among the most common autoimmune and neurodegenerative disorders manifesting during the prime of one's life, yet the cause and underlying processes driving neurodegeneration in MS remain unknown. Currently it has been proposed that there are three crucial, though broad, factors involved in MS susceptibility and development. These include genetic predisposition to MS (most prominently HLA related genes), environmental factors (i.e. smoking, Epstein-Barr Virus infection, vitamin D levels) and finally a triggering event (i.e. physical/emotional trauma) (Didonna & Oksenberg, 2017; Olsson *et al*, 2017). As the exact cause of MS hasn't been identified a number of models (and subsets thereof) are used to understand and develop therapeutics for candidate inflammatory or neurodegenerative processes that are difficult to access in the human disease for ethical or other reasons. MS is a complex disease that no individual model available to date accurately replicates, however models are critical in order to identify and characterise molecular players in the disease process with the aim of developing treatments to preserve neural tissue (Lassmann & Bradl, 2017). That no MS model accurately portrays the multiple facets of the disease is a valid critique. On the one hand, overinterpretation of data from a model that only partially recapitulates the human counterpart of the disease has led to unsuccessful therapeutics or problems that an individual model had not and possibly could not predict (Baker & Amor, 2014; Baker *et al*, 2011). On the other hand, it is due in part to these very models that many of the current suite of available therapeutics, as well as others developed in the future, are safely made available at all (Ben-Nun *et al*, 2014; Constantinescu *et al*, 2011). A second major criticism of MS models is that MS is primarily a disease of the brain, while experimental autoimmune encephalomyelitis (EAE) most prominently affects the spinal cord (SC). Due to the very different structural and neuronal composition, it is argued that a model centred around SC pathology may not be the most relevant for neurodegeneration in the brain. To this end, this

thesis will explore the cerebellum as an additional region of interest for understanding and treating progressive disease in MS. The cerebellum has been underutilised in part due to its complexity relative to the easier to access and simple structure of the SC, as well as a history of focus on WM pathology that has proved easier to study in animal models.

A brief overview of the pathogenesis of multiple sclerosis

 While the symptoms of MS are diverse, the broad overarching path the disease takes generally fits into a well-described set of subtypes (Klineova & Lublin, 2018). Relapsing remitting multiple sclerosis (RRMS) is the most commonly seen form, characterised by periods of clinical disease typically coupled with lesions identifiable using magnetic resonance imaging (MRI), and an initially MRI silent loss in grey matter (GM) volume occurring over many years with similarly subtle impacts on cognitive and motor functions (Fig. 1-1a). This global volume loss/neurodegeneration is thought to eventually reach a threshold where one's neurological reserve is exhausted from which time permanent deficiencies are observed. In many cases, RRMS patients reach a point where they rarely experience relapses and remissions, but the progressive component persists. This transition from RRMS is termed secondary progressive multiple sclerosis (SPMS; Fig. 1-1a). A less common subtype is primary progressive multiple sclerosis (PPMS; Fig. 1-1b), that presents as a continuous decline in function in the same manner as SPMS, however patients do not normally present with a relapse/remission phase earlier in the disease. Lastly, other rarer forms include paediatric multiple sclerosis (PdMS; Fig. 1-1d) with a much more aggressive course of disease with an earlier onset (Diaz *et al*, 2019) and benign MS (not shown) which shows very little progression over several decades (Reynders *et al*, 2017). Much debate has been had over how fundamentally different these subtypes are from one another and whether MS is closer to an umbrella for several different diseases that result in similar pathology akin to a syndrome, where the diversity in genetics, environment and trigger

result in one following a number of broad disease paths (Dwyer *et al*, 2020). For instance, when comparing measures of extent and rate of progressive disease between SPMS and PPMS the literature reveals more similarities than differences. Though far from a complete picture, the similar rate of progression, lesion pathology and clinical disease between the two suggests a common driver of disease (Lassmann, 2018). In all its forms, it is this progressive aspect that we are currently most unequipped to treat. In the most common forms of MS this occurs over a time course of decades giving some time to determine the most suitable treatment plan for an individual patient with the goal of preserving as much of the neuropil as possible. However, the few treatment options available only appear to offer a modest preservation of GM volume over time (Bross *et al*, 2020). To maximise the efficacy of the current treatments available, it stands to reason that the sooner clinicians diagnose and prescribe the most effective treatment for an individual patient the greater the tissue that is saved. This raises the crucial questions of when does neurodegenerative disease begin, and how do we determine an individual patient is on the most appropriate treatment plan? In light of a breakthrough, tests more sensitive to neurodegeneration such as those associated with balance and cognition are required for both earlier intervention and also to swiftly determine whether patients are responsive to the current prescribed therapeutic to maximise the amount of time spent with the right treatment.
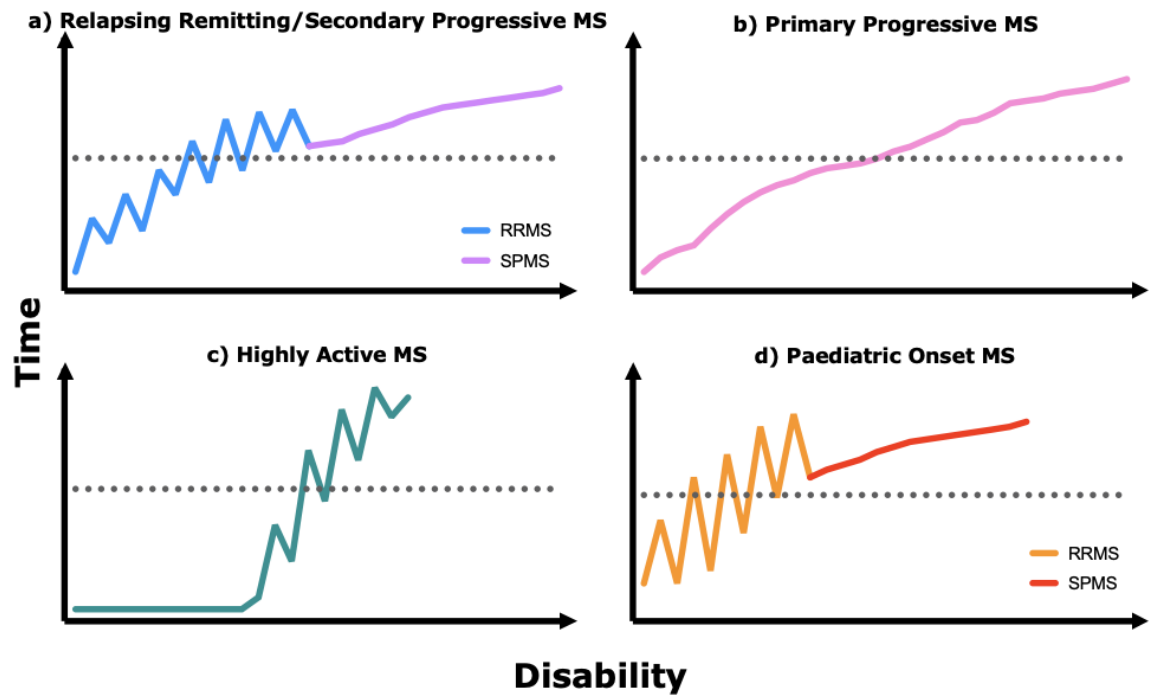
Fig. 1-1 Common forms of MS. (a) Relapsing-remitting MS (blue) is the most frequently seen form of MS. This often progresses into a secondary stage, secondary progressive MS (purple). (b) Primary progressive MS (pink). (c) Highly active MS (green), the name given to the poorly defined spectrum of rapid onset MS subtypes with severe disability and potentially death occurring in a much shorter time frame relative to other subtypes. (d) Paediatric onset MS shows a similar pattern to adult-onset relapsing remitting disease, though occurring much earlier in life (orange) which usually converts to secondary progressive MS (red).

Almost all regions of the brain may show disease activity in some form, though not all occur in the same individual hence the diversity of symptoms observed across those with MS. As with all things MS, a multitude of disease processes have been observed, with some unique to certain brain regions with others overlapping white matter (WM) and GM. Furthermore, analysis and interpretation of post-mortem histology becomes especially complex when one considers that any given patient will present a variety of lesions at a variety of developmental stages. The most salient feature is the presence of inflammatory lesions in both WM and GM, though significantly more florid and cellular in WM. Broadly, WM inflammatory lesions are characterised by infiltration of immune cells including monocytes, T cells (predominantly CD8+ Th$_1$ (T helper)) and some B cells resulting in extensive demyelination, axonal damage and glial scarring (Arneth, 2020; Arneth, 2019; Chu *et al*, 2018; Voskuhl *et al*, 2009). In GM, this type of pathology is mainly associated with deep GM nuclei (albeit less inflammatory). Lesions may become confluent, especially in later stages of the disease but typically a post-capillary venule can be found within the confines of the lesion which serves as the main point of entry for the peripheral immune system (Kuhlmann *et al*, 2017). In addition, a diffuse presence of T cells likely associated with demyelination and axonal damage which may extend into regions beyond the immediate lesion boundary are observed. To varying extents, these are present in all subsets of MS, with inflammatory lesions typically associated with relapsing/remitting disease and GM atrophy associated with progressive disability. However analysis and interpretation of post-mortem histology and gleaning useful information about the disease processes involved becomes especially complex when one considers that not only must investigators factor in the different lesion types and their development cycles, but that any given patient at any given time will present a variety of lesions types at a variety of developmental stages. Various groups have attempted create a number of WM lesion classification systems based on factors such as lesion morphology, developmental stage, presence or absence of specific

immune cell types or components and the presence of specific myelin proteins (Jarius *et al*, 2017; Lucchinetti *et al*, 2000; van der Valk & De Groot, 2000). Among the more recent classifications combines the crucial aspects of these into a simple system where lesions are termed active (large numbers of microglia/macrophages and T cells present), inactive (very few microglia/macrophages and T cells observed) and mixed active/inactive. These can be further subdivided into demyelinating or post demyelinating based upon the presence of myelin proteins within phagocytes in the lesion (Kuhlmann *et al.*, 2017).

Similar to WM lesions, cortical GM also display heterogeneity. However, contrary to the classic WM lesions described above GM lesions are associated with an absence of inflammatory cell infiltration though still show severe demyelination, microglial reactivity and neurodegeneration. The literature also suggests the existence of a soluble factor, produced by B cells often found in the meninges which may drive neurodegeneration and/or demyelination directly or potentially via the provocation of microglia into reactivity (Lisak *et al*, 2012). Furthermore, only a fraction of cortical GM lesions are detected with standard MRI procedures. Specifically, these are split into four types (Bo *et al.*, 2003; Calabrese *et al*, 2010a; Kidd *et al*, 1999): Type I appear occurs at the GM/WM boundary in the cortex; Type II lesions are purely intracortical surrounding a blood vessel; Type III presents as extensive subpial demyelination of the outermost cortical GM layers; Type IV lesions show complete demyelination from the pial surface to the WM/GM boundary, though not extending into the WM (Fig. 1-2). As an aside, this type of extensive subpial demyelination (Type III) has not been observed in diseases other than MS (Junker *et al*, 2020). Lastly, concurrent to the relatively focal pathology described above, a global loss in cerebral and cerebellar cortical brain volume is also observed over time. It is argued that this loss of GM volume, the mostly untreatable aspect of MS is the "real multiple sclerosis" having the greatest contribution to overall disability. However, the disease processes behind this

continual loss of neuronal cell bodies and processes that lead to GM volume reduction are not understood.
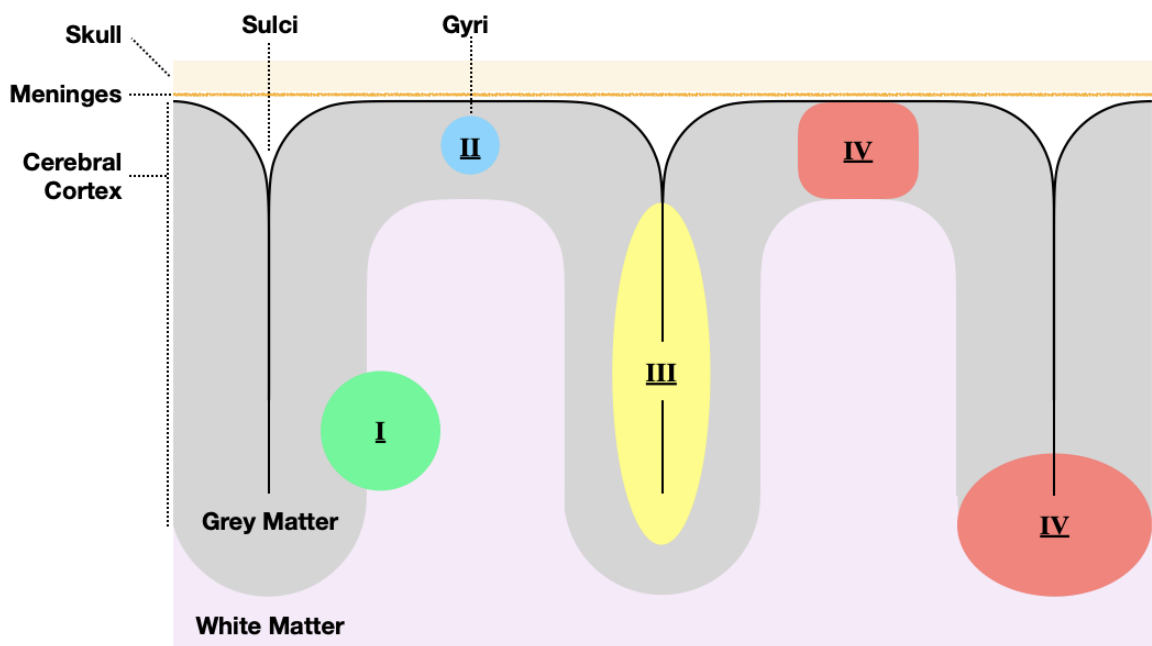
Fig. 1-2 GM lesion classifications. Type I (green) occur at the boundary of WM and GM and extend into both. Type II (blue) are purely intracortical and do not reach either pial surface or WM boundary. Type III (yellow) lesions present as extensive subpial demyelination extending a short way into the cortical surface. Type IV (red) span the entire GM cortex reaching but not extending into the subcortical WM (Bo et al, 2003).

Due to the incredibly long disease duration, end stage pathology being oversampled and limited early biopsies it is unclear if the heterogeneity of these lesions is a case of accessing them at different stages of development, or whether they're a consequence of the complex genetic/immunological/environmental factors resulting in subtly different processes of the same disease. The challenges of studying a central nervous system (CNS) disease combined with the various unknowns, particularly in the early stages have made developing effective therapeutic treatments challenging. In all, therapeutic approaches that appear to mostly target mechanisms leading to WM disease as visualised by MRI are generally quite successful at reducing lesion burden/frequency in the early stages of RRMS. However, they do not appear have a significant impact on preventing cortical volume loss, conversion to SPMS and the only approved for treatment of the progressive MS (ocrelizumab) has shown a mild at best reduction in the rate of progressive disease. This lack in neuroprotective or restorative therapeutics targeted at the progressive neurodegenerative aspect is in part due to the difficulty in studying the CNS and to not exacerbate the disease in an already at-risk region with invasive procedures. Furthermore, heavy focus has been placed on addressing WM disease likely due to its visibility on MRI and in animal models. To improve the understanding of 'the real MS', examination of the cerebellum would be beneficial because of the evidence in the literature that damage in this CNS region may occur earlier than in the cerebral hemispheres (Kutzelnigg *et al*, 2007) and the association of motor/balance/gait symptoms with converting to a progressive disease (Khaleeli *et al*, 2008; Rzepinski *et al*, 2019).

Modelling multiple sclerosis

The difficulty in determining what is driving the chronic neurodegeneration in MS is in part due to the variety of disease processes seen in terms of region (cortical GM, WM and deep GM) and lesion subtypes. Furthermore, the earliest stages of MS are either clinically silent

or subtle enough to escape notice, meaning that the disease has been progressing for some time prior to patient presentation. As mentioned above, due to the sensitivity of the brain and how crucial it is to preserve neural tissue, analysis is typically limited to non-invasive procedures which provides an incomplete picture of the processes driving the disease. As such, most histology done on MS brain tissue is heavily skewed towards post-mortem samples where the original pathological mechanisms may be obscured by secondary disease processes. To begin to understand the pathogenesis behind the mostly untreatable progressive disease (Montalban *et al*, 2017), three main models and an array of subtypes have been developed (Kipp *et al*, 2017; Lassmann & Bradl, 2017). Broadly, these focus on aspects of MS such as autoimmune mechanisms directed at particular myelin components (EAE model), an alternate inflammatory model mediated by viral infection of CNS cells and immune recognition and destruction (Theiler's murine encephalomyelitis virus model) and toxin mediated demyelination in the CNS (cuprizone model) to understand mechanisms underlying adult remyelination. While any individual model is not an accurate representation of MS in its entirety, each offers its own perspective of pathological processes that have been shown to occur in MS. When used with a full understanding of the limits of the chosen model they can provide a highly reproducible view of processes involved in neuroinflammation.

EAE is one of the most widely used models to investigate the consequences of inflammatory demyelination on the surrounding CNS architecture. This model relies on initiating an autoimmune response against CNS specific antigenic fragments of quantitatively major or minor myelin proteins with the aid of powerful adjuvants such as Complete Freund's adjuvant (CFA; mineral oil with powderised, heat inactivated *Mycobacterium tuberculosis*) and *Bordetella pertussis* toxin to overcome tolerance (Bittner *et al*, 2014). The exact method of induction varies somewhat between laboratories (i.e.

where the neuroantigen/CFA emulsion is injected) though this appears to have no impact on the disease course. Significant changes to the concentration of the neuroantigen or *M. tuberculosis* however do impact the severity and speed of onset of the EAE, with lower concentrations of neuroantigen, *M. tuberculosis* and *B. pertussis* toxin producing a less aggressive and much longer disease course that may provide insight into pathological mechanisms that may take months to materialise, versus higher concentrations of neuroantigen/adjuvants that causes a much more aggressive disease that's much more reliable in its timing (Dias *et al*, 2015; Hasselmann *et al*, 2017; Miller & Karpus, 2007). Common antigenic fragments used include MOG_{35-55} (myelin oligodendrocyte glycoprotein), $PLP_{139-151}$ (proteolipid protein) and MBP_{84-104} (myelin basic protein) that are used to induce an immune mediated response in mouse strains such as C57Bl/6, SJL/J and NOD/Lt (Miller & Karpus, 2007). Curiously, not all antigenic fragments can be used to induce EAE in all strains. For example, MOG_{35-55}, a neuroantigen used in C57Bl/6 and NOD/Lt cannot be used to induce EAE in SJL/J. The most common combinations include C57Bl/6 ~ MOG_{35-55} resulting in a chronic progressive ascending paralysis with no recovery and NOD/Lt ~ MOG_{35-55} or SJL ~ $PLP_{139-151}$, which induce a multiphasic disease with periods of worsening ascending paralysis coupled with recovery, reminiscent of the pattern observed in RRMS. As such, careful consideration to the strain, neuroantigen and induction must be given with respect to what aspects of MS the investigator wishes to model.

As can be the case when trying to model a disease that spans a period of time that is over an order of magnitude greater than the lifespan of the animal used, there are a number of issues that one must consider when interpreting the results. For one, the course of MS may run several decades depending on the subtype and patient. Slowly progressing models may run for over 60 days (Hamilton *et al*, 2019), but any long-term impact studies in rodents

will be limited. Many experiments use EAE models that have an endpoint of under four weeks duration. What these may lose in terms of the effect of the more chronic effects of neuroinflammation is mitigated in part by the increased reliability in inter-mouse progression of disease, especially important if the goal is discovery of preclinical effects. Key effector cell types seen as crucial to pathogenesis vary between MS and its models. Specifically, active EAE induced using short antigenic fragments (i.e. MOG_{35-55} or $PLP_{139-151}$) relies heavily on the CD4+ Th1 subset to initiate and drive inflammation that is supported by local and recruited macrophage populations (Chu *et al.*, 2018; Sonobe *et al*, 2007). Whereas cytotoxic CD8+ T cells, a major component of MS pathology (Babbe *et al*, 2000), have yet to be shown to have a major pathogenic role in EAE (Saligrama *et al*, 2019; Sonobe *et al.*, 2007). Furthermore, while B cells are involved in antigen presentation in short fragment EAE induction, demyelinating autoantibodies are typically only observed in EAE induced using the complete extracellular fragment MOG_{1-125} (Mann *et al*, 2012). However, a major risk factor associated with developing MS is related to the gene *HLA-DRB1* which is critical to protein presentation to CD4+ T cells, one of the main effector cell types in EAE. Recent studies have identified cytotoxic CD4+ T cells in MS and EAE though the exact role these play is currently unclear (Parnell & Booth, 2017; Peeters *et al*, 2017). As briefly touched on above, reactive microglia and macrophages are readily seen in both MS and EAE and appear to be crucial effectors of reactive oxygen/nitrogen-based damage and demyelination in both WM and GM (Chu *et al.*, 2018; Lassmann & van Horssen, 2016). These cells release a multitude of pro-inflammatory cytokines associated with cellular stress and death and are key to CNS recruitment of the rest of the immune system (Dong & Yong, 2019). Their deleterious effect is highlighted in EAE whereby a less aggressive disease course is seen when the pro-inflammatory aspects of microglia/macrophages are attenuated (Heppner *et al*, 2005; Sloka *et al*, 2013). However, there are also crucial reparative functions facilitated by microglia and macrophages such as

clearing myelin debris to enable remyelination to occur, release of neurotrophic factors and driving anti-inflammatory processes to resolve lesions (Plastini *et al*, 2020). With new technologies advances have been in the separation of macrophage type populations into those derived from CNS resident microglia and those from monocytes recruited from the periphery (Bennett *et al*, 2016). Interestingly it appears that microglia derived macrophages may be more involved in reparative (i.e. myelin debris clearing) and resolution aspects of the inflammatory process while monocyte derived macrophages are crucial to the post recruitment inflammatory stage (Yamasaki *et al*, 2014). Unfortunately this is not so simple as microglia ~ good, monocytes ~ bad. Rather, it is likely a strong inflammatory response is crucial to efficient removal of antigenic/pathogenic material from the CNS environment as is an efficient resolution of said inflammatory environment to enable remyelination and axonal/neuronal repair to take place. Due to the prominent role microglia have in EAE, this model may prove useful in understanding what processes go awry leading to remyelination failure in chronic inflammatory lesions, and the impact microglia and monocyte derived macrophages may have on neuronal components of GM and WM over time.

The difference in size between the mouse and human brain is also significant, particularly in terms of the relative size and structure of the cerebral and cerebellar cortices as well as the expansive regions of WM underlying them. The complexity of the folds the human brain as opposed to their absence in the mouse cerebral cortex are of particular significance in light of cortical volume loss being an especially crucial measure of the extent of disease progress and disability. Furthermore, cortical lesions and demyelination appear to be often centred around sulci, especially in the highly infolded regions of the insular cortex (Kutzelnigg & Lassmann, 2006). The role that a folded cortex has on MS development is as of yet unclear, however it has been suggested that such convolutions in the human cortex may either reduce blood flow enabling greater diffusion of peripheral myelinotoxic

substances into the surrounding GM, or that the slower blood flow may increase the likelihood of rolling/adhering lymphocytes extravasating to initiate lesion formation. To this end, one of the criticisms of using EAE is that pathology is predominantly of the SC, rather than the brain and cerebral cortex. That is not to say that the SC is free of pathology in MS. As non-invasive techniques such as MRI become more sophisticated, SC lesions and loss of volume have been observed (Moccia *et al*, 2019), with one study showing loss of spinal cord GM volume greater than that seen in the GM of the brain (Schlaeger *et al*, 2014). Regardless, this apparent vulnerability of the MS cerebral cortex extends to the cerebellum. In the seminal piece investigating the extent of cerebellar cortical demyelination it was found that in PPMS and SPMS patients on average 38.7% of the cerebellar cortex was demyelinated, with extreme cases reaching up to 92% (Kutzelnigg *et al.*, 2007; Kutzelnigg *et al*, 2005). This demyelination also strongly correlated with the extent of demyelination seen in the cerebral cortex (Kutzelnigg *et al.*, 2007; Kutzelnigg *et al.*, 2005). Furthermore, in a study investigating patterns between WM and GM lesions in RRMS, a cerebellar pattern was associated with increased future disability/EDSS (expanded disability status scale) scores in follow up tests a year later (Muthuraman *et al*, 2020; Weinshenker *et al*, 1991). However, care must be taken when considering the impact of infratentorial lesions alone, as brainstem lesions are typically much more impactful than other infratentorial structures including the cerebellum (Tintore *et al*, 2010). WM lesions and, importantly, GM volume loss is observed in the EAE cerebellum. In one of the first studies measuring GM atrophy in EAE MacKenzie-Graham *et al* (2006) found progressive reduction in cerebellar volume in a longitudinal assessment involving repeated measurement over the course of 60 days. This was further expanded on finding a prominent volume reduction in the outermost molecular layer (ML) of the cerebellum coinciding with a reduction in the number of Purkinje neurons (a major group of large inhibitory neurons in the cerebellar cortex) (MacKenzie-Graham *et al*, 2012; MacKenzie-Graham *et al*, 2009).

In all, these studies were crucial in pushing the concept of modelling major GM disease processes in MS such as atrophy and neurodegeneration using the EAE cerebellum.

Cerebellar disease in multiple sclerosis and models

General structure and function of the cerebellum

The cerebellum is located just below the occipital lobe at the back and base of the skull. It is a highly folded structure densely packed with neurons and consists of several well delineated regions (Gruol *et al*, 2016), namely the ML, Purkinje layer (PL), granular layer (GL), WM and deep cerebellar nuclei (DCN; Fig. 1-3). The very outermost layer of the cerebellum is almost completely devoid of myelin, consisting of the enormous dendritic arbors of the Purkinje neurons projecting from the layer below, excitatory projections from granular neurons deeper again that interact with these arbors, as well as a number of interneurons within the ML. Beneath this is a monolayer of large inhibitory Purkinje neurons. These are especially crucial being the only neurons that project from the cortex. Underlying the PL monolayer is the densely packed GL, so called for the many excitatory granular neurons that make up the bulk of the cells in this region. Buried deep within the convoluted WM consisting of axons to and from the cerebellar cortex is the DCN. As the Purkinje neurons are for the cerebellar cortex, the neurons within the DCN are responsible for almost all output of the cerebellum and any damage to this structure may lead to large swathes of cerebellar cortical processing effectively removed the from the CNS circuit (Gruol *et al.*, 2016).

Despite its proximity to the cerebral cortex the cerebellum is actually connected to the brainstem via three WM tracts, the cerebellar peduncles (superior, middle and inferior). Projections into the cerebellum pass through the superior, middle and inferior peduncles along mossy or climbing fibres which project from the pons and spinal cord, and the inferior

olive to the cerebellar cortical and deep GM areas. Broadly speaking, information travels through the cerebellar WM to the cortex, is processed in the ML and sent from the cortex to the DCN via the PL before leaving the cerebellum once again via the superior and inferior peduncles (Fig. 1-4).

The Mouse Brain
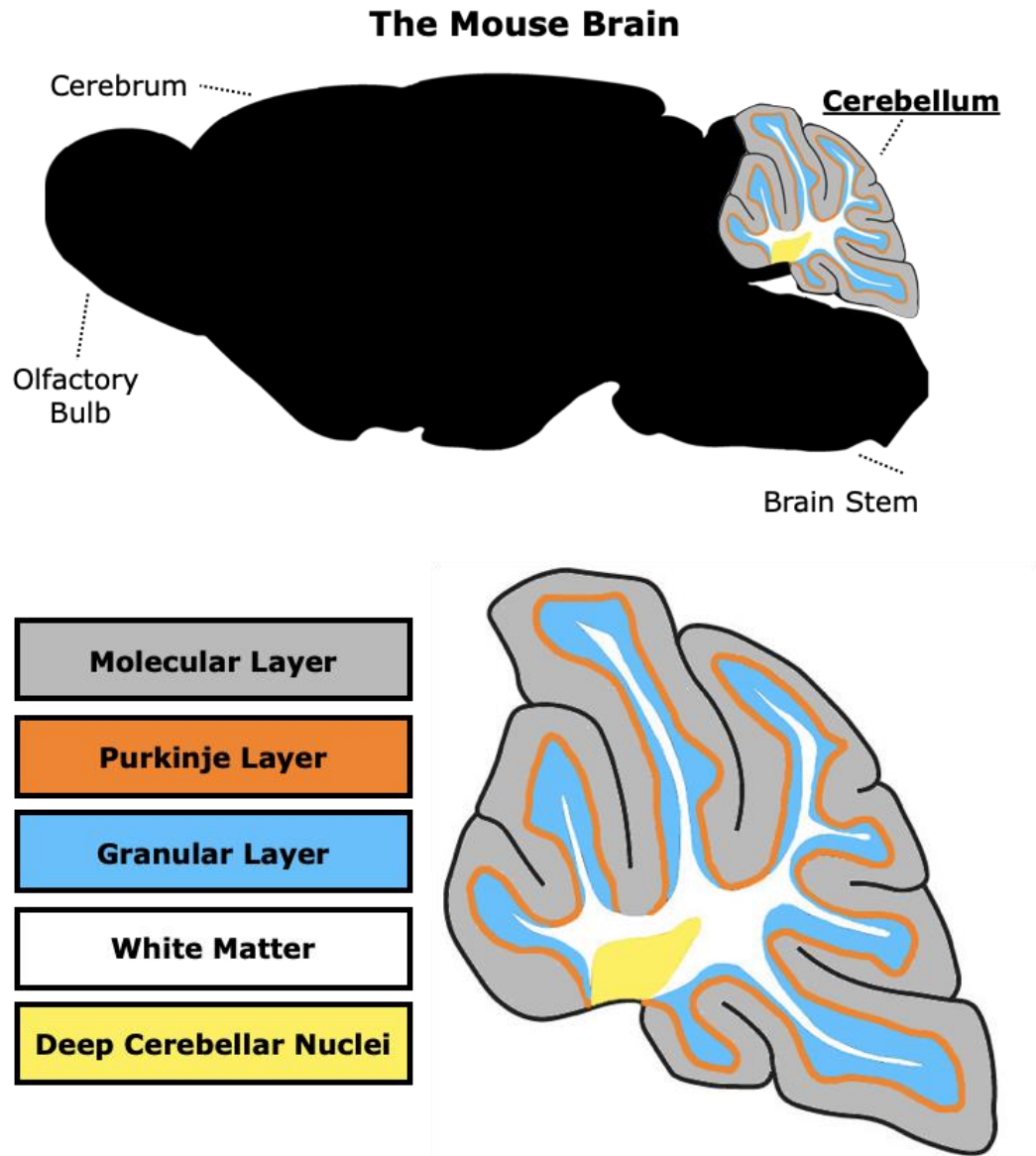
Fig. 1-3 A sagittal view of an adult mouse cerebellum. Immediately beneath the meningeal surface is the ML (grey), the bulk of which is made up of the expansive dendritic arbors of the Purkinje neurons located immediately beneath in the PL (orange). The last layer of the cerebellar cortex, the GL, so named for the numerous granular neurons (blue). Beneath the cerebellar cortex lies the WM (white) which in turn surrounds the deep GM, the DCN (yellow).
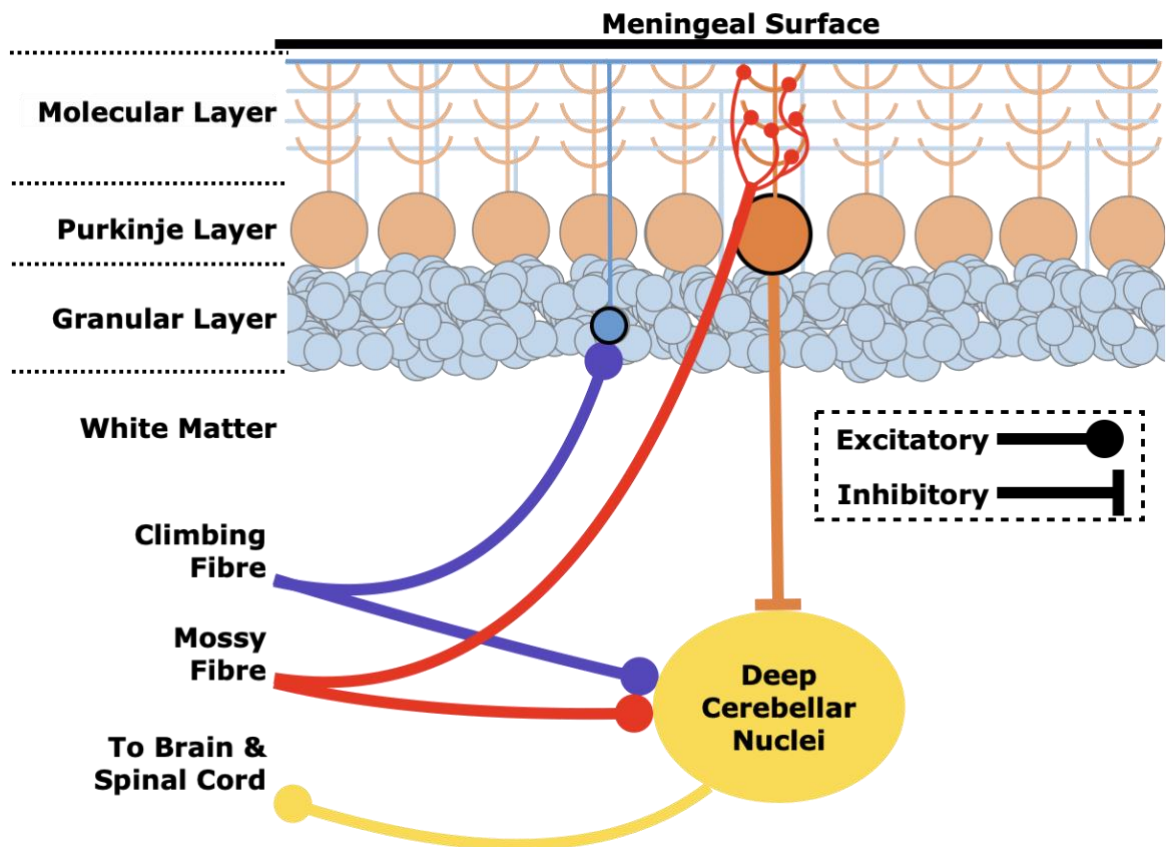
Fig. 1-4 Simplified cerebellar circuit. Inputs into the cerebellum enter the super, middle or inferior peduncles (not pictured). Climbing fibres (emanating exclusively from the inferior olive) pass through the WM and connect to granular neurons in the GL, that then relay information through to Purkinje neurons in the PL via their dendritic arbor in the ML. All other inputs into the cerebellum take the form of mossy fibres, so named for their extensive connections they make to a small number of Purkinje neurons (usually less than 10). Regardless of input (climbing or mossy fibre), all cerebellar cortical output is derived from the Purkinje neurons, almost all of which project to one of the four DCN (fastigial, interposed (emboliform and globose) and dentate) which in turn project to targets throughout the brain and SC. Alternatively, both climbing and mossy fibres also project directly to the deep cerebellar nuclei.

Cerebellar cortical disease in EAE and MS

The cerebellum is an established target region of MS pathology and plays a key role in both the deterioration of balance and freedom of movement as well as aspects of cognition (Parmar *et al*, 2018). However, it is only recently that more focus is being directed to this region of the brain. WM lesions and cortical volume loss have been observed via MRI and symptoms of cerebellar pathology such as ataxia and balance can be detected at the time of presentation and may offer a more sensitive measure than traditional EDSS scores (Findling *et al*, 2018; Martin *et al*, 2006; Spain *et al*, 2014). Focus has mainly been on the cerebellar cortical regions due to extensive demyelination and volume loss being observed, not dissimilar to that seen in cerebral cortex (Cocozza *et al*, 2017; Kutzelnigg *et al.*, 2007; Kutzelnigg *et al.*, 2005). Non-cortical, deep GM structures in the brain have also been implicated in the progression of disease including but not limited to the thalamus, hypothalamus, basal ganglia, hippocampus and DCN (Gilmore *et al.*, 2009).

The extent of cortical demyelination seen in the cerebellum varies significantly from patient to patient with more extensive cortical demyelination seen in SPMS and PPMS patients relative to RRMS (Kutzelnigg *et al.*, 2007). The pattern of demyelination is suggestive of a myelinotoxic factor diffusing from the outer meningeal layer, with myelin being lost from the outermost areas first in order of supra/infra-PL myelin, GL then WM of the folia and arbor vitae (Gilmore *et al.*, 2009). Its currently unclear if GM myelin is more vulnerable to whatever factor this may be, that the densely packed unidirectional myelinated axons in the WM present a natural diffusion barrier limiting its spread or some other as yet undiscovered process is at work. This is most strikingly observed in the SC where the relation between WM and GM juxtaposition is reversed (i.e. GM is located deeper inside the SC while the WM is present at the outermost edge) (Gilmore *et al*, 2006; Gilmore *et al.*, 2009). Here we see GM demyelination in the regions near surface SC lesions while WM between the

GM/SC surface lesion may appear relatively intact (Gilmore *et al.*, 2006; Gilmore *et al.*, 2009).
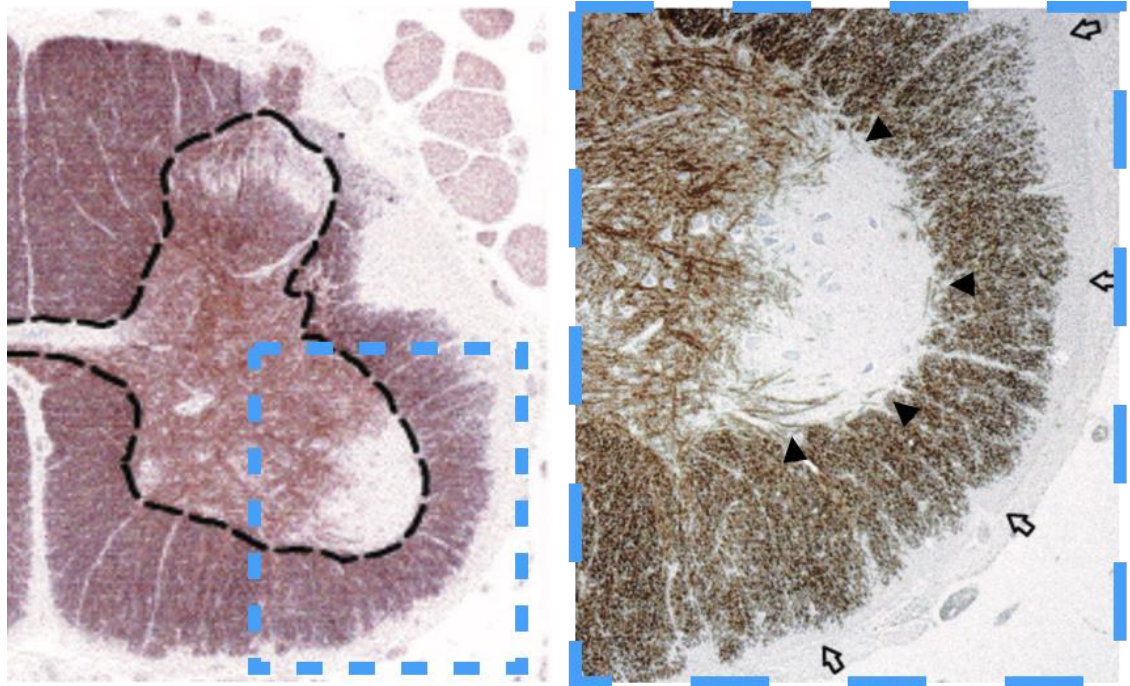
Fig. 1-5 Demyelination identified using IHC for PLP in the MS SC is regularly seen occurring from the outermost edge inwards (open arrows). GM demyelination may also occur from the outermost edge near to surface WM demyelination, though WM between these regions may be preserved (closed arrow heads). This figure was adapted from adapted from Fig. 3 - F and 3 - G from Gilmore et al (2009).

However, blood vessels supplying the GM do not anastomose with vessels that supplies the surface WM, and any myelinotoxic factor released from these deeper vessels may diffuse more freely through the GM than the WM. A further consideration is that because the blood brain barrier (BBB) is induced by the local CNS environment (Blanchette & Daneman, 2015), different regions may result in anatomically and functionally distinct barriers, some of which may be more permeable to this predicted soluble factor (Nyul-Toth *et al*, 2016; Wilhelm *et al*, 2016). Cortical demyelination of the cerebellar cortex has also been observed in EAE, albeit far less extensive and complete relative to what is seen in the MS cerebellum (Kutzelnigg *et al.*, 2007; MacKenzie-Graham *et al.*, 2006; MacKenzie-Graham *et al.*, 2009). That EAE shows a quantifiable but far less extensive and severe pathology may be a consequence of the relatively short time frame EAE occurs in relative to MS. Alternatively, remyelination efficacy is closely tied to age (Neumann *et al*, 2019), and while aged mice are used in EAE experiments, these are typically the exception rather than the rule. As such, recovery may much more rapid in MS models. Whatever the case, a number soluble myelinotoxic factors have been put forward (i.e. TNF, reactive nitrogen and oxygen species and antibodies) though, thus far no single factor has been identified to be the causative agent of demyelination in either MS or EAE. Due to the seemingly syndromic nature of MS, a soluble myelinotoxic factor may the convergence point of subtly different diseases.

Cortical volume loss as a consequence of dendritic/axonal loss and neurodegeneration is one of the strongest correlates of the as of yet untreatable progressive component of MS. This process appears to occur for quite some time prior to any sort of detectable symptoms being evident until the neurological reserve of the brain is exceeded. While aspects of cerebellar disease in MS may be on the more subtle end of the spectrum, cerebellar cortical GM loss is detectable both via MRI and physical tests assessing cerebellar function. Due

to its convoluted structure consisting of WM surrounding, and itself surrounded by several different types of GM (DCN, GL and ML) quantitatively measuring changes in volume has proven challenging. Furthermore, the heterogeneity and long time-course of MS, multiple subtypes, various MRI modalities used and sometimes limited patient numbers have made definitive broad conclusions rare. For instance, despite extensive demyelination there are reports of no loss in cortical volume (Ramasamy *et al*, 2009), no reduction in Purkinje cells numbers (Howell *et al*, 2015) or synaptic density (Howell *et al.*, 2015). Others show significant a reduction in volume across major MS subtypes (RRMS, SPMS and PPMS) (Calabrese *et al*, 2010b). Likewise, Purkinje cells numbers or synaptic density do not appear to be reduced globally (Howell *et al.*, 2015). However, when Purkinje neurons counts were compared between normal appearing cortex, cortex with intracortical lesions/GM demyelination leukocortical/juxtacortical lesions, Purkinje numbers were significantly reduced in the leukocortical group only (intracortical numbers showed a downward trend that did not reach significance). More subtle Purkinje cell abnormalities such as altered phosphorylation states of neurofilament proteins have also been observed (Kemp *et al*, 2018; Redondo *et al*, 2015). Similar pathology has been described in EAE with extensive disruption of Purkinje dendritic arbors, reduced Purkinje cell numbers and the presence of axonal ovoids alongside a global reduction in cerebellar cortical volume (MacKenzie-Graham *et al.*, 2012; MacKenzie-Graham *et al.*, 2006; MacKenzie-Graham *et al.*, 2009). Altered cerebellar protein expression has also been observed. Na$_v$1.8 channel proteins and annexin light chain (p11; required for functional channel expression) normally expressed in the peripheral nervous system have been detected in Purkinje neurons in both MS and EAE which have been found to lead to abnormal firing patterns in EAE (Craner *et al*, 2003). Similarly, reduced expression of mGlut1a and increased expression of mGlut5 receptors normally restricted to early development were observed which was also associated with altered firing patterns and motor symptoms (Black *et al*, 2000; Fazio *et al*, 2008; Shields *et*

al, 2015; Shields *et al*, 2012). However, motor performance was improved upon treatment with an mGlut1a enhancer in EAE. Alongside a loss of cortical volume and Purkinje channelopathies are a reduction in the number of the inhibitory interneurons located in the ML also likely contributing to the altered firing patterns (Mandolesi *et al*, 2012). Increased numbers of binucleate Purkinje neurons are also observed, which are assumed to be a self-preservative response seen almost exclusively in this neuron type. Lastly, Purkinje knockout models suggest that denervation of the DCN from the PL may result in atrophy over time, though the extreme atrophy of the whole cerebellum may impact these results somewhat. Damage to the PL is particularly impactful as these are the only projections that leave the cerebellar cortex, with almost all projecting to one of the four DCN.

Deep grey matter disease in EAE and MS

Studies focussed on the DCN in MS patients are even fewer in number than those focussed on the cerebellar cortex and usually only limited to the largest of the DCN, the dentate nucleus. While some observations have been made, such as the DCN appearing hyper/hypointense in T1 (Kasahara *et al*, 2011; Roccatagliata *et al*, 2009; Tedeschi *et al*, 2016) and T2 weighted images respectively, these results have been found to be more related to retention of contrasting agent and age related iron deposition rather than any MS related disease process (Bakshi *et al*, 2001; Maschke *et al*, 2004; Tjoa *et al*, 2005) Discoveries more relevant to the underlying deep GM pathology in MS have been made at the histological level in the dentate nuclei. Specifically, a significant reduction in the number of synapses present in both normal appearing and demyelinated dentate nuclei compared to healthy controls as well as a significant reduction in the number of neurons in the demyelinated dentate nucleus specifically. Furthermore, neuronal soma in the dentate nucleus appeared shrunken and chromatic, however this trend did not reach significance (Albert *et al*, 2017). Qualitatively, ionised binding adapter molecule 1 (Iba1) staining

macrophages and microglia appeared morphologically more reactive, however there was no significant difference in the area staining positive for Iba1 or glia positive for glial fibrillary acidic protein (GFAP) (Albert *et al.*, 2017). More detailed confocal and SEM analysis revealed free postsynaptic densities opposed to astrocytic processes, while other astrocytic processes were positioned in between pre/post synaptic elements resulting in wider intercellular clefts (Albert *et al.*, 2017). Synaptic vesicles also appeared misaggregated away from the active zone of the synapse with vesicular fusion also being observed (Albert *et al.*, 2017). Autophagosomes were also observed containing synaptic components suggestive of remodelling (Albert *et al.*, 2017). However, as only one MS patient and control were investigated this needs to be further investigated in a broader cohort (Albert *et al.*, 2017). Lastly, as the cerebellum shows extensive connections to many circuits throughout the brain, Margoni *et al* (2021) investigated a major projection site from the cerebellum, the red nucleus (RN). Margoni *et al.* (2021) showed a reduction in RN volume that correlated strongly with WM lesion volume but appeared to have no relation to GM lesion volume, supratentorial lesion volume or cortical thickness. As this study was done in RRMS patients with a very short disease duration, this supports the notion of early cerebellar disease. Having such early targets with which to track progressive disease, atrophy in GM structures to gauge neuron somal and dendritic arbor health and projections to other structures for axonal integrity, may improve the speed with which patients find the drug most suitable for them in a disease that may require a more personalised approach than most.

Summary

Clinical, MRI and histological evidence of the diverse range of disease processes that make up MS are seen in the cerebellum. These begin early and appear to continue throughout the lifetime of the patient having a sizable impact on reported quality of life measures of those

with MS. Greater focus on developing accurate measures of cerebellar functional capacity such as gait analysis, motor coordination and cerebellar associated cognitive function may make earlier detection of MS possible increasing the time neuroprotective treatments have to preserve as much neural tissue as possible. While current animal models have limited cerebral cortical pathology and most studies using them tend to focus on highly reproducible and accessible SC pathology, the similar elements of pathology seen in the cerebellum may offer useful insights into progressive disease that is currently poorly treated. Furthermore, development of tests capable of measuring more subtle changes in cerebellar function may also enable faster assessment of patient responsiveness to therapeutics in MS, and more subjective and sensitive assessment of efficacy of potential therapeutics in EAE. Using an EAE mouse model of MS, this study aims to further support the notion that the cerebellum is a valuable region to investigate the diverse forms of neuropathology that occur in various GM and WM regions in both MS and EAE. By improving our understanding of the processes surrounding neuroinflammation, the effect an inflammatory environment has on neural tissue and how tissue of various GM tissues respond will improve the efficacy of drugs aiming to protect against neurodegeneration and may offer new points of intervention.

Hypothesis & Aims

Clinical disease associated with cerebellar dysfunction is frequently observed in MS and is not limited to WM lesions and cortical GM atrophy. The DCN, through which almost all cerebellar output must pass is a region that must be better understood in the context of neuroinflammation in EAE to guide MS research in treating both cerebellar related pathology and preserving neural tissue. This thesis will address the following hypotheses:

❖ ***The DCN displays early and significant pathological changes in EAE that are hallmarks of deep GM pathology.***

➤ Use defined markers of astrocytic and macrophage reactivity and of neuron/myelin integrity to determine if the local DCN environment has been disrupted.

➤ If the local environment appears altered, determine if there is cell death associated with this, focusing on the neuronal population.

➤ Provide proof of principle for a more rigorous investigation of the DCN pathology in EAE and to justify greater attention to this region in MS tissue.

❖ ***Early cerebellar damage is more accurately evaluated by the rotarod performance test compared with the standard clinical scoring system.***

➤ Investigate EAE mouse performance on an accelerating rotarod as a means of detecting pre-ascending paralysis pathology, particularly that associated with cerebellar disease.

➤ Evaluate the accelerating rotarod test as a more objective means of assessing EAE disease progression compared to the standard clinical score system.

Chapter 2 Materials and Methods

<u>Strains of mice and housing conditions</u>

C57Bl/6 were bred from breeding pairs purchased from the Animal Resource Centre (Canning Vale, WA) and housed in the clean conventional wing of the La Trobe Animal Research and Teaching Facility (LARTF; Melbourne, Vic). SJL/J mice were purchased from the Animal Resource Centre and housed in the clean conventional wing of The Austin Health BioResources Centre (Melbourne, Vic). Up to five mice were housed in open top cages with a 12:12 hr day:night cycle at 23 °C, with free access to standard rodent chow (Barastoc Rat and Mouse Feed, Ridley AgriProducts, Melbourne, Vic.) and tap water ad libitum. Mice displaying ambulatory difficulties were provided with food and water in petri dishes on the floor of the cage.

Mice used for experimentation were female, weighed at least 21 g and were of at least 9 weeks of age. Mice were weighed on the day of induction to ensure that they were of the correct weight and are monitored for at least 30 minutes after any procedures were performed. All animal experiments were performed in accordance with the National Health and Medical Research Council (NHMRC) and La Trobe Animal Ethics Committee guidelines under the ethics code AEC 14-53.

<u>EAE Induction</u>

Prior to induction, the following stock solutions were prepared.

Myelin antigen solution

Myelin antigen solution (2 mg/mL) was prepared using freeze dried MOG_{35-55} (ModPep, Melbourne, Australia) or $PLP_{139-151}$ (ModPep) protein made up in phosphate buffered saline (PBS; 7.68 mM Na_2HPO_4, 2.67 mM NaH_2PO_4, 154 mM NaCl, pH 7.4).

Adjuvant preparation

Finely ground *Mycobacterium tuberculosis* H37 Ra (*M. tuberculosis*; *231141,* Becton Dickinson, Franklin Lakes, NJ, USA) was added to CFA (F5881, Sigma-Aldrich, St Louis, MO) to create an adjuvant with a minimum concentration of *M. tuberculosis* of 4 mg/mL. The supplemented adjuvant was stored at 4 °C until use. Prior to use, the adjuvant was thoroughly mixed until turbid.

Emulsion

An EAE induction emulsion was made by mixing equal parts CFA with the relevant neuro-antigen in PBS and homogenised until the solution became and remained uniformly opaque, white and viscous (2 mg/mL *M. tuberculosis*, 1 mg/mL CNS antigen). A vehicle only emulsion was made by mixing equal parts CFA with PBS (2 mg/mL *M. tuberculosis*). Both emulsions were stored on ice until needed and used on the day of preparation.

Pertussis toxin solution

Pertussis toxin stock solution was prepared from lyopholised *B. pertussis* toxin (P7208, Sigma-Aldrich, Saint Louis, MO, USA) made up to 0.1 mg/mL using PBS and stored at -4 °C. On the day of induction and 2 days post induction (DPI) pertussis solution was prepared by making 3.5 µL of stock solution up to 300 µL with PBS (0.116 mg/mL; 350 ng pertussis toxin per injection) per mouse and kept on ice until use.

Induction

Mice received one subcutaneous injection at day 0 in each inguinal region (two injections total). C57Bl/6 were given the myelin antigen solution containing MOG_{35-55}, whilst SJL/J were given the solution containing $PLP_{139-151}$. Vehicle only mice (VO) from all strains were given the same vehicle only emulsion. At 0 DPI and at 2 DPI, pertussis solution was

administered intraperitoneally (IP; C57Bl/6J and SJL/J) in groups that received either the EAE or VO emulsion (Fig. 2-1). Uninjected normal mice were also included as controls (Miller & Karpus, 2007).

Mice were weighed and monitored 24 hours post each injection and every other day until 10 DPI, whereupon monitoring was carried out on a daily basis unless stated otherwise. Disease progression was evaluated by observing general behaviour, state of grooming, weight loss and by assessing their clinical score (CS). The CS system is used to gauge EAE disease progression by assigning a value from CS 0 (normal) to CS 5 (moribund) representing the extent of ascending paralysis. The condition shown by the mouse, along with the relevant CS is detailed in Fig. 2-2. Upon reaching the endpoint of the experiment, mice were asphyxiated by oxygen displacement using carbon dioxide at a rate of 0.5 L/min.

EAE was also monitored in part by assessing performance on the rotarod for mice involved in the rotarod testing.
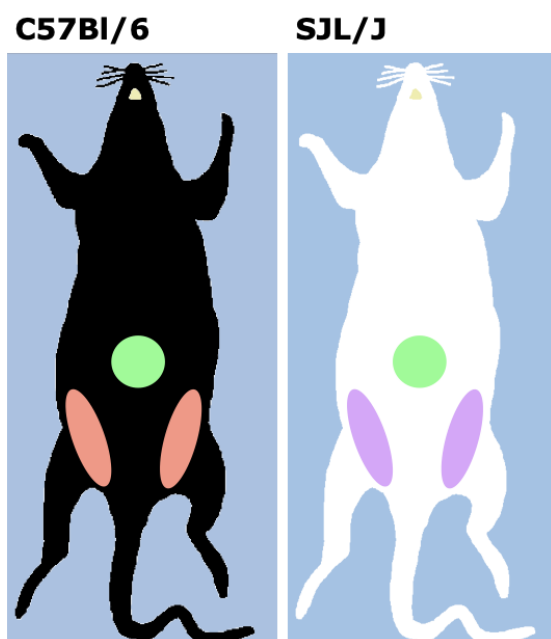
Fig. 2-1 All mice receive an injection of a neuroantigen emulsified in Freund's adjuvant on the day of induction with C57Bl/6 given MOG_{35-55} (red) and SJL/J given $PLP_{139-151}$ (purple) for the neuroantigen. All mice also receive an injection of pertussis toxin (green) given intraperitoneally for C57Bl/6 and SJL/J on the day of induction (DPI 0) and a second two days later (DPI 2).
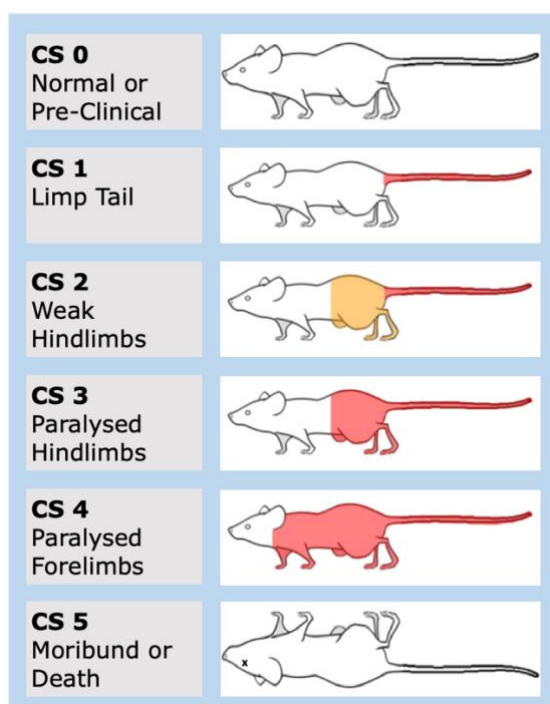
Fig. 2-2 EAE is monitored using the clinical score system, a measure of the ascending paralysis due to inflammation in the spinal cord ranging from a score of 0 indicating a mouse showing no sign of disease, up to a score of 5 indicative of a moribund state. Mice are taken at scores ranging from 0 to 3.

Rotarod test

Mice were brought to the rotarod room and left to acclimate for 20 minutes prior to training or testing. For the very first training session mice were placed on the rotarod (47650, Ugo Basile, Italy) with the apparatus switched off for 1 minute to provide opportunity for the animals to familiarise themselves with the equipment (Fiander *et al*, 2017). During the rotarod training phase mice received three training sessions per day each lasting 300 seconds with at least 10 minutes rest in between each session for both training and experimental phases, after which the mice are returned to their housing unit (Fiander *et al.*, 2017). Mice that fell before the end of the training session were placed back on the rotarod. During the experimental phase mice were left at the bottom until the test ended so as to not disturb the mice still on the rotarod. Trials were averaged to get a single measurement of time to fall each day.

Protocol 1

Mice were put through a training phase of two training sessions at DPI -1 and 6 consisting of three trials on an accelerating rotarod (5-16, 5-40, 5-40 revolutions per minute (RPM)). Testing was performed on DPI 8 and 14 with all three trials at 5-40 RPM (Table 2-1a). Mice at DPI 14 that had a CS of 2 or above were not placed on the rotarod due to ethical concerns.

Protocol 2

Mice were trained on the rotarod daily from -4 DPI to DPI 0 (Bernardes & Oliveira, 2017; Fiander *et al.*, 2017; Gilli *et al*, 2016). Training sessions consisted of three identical trials per day where the final RPM was increased each day as per Table 2-1b. The experimental phase began at 5 DPI which allowed the mice time to recover from induction procedures performed on DPI 0 and 2 as evidenced by a return to pre-induction weights. Testing continued daily until mice exhibited early evidence of motor symptoms associated with

EAE, namely hind limb weakness (clinical score ≥ 1.5)(van den Berg *et al*, 2016). Over the course of the experimental phase, mice underwent three trials per day on an accelerating rotarod (5-40 RPM; Table 2-1b)(van den Berg *et al.*, 2016).

Protocol 3

Identical to protocol 2 except the max speed for the training and testing phase was increased to 60 RPM (Table 2-1c).

a) Protocol 1

Training Phase	Trial 1	Trial 2	Trial 3
DPI -1	5-16 RPM	5-40 RPM	5-40 RPM
DPI 6	5-16 RPM	5-40 RPM	5-40 RPM

Experimental Phase	Trial 1	Trial 2	Trial 3
DPI 8	5-40 RPM	5-40 RPM	5-40 RPM
DPI 14	5-40 RPM	5-40 RPM	5-40 RPM

b) Protocol 2

Training Phase	Trial 1, 2 & 3
DPI -4	5-16 RPM
DPI -3	5-24 RPM
DPI -2	5-32 RPM
DPI -1	5-40 RPM
DPI 0	5-40 RPM

Experimental Phase	Trial 1, 2 & 3
DPI 5+	5-40 RPM

c) Protocol 3

Training Phase	Trial 1, 2 & 3
DPI -4	5-16 RPM
DPI -3	5-24 RPM
DPI -2	5-32 RPM
DPI -1	5-40 RPM
DPI 0	5-60 RPM

Experimental Phase	Trial 1, 2 & 3
DPI 5+	5-60 RPM

Table 2-1 Training and experimental speeds (RPM) for mouse rotarod protocols. (a) Protocol 1 was insufficient in that the mice showed improvement during the testing phase and did not have enough points of assessment to determine onset of disease. (b) Protocol 2 did not have a high enough top speed to properly assess the maximum capabilities of all mice, (c) therefore the maximum RPM was increased from 40 to 60 RPM for Protocol 3.

<u>Tissue Collection</u>

Prior to taking the mice, a stock solution of paraformaldehyde (4 % w/v) in PBS was prepared, with 50 mL aliquots stored at -20 °C. After carbon dioxide asphyxiation, mice were perfused transcardially with 10 mL of PBS followed by 10 mL of paraformaldehyde solution. Soft tissues were then dissected and discarded such that just the head and vertebral column remained which were stored in individual 50 mL tubes filled with paraformaldehyde and left on a tube roller for at least 48 hours before further dissection. The brain was then removed and quartered using a matrix guide (Alto 1 mm acrylic brain matrix, Roboz Surgical Instrument Co., Gaithersburg, MD, USA) separating the cerebellum from the rest of the brain and also cutting the cerebellum in half in the sagittal plane into right and left hemispheres (Fig. 2-3).

Paraffin sections

Tissue dye (The Davidson Marking System™, Bradley Products Inc., Bloomington, MN, USA) was used to mark the sagittal faces of the right and left hemispheres of the cerebellum. Dyed tissue was then processed (Leica TP 1020 Leica Biosystems GmbH, Wetzlar, Germany) as per Table 2-2, and using a tissue embedder (Leica EG 1150 H), embedded medial sagittal side down in paraffin wax (Histotec Pastilles with DMSO, 1151612504, Merck, Darmstadt, Germany). Each wax block consisted of the sagittal sections of three to six mice within the same experimental group as seen in Fig. 2-3. Duplicate sections were cut using a microtome (Model No. RM2235, Leica Biosystems) at 7 μm and collected on positively charged glass slides (SuperFrost Plus®, SF41296SP, Menzel Glaser, Braunschweig, Germany). Slides were left to dry overnight before storage at room temperature.
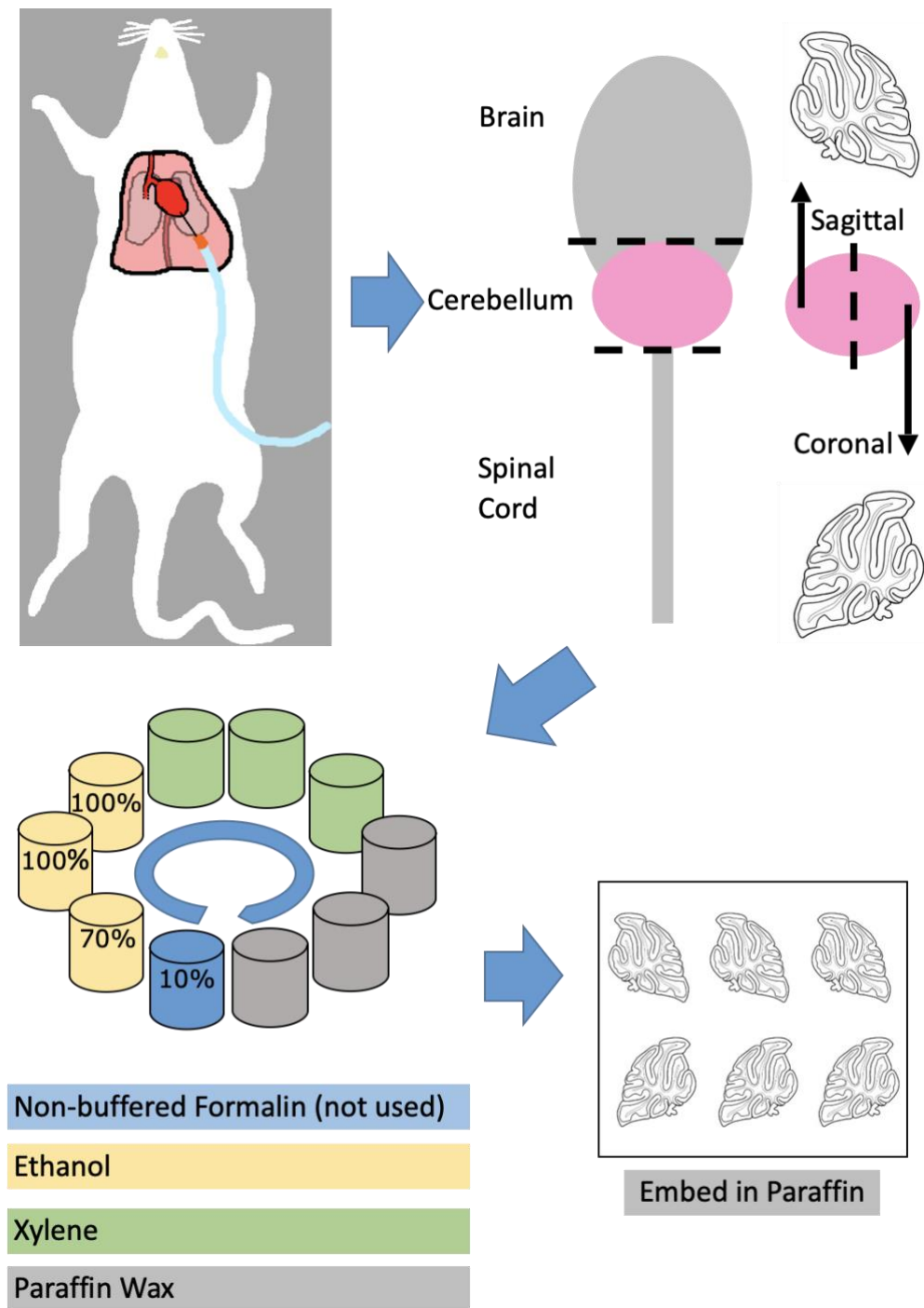
Fig. 2-3 Mice are immediately perfused with PBS, then 4 % (v/v) paraformaldehyde after asphyxiation with carbon dioxide. After perfusion, soft tissues and body are placed on a tube roller for at least two days before CNS tissues are removed. Using a matrix, the cerebellum is cut away from the brain and then halved in the sagittal plane. Tissue for wax sections were then placed into a tissue processor and embedded medial-sagittal side down in paraffin wax.

Step	Solution	Time (hours)
1	70% Ethanol	1
2	Absolute Ethanol	1.5
3	Absolute Ethanol	2
4	Absolute Ethanol	3
5	Xylene	0.5
6	Xylene	1
7	Xylene	2
8	Xylene	2
9	Wax	2
10	Wax	2
11	Wax	2.5
	Total time	19.5

Table 2-2 Cerebellar tissues are prepared for paraffin sectioning using a series of ethanol, xylene to dehydrate and then perfused with wax. This is performed using a tissue processor (Leica TP 1060) with tissues spending a set time inside each solution or liquid as indicated.

Cryostat sections

After fixation, cerebellar hemispheres for cryosectioning were placed into individual 10 mL tubes (one tube per mouse) containing a 30 % (w/v) sucrose solution for cryoprotection then placed onto a tube roller at room temperature. Cerebellar tissue was left on the tube roller for several days until it no they longer floated in the cryoprotectant, with the cryoprotectant being replaced daily with fresh solution. Cerebellar tissues were removed after the cryoprotectant had fully diffused through the tissue, dried with paper towelling, then positioned in cryomolds (4557 Tissue-Tek®, Torrance, CA) with the medial-sagittal surface face down. Tissue in the cryomolds was then completely immersed in Optimal Cutting Temperature (OCT; 4583, Tissue-Tek®) taking care not to introduce any air pockets and left for approximately 5 minutes to ensure the OCT had fully bonded with the tissue. To evenly freeze the contents of the cryomold a small beaker was filled with enough isopentane to fully submerge the mold and tissue. This was cooled using a second larger beaker containing liquid nitrogen with the isopentane stirred until crystals began to form at the bottom. Cryomolds were carefully lowered into the almost frozen isopentane to the top of the mold, then fully submerged when the OCT has almost completely frozen solid. Frozen OCT and tissue were left in the cryomold and stored on dry ice until all tissue had been frozen, whereby blocks are stored at -80 °C until sectioning. Sections were cut using a cryostat (Leica) at -21 °C at 10 µm and collected on positively charged slides (SuperFrost Plus ®) and left to dry for approximately an hour at room temperature before storing at -20 °C.

Histological Staining

Paraffin and cryostat sections were stained with Mayer's haematoxylin (MH; Amber Scientific, Midvale, WA, Australia) and eosin (EOA1, Amber scientific) in accordance with a progressive staining protocol used in the laboratory detailed in Table 2-3 and Table

2-4 respectively. Cresyl violet staining was performed on paraffin sections as detailed in Table 2-5.

Step	Solution	Purpose	Time (min)
1	Xylene	Dewaxing	4
2	Xylene		4
3	Ethanol	Transition from a non-polar to polar/aqueous solution	2
4	Ethanol		2
5	Tap water	Aqueous environment required for staining	5
6	Haematoxylin	Nuclear stain	3
7	Tap water	Remove excess haematoxylin	0.5
8	Scott's Tap water*	Develop the hematoxylin into a deep blue	1.5
9	Eosin	Cytoplasmic stain	3.5
10	Tap water	Removal of excess eosin	Rinse until water is clear
11	70% (v/v) Ethanol	Graduated removal of water and returning to a non-polar environment.	10 quick dips
12	100% Ethanol		10 quick dips
13	100% Ethanol		10 quick dips
14	Xylene	Enables DPX** to mix seamlessly with tissue.	2
15	Xylene		2

*Table 2-3 Paraffin sections are dewaxed and stained with fresh haematoxylin and eosin. *Scott's Tap water (20.18 mM KCO_3, 166.15 mM $MgSO_4$, pH 8.9), ** Dibutyl phthalate Polystyrene Xylene (DPX; Thermo Fisher Scientific).*

Step	Solution	Purpose	Time
1	1 x PBS	Removes OCT and provides aqueous environment required for staining	10m
1	Tap water		Quick Rinse
2	Haematoxylin	Nuclear stain	40s
3	Tap water	Remove excess haematoxylin	10s
4	Scott's Tap water	Develop the hematoxylin into a deep blue	15s
5	Tap water	Bring back to aqueous state	30s
6	Eosin	Cytoplasmic stain	35s
7	Tap Water	Removal of excess eosin	Rinse until water is clear
8	70% (v/v) Ethanol	Graduated removal of water and returning to a non-polar environment.	10 quick dips
9	100% Ethanol		10 quick dips
10	100% Ethanol		10 quick dips
11	Xylene	Enables DPX to mix seamlessly with tissue.	2m
12	Xylene		2m

Table 2-5 Cryostat sections are stained with haematoxylin and eosin using a much shorter version of the paraffin protocol without dewaxing steps.

Step	Solution	Purpose	Time (min)
1	Xylene	Dewaxing	5
2	Xylene		5
3	Ethanol	Transition from a non-polar to polar/aqueous solution	5
4	Ethanol		5
5	Tap water	Remove excess ethanol	2 Dips
6	dH2O	Remove excess ethanol	2 Dips
7	0.1% Cresyl Violet	Stain rough endoplasmic reticulum	14
8	dH2O	Rinse excess stain	2 Dips
11	95% (v/v) Ethanol	Graduated removal of water and returning to a non-polar environment.	2
12	100% Ethanol		1
13	100% Ethanol		1
14	Xylene	Enables DPX to mix seamlessly with tissue.	2
15	Xylene		2

Table 2-4 Paraffin sections stained with cresyl violet were dewaxed, stained and mounted as per the above protocol.

Step	Solution	Purpose	Time (min)
1	Xylene	Dewaxing	4
2	Xylene		4
4	Ethanol	Transition from a non-polar to polar/aqueous solution	2
5	Ethanol		2
6	Tap water	Rinse off remaining ethanol	2
7	PBS	Return tissue to homeostatic conditions	15
8	Citrate Solution	Antigen retrieval	Boiling ~ 1 Cooling ~ 40
9	2 x Wash in PBS	Remove citrate buffer	5 & 10
10	Blocking Solution	Prevent non-specific primary antibody binding	40
11	Primary antibody	Label proteins of interest	Overnight at 4°C
12	Wash in PBS-Tween 0.5% (v/v)	Remove non-specific binding of primary antibody	5 & 10
13	Amplification	Apply biotinlyated antibody solution if required	13
14	Wash in PBS-Tween 0.5% (v/v)	Remove non-specific binding of biotinylated antibody	5 & 10
15	Secondary antibody and Streptavidan conjugates	Highlight bound primary antibody with fluorophore	60
16	Wash in PBS-Tween 0.5% (v/v)	Remove non-specific binding of secondary antibody	5 & 10
17	DAPI	Stain nucleus	5
18	Coverslip	Protect tissue	Drying ~ 60

Table 2-6 Standard protocol for performing IHC on paraffin sections. For frozen sections, steps 1-5 relating to dewaxing can be skipped starting at step 7.

Immunochemistry

Paraffin sections or frozen sections were brought to an aqueous state as detailed in Table 2-6. Antigen retrieval was performed by boiling in sodium citrate solution (113.93 mM $Na_3C_6H_5O_7$, pH 6) for 1 minute (min) and left to cool for 40 min. Slides were then washed in PBS 1×5 min and 1×10 min before tissue sections were encircled with a hydrophobic barrier pen (PAP pen, Z672548, Sigma-Aldrich). Blocking solution was applied to all sections for 40 min (3 % v/v non-immune horse or goat serum, 0.3 % v/v Triton X-100, made up in PBS) before being washed off with PBS 1x 5 min and 1 x 10 min. Primary antibodies (Table 2-7) were diluted in blocking solution before application to sections and left in a humid chamber overnight at 4°C after which they were washed off in PBS-Tween 0.5 % (v/v) 1 x 5 min and 1 x 10 min. Where appropriate, biotinylated antibodies (Table 2-8) diluted in blocking solution against the primary were applied for 1 hour at room temperature before being washed off with PBS-Tween 0.5 % (v/v) 1 x 5 min and 1 x 10 min. In a dark room, Alexa-conjugated fluorescent secondary antibodies (Table 2-10) or streptavidin-fluorophore conjugates (Table 2-9) were diluted in blocking solution and left on the sections for 60 min before being washed with PBS-Tween 0.5 % (v/v) 1 x 5 min and 1 x 10 min.

When even greater amplification was required, this was performed using a Tyramide SuperBoost™ Kit (B40944, Thermo Fisher Scientific, Waltham, MA). Required components are made up as prescribed by the included protocols. In brief, prior to primary antibody application endogenous peroxidase activity was quenched covering the tissue with hydrogen peroxide solution (prepared on day of use, 3 % in dH_2O, Component C2) for 60 min at room temperature in a humid chamber, then washed 3 x 5 min with PBS. Enough blocking buffer (Component A) was applied to cover the tissue and left for 60 min in a humid chamber at room temperature. Primary antibody diluted in blocking solution was

then applied and left to incubate overnight at 2-8 °C in a humid chamber, then rinsed with three washes of PBS for 10 min at room temperature. Enough poly-HRP conjugated secondary antibody (Component B) to cover the tissue and left overnight at 2-8 °C, then washed 3 times with PBS for 10 min at room temperature. Tyramide solution (prepared within 2 hours of use) was applied covering the entire tissue section and left to incubate for 2-10 min depending on required intensity, whereby 100 µL of Reaction Stop Reagent (95 % ethanol) was applied to end the reaction. Sections were then washed with PBS 3 x 10 min.

Lastly, 4', 6-diamidino-2-phenylindole (DAPI) in PBS (1:1000), was applied for 5 min before briefly rinsing in PBS. Coverslips were applied using fluorescent mounting medium (Dako, Santa Clara, CA) with excess media removed and slides left dry for several hours, then stored at 4 °C (Table 2-6).

Target	Host	Manufacturer	Product Code	Working Dilution
CD3	Rabbit	Dako, Santa Clara, CA	A 0452	1/400
Crystallin αB	Goat	R&D Systems, Minneapolis, MN	AF4849	1/100
GFAP	Mouse	Merke Millipore	MAB360	1/400
Iba1	Rabbit	WAKO, Richmond, VA	019-19741	1/200
Iba1	Goat	Novus Biologicals, Centennial, CO	NB100-1028SS	1/200
MBP	Rabbit	Dako	A0623	1/200
Hypo-phosphorylated Neurofilament H	Mouse	Sternberger Monoclonals, Lutherville, MD	SMI-32R	1/200
Phosphorylated Neurofilament H	Mouse	Sternberger Monoclonals	SMI-31R	1/200
PLP	Mouse	R&D Systems	MAB388	1/500
TMEM119	Rabbit	Abcam, Cambridge, UK	ab209064	1/100

Table 2-7 Details of primary antibodies including target, host, manufacturer, working dilution and product code.

Target	Host	Manufacturer	Product Code	Working Dilution
Goat IgG	Donkey	Abcam	ab208000	1/200
Rabbit IgG	Goat	Vector Laboratories Inc., Burlingame, CA	BA-1000	1/500
Mouse IgG	Horse	Vector Laboratories Inc.	BA-2000	1/500

Table 2-8 Details of biotinylated antibodies used to enhance the signal of weakly staining primary antibodies.

Streptavidin Conjugates	Fluorophore Excitation/Emission (nm)	Manufacturer	Product Code	Working Dilution
Alexa Fluor 488	Alexa 488 - Green 495/519	Thermo Fisher Scientific	S11223	1/200
Alexa Fluor 555	Alexa 555 - Red 555/565	Thermo Fisher Scientific	S21381	1/200

Table 2-9 Details of streptavidin-fluorophore conjugates used to visualise primary antibody staining amplified with the addition of a biotinylated antibody.

Target	Host	Fluorophore Excitation/Emission (nm)	Manufacturer	Product Code	Working Dilution
Mouse IgG	Goat	Alexa 488 - Green 495/519	Abcam	ab150113	1/200
Mouse IgG	Goat	Alexa 488 - Green 495/519	Thermo Fisher Scientific	a11029	1/200
Rabbit IgG	Goat	Alexa 488 - Green 495/519	Abcam	ab150077	1/200
Goat IgG	Goat	Alexa 488 - Green 495/519	Abcam	ab150129	1/200
Mouse IgG	Mouse	Alexa 488 - Green 495/519	Abcam	ab150109	1/200
Rabbit IgG	Donkey	Alexa 488 - Green 495/519	Abcam	ab150061	1/200
Mouse IgG	Goat	Alexa 546 - Red 556-573	Thermo Fisher Scientific	A-11003	1/200
Mouse IgG	Donkey	Alexa 555 - Red 555/565	Abcam	ab150110	1/200
Rabbit IgG	Donkey	Alexa 594 - Red 590/617	Abcam	ab150064	1/200
Mouse IgG	Goat	Alexa 594 - Red 590/617	Abcam	ab150116	1/200
Rabbit IgG	Goat	Alexa 594 - Red 590/617	Abcam	ab150080	1/200
Rabbit IgG	Donkey	Alexa 647 - Far Red 650/665	Abcam	ab150063	1/200

Table 2-10 Details of secondary antibodies used to visualise primary antibody staining.

TUNEL Staining

Tissue for TUNEL staining was brought to an aqueous state in the same manner as paraffin or cryostat sections used for immunohistochemistry (IHC), including antigen retrieval and permeabilisation steps. TUNEL staining was performed prior to the addition of primary antibodies to visualise other targets. Solutions were prepared as directed by the manufacturer's protocol (In Situ Cell Death Detection Kit, Fluorescein, 11684795910, Roche Diagnostics GmBH, Mannheim, Germany) producing an Enzyme+Label mix for the experimental tissue and a Label-Only mixture to function as a negative control.

Prior to performing the TUNEL assay, two positive controls were prepared where one cerebellar section was treated with enough DNase I (approx. 50 µL) to cover the section for 15 min at room temperature in a humid box, then removed with three washes of PBS. Tumour tissue (4T1) was included as a second positive control untreated with DNase I.

For the TUNEL stain itself, approximately 50 µL of the Enzyme+Label and Label-Only solutions were applied to the relevant sections in a carefully sealed humid box for 60 min at 37 °C. TUNEL solutions were removed from the tissues with three washes of PBS before commencement of blocking steps required for additional antibodies.

Neuronal Counting

Cerebellar tissue was taken from normal, VO and EAE induced mice and embedded in paraffin. Three out of every ten slides (#2/5/8, 12/15/18, etc) were stained with cresyl violet as per Table 2-5. Using an Olympus (CH-2, Olympus, Japan) and a USB microscope camera (MD500L, AmScope, Irvine CA, USA), images were taken at 10 x magnification and stitched together where applicable to get a complete image of the fastigial and interposed nuclei. Sagittal images were positioned alongside each other with sections being

selected for counting that most accurately aligned with other sections taken from other mice (Supp. 3-1). Neurons were manually counted if the soma was intact and larger than 10 μm and contained a clear well-defined nucleus, with neurons smaller than 10 μm requiring a clearly identifiable axonal/dendritic process to be counted as such (Fig. 2-4). The researcher counting the neurons was partially blinded in that they were not involved in all aspects of the initial rotarod experiment, tissue collection, histology and imaging. While normal, VO and EAE (CS 2.5+) with low cerebellar inflammation groups were broadly indistinguishable, the EAE (CS 2.5+) with high cerebellar inflammation group was immediately distinguishable due to the large inflammatory lesions surrounding the DCN. Regions counted extended from medial edge of the fastigial cerebellar nucleus to the medial dorsolateral protuberance.
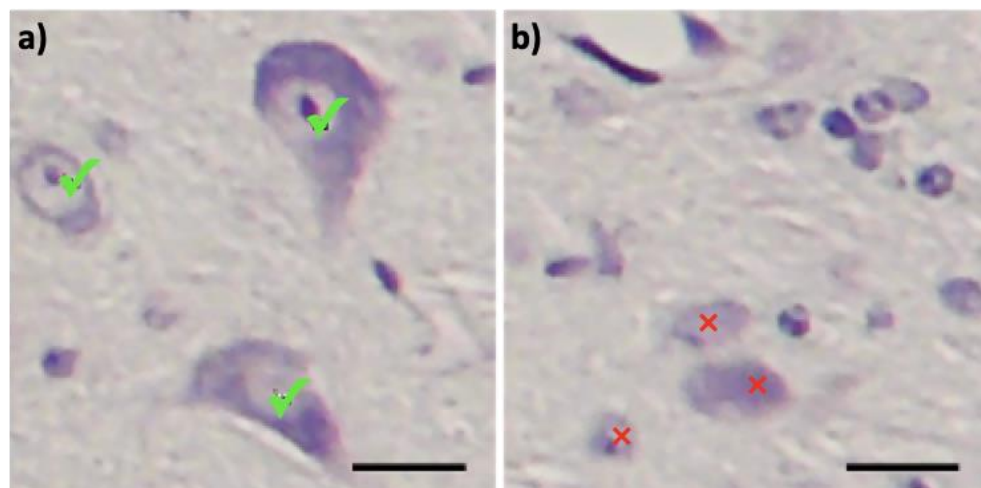
Fig. 2-4 (a) Paraffin sections stained with cresyl violet was used to estimate neuron numbers (green tick) in the cerebellar DCN. Cresyl violet positive cells in (b) were not counted due to being too small or missing a clearly identifiable nucleus (red cross).

Microscopy and imaging

Brightfield

Brightfield H&E images were taken using the Nikon Ti Eclipse (Nikon Corporation, Chiyoda, Tokyo, Japan) with a DS-Fi2 colour camera (Nikon Corporation) and controlled with the software NIS-Elements (Nikon). Images were captured using one of several objectives including: 10 x (Plan Fluor DL 10 x/0.30 Air), 20 x (Super Plan Fluor 20 x/0.45 ELWD ADM [correction collar] Air), 40 x (Super Plan Fluor 40 x/0.60 ELWD ADM [correction collar] Air) or 100 x (Plan Apochromat VC Oil) objective, all of which could be magnified by a further 1.5 x zoom inbuilt into the microscope. Images were stitched together using the NIS elements tile feature where required.

Epifluorescence

Fluorescently labelled tissue was imaged using the Zeiss AxioObserver Z1 microscope (Carl Zeiss International, Oberkochen, Germany) using an Axio Cam MRm monochrome camera (Carl Zeiss International) controlled with Zen Blue (Carl Zeiss International). Objectives included 10 x (A-Plan 10 x/0.25 Ph1 M27), 20 x (LD Plan-NeoFluar 20 x/0.4 Corr Ph2 M27), 40 x (LD Plan-NeoFluar 40 x/0.6 Corr Ph2 M27) and 100 x (Plan NeoFluar 100 x/1.30 Oil M27).

Cerebellar Atlas

A series of sagittal traces was taken from The Mouse Brain in Stereotactic Coordinates (Franklin & Paxinos, 2008) and edited using Adobe Illustrator. These vector lines were then imported into the 3-D rendering program Blender (https://www.blender.org). Traces of the outer edge of the cerebellum, outer edge of the GL, WM and DCN were used as a scaffold to create a model of the multiple layers present within the cerebellum. Using H&E-stained sections, the location of inflammatory infiltrates was recorded for each mouse. To

create the cerebellum model, Adobe Illustrator was used to transfer all relevant sagittal vector paths that made up the sagittal cerebellar series from The Mouse Brain in Stereotactic Coordinates (Franklin & Paxinos, 2008). Once imported into Blender, sagittal vectors denoting the ML, GL, WM and DCN were moved to their respective planes as per the lateral position. Vertical sections were aligned with the underlying grid. Once in position, vector paths were converted to meshes and connected to create a 3-D model of the outermost layer of the cerebellum, the outermost edge of the GL, the underlying WM and the innermost DCN. Non-destructive modifiers were applied to smooth the whole mesh, colour layers and make them transparent (Fig. 2-5). To record inflammatory disease, paraffin sections (1/10) were stained with H&E with images taken at 6 x magnification and stitched together using an inverted bright field colour microscope (Nikon Ti Eclipse). Lesions observed were recorded on a series of traces taken from the mouse atlas with each mouse being recorded as an individual layer using GIMP (GNU image manipulation program, https://www.gimp.org).

Statistics

Analysis of neuron counts and rotarod data and production of graphs was performed using GraphPad Prism (Bit Plane) with findings considered significant if $p < 0.05$. For any given experiment, the number of mice per group and details of the statistical test used is described in the corresponding figure legend.
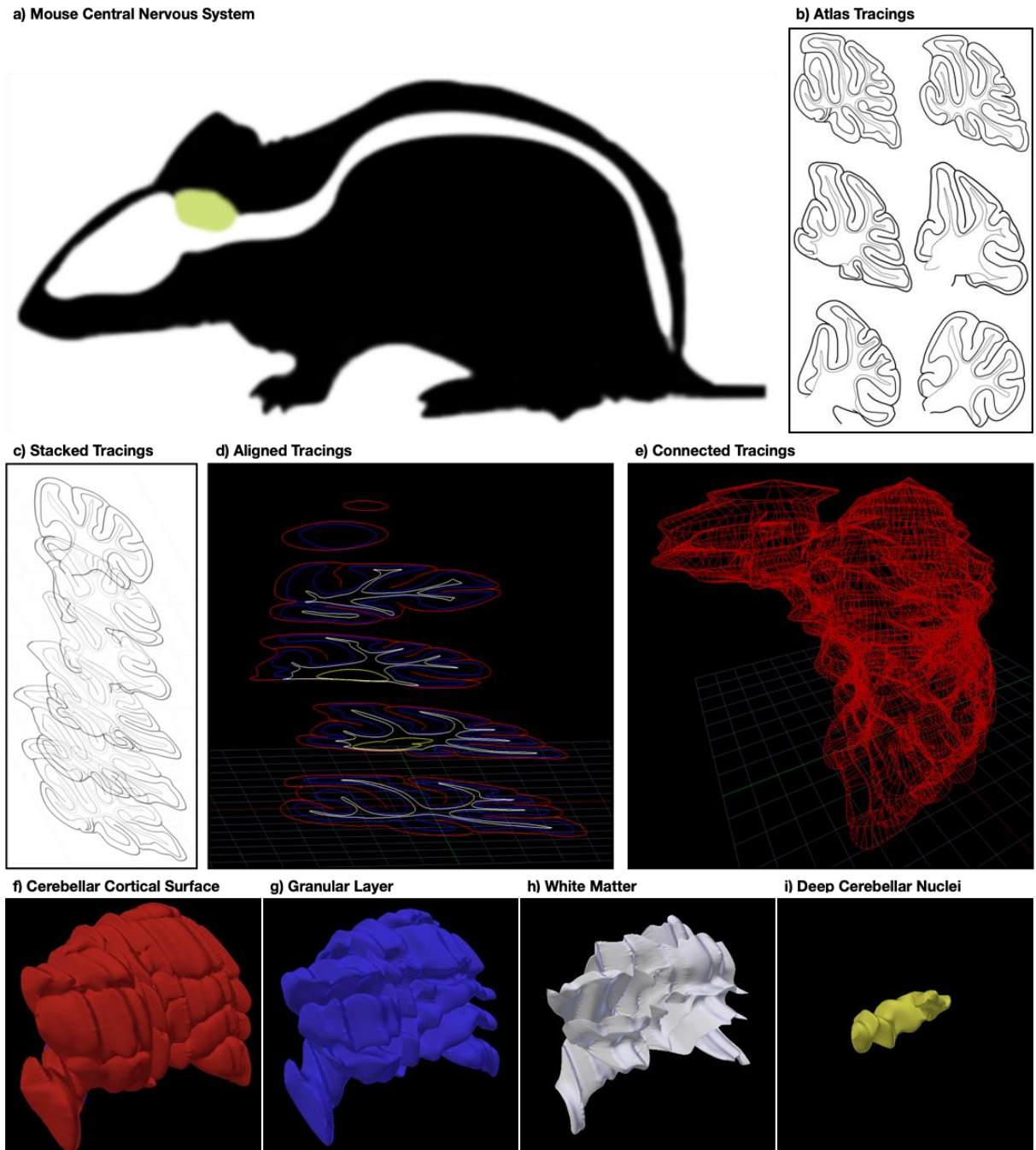
Fig. 2-5 Three-dimensional cerebellar reconstruction. (a) Location of mouse cerebellum (green) relative to rest of CNS (white). (b) Traces of the cerebellum were taken from the Mouse Brain Atlas (Franklin & Paxinos, 2008). (c) These traces were aligned and (d) used to create vector lines for the outermost layer (red), the GL (blue), the WM (white) and the DCN (yellow) using the free 3-D rendering program Blender (https://www.blender.org). (e) These traces were connected, and non-destructive modifiers were applied resulting in a 3-D model of (f) the cerebellar cortical surface, (g) the GL, (h) the underlying WM and (i) the DCN.

Chapter 3 "Contrasting levels of pathology between the deep cerebellar nuclei and adjacent white matter in experimental autoimmune encephalomyelitis"

The following chapter is being prepared as a manuscript submission to a neuropathology journal hence there will be some repetition in the contents of this chapter and the rest of the thesis. Due to time constrains, some data shown as supplementary data are presented in qualitative form only. However, quantification, where required will be completed prior to submission of the manuscript.

Title: Contrasting levels of pathology between the deep cerebellar nuclei and adjacent white matter in experimental autoimmune encephalomyelitis

3-2

Authors: Dain L Maxwell[a], Nishat Tabassum[a], Claretta S D'Souza[a], Stuart McDonald[b] and Jacqueline M Orian[a, c]

a) Department of Biochemistry and Genetics, La Trobe Institute for Molecular Science, La Trobe University, Bundoora 3086, Victoria, Australia.

b) Department of Neuroscience, Central Clinical School, Monash University, Clayton 3800. Victoria, Australia.

c) Corresponding author.

email addresses: j.orian@latrobe.edu.au (Jacqueline M Orian); d.maxwell@latrobe.edu.au (Dain L Maxwell); claretta.dsouza@latrobe.edu.au (Claretta S D'Souza); n.tabassum@latrobe.edu.au (Nishat Tabassum); stuart.mcdonald@monash.edu.au (Stuart Macdonald).

Running title: Spatiotemporal mapping of cerebellar inflammation in EAE

List of abbreviations:

CFA	Complete Freund's Adjuvant
CNS	Central nervous system
CR	Chronic remitting
CP	Chronic progressive
CS	Clinical score
DAPI	4', 6 diamidino-2-phenylindole
DCN	Deep cerebellar nuclei
DPI	Days post induction
EAE	Experimental autoimmune encephalomyelitis
GFAP	Glial fibrillary acidic protein
GL	Granular layer
GM	Grey matter
H&E	Haematoxylin & eosin
Iba1	Ionised binding adapter molecule 1
IHC	Immunohistochemistry
MBP	Myelin basic protein
Men.	Meninges
ML	Molecular layer
MOG	Myelin oligodendrocyte glycoprotein
MS	Multiple sclerosis
MRI	Magnetic resonance imaging

NF   Hypo-phosphorylated neurofilament

OCT   Optimal Cutting Temperature

PBS   Phosphate buffered saline

PLP   Proteolipid protein

PPMS   Primary progressive multiple sclerosis

RRMS   Relapsing remitting multiple sclerosis

SPMS   Secondary progressive multiple sclerosis

TUNEL   Terminal deoxynucleotidyl transferase dUTP nick-end labelling

VO   Vehicle only

WM   White matter

Abstract

The elucidation of grey matter (GM)-specific mechanisms in multiple sclerosis (MS) is key to the generation of neuroprotective approaches for this condition. Investigations of post-mortem MS tissue have identified the cerebellum as a major predilection site for cortical pathology, characterized by severe demyelination and significant reduction in Purkinje cell density. In parallel, longitudinal studies of cerebellar changes in murine experimental autoimmune encephalomyelitis (EAE), the preferred MS model, have revealed remarkable similarities in pathological hallmarks between MS and EAE in this region. These include demyelination, Purkinje cell loss and significant whole cerebellar volume reduction by late disease, thereby validating EAE for providing proof-of-concept for GM-specific mechanisms. Surprisingly, these studies have neglected the deep cerebellar nuclei (DCN), a functionally significant group of nuclei at the centre of the cerebellum associated with relaying information from the cerebellum to the brainstem and thalamus. As a first step to the characterisation of pathology in the DCN and functional consequences of such damage, we performed spatiotemporal mapping of lesion development in the cerebellum in two EAE variants, namely $MOG_{35\text{-}55}$ induced C57Bl/6 mice which exhibit chronic-progressive (CP) EAE and $PLP_{139\text{-}151}$ induced SJL/J mice, exhibiting chronic-remitting (CR) EAE. We found that although surrounded by florid white matter (WM) inflammation, the DCN remains remarkably free from inflammatory infiltration. On the other hand, highly elevated microglial reactivity is observed as well as terminal deoxynucleotidyl transferase dUTP nick-end labelling (TUNEL)+ activity above that of controls. These hallmarks suggest significant functional disturbances in the DCN, independent of inflammatory cell infiltration.

Key words: Cerebellum, neuroinflammation, deep cerebellar nuclei (DCN), experimental autoimmune encephalomyelitis (EAE), microglial reactivity, multiple sclerosis (MS).

Introduction

MS is a central nervous system (CNS) autoimmune disorder with a neurodegenerative component (Dendrou *et al*, 2015; Stys *et al*, 2012; Trapp & Nave, 2008). In its commonest form, which accounts for 80-85% of cases, it manifests as a relapsing-remitting disease with periods of neurological impairment interrupted by partial or total recovery (Compston & Coles, 2002; Goodin, 2014). In the majority of relapsing-remitting MS (RRMS) patients the disease evolves into a progressive form without remissions, known as secondary progressive MS (SPMS)(Compston & Coles, 2002; Goodin, 2014). The next most common form is primary progressive MS (PPMS), affecting about 10% of cases and characterized by steady increase in neurological disability from first presentation (Compston & Coles, 2002; Goodin, 2014). Different pathological processes have been identified in WM and GM (Matthews *et al*, 2016; Prins *et al*, 2015). In WM, pathology is characterised by inflammatory demyelination, associated with reactive gliosis, oligodendrocyte loss and axonal degeneration (Lucchinetti *et al.*, 2000; Popescu & Lucchinetti, 2012). WM damage can be visualised with magnetic resonance imaging (MRI) (Lucchinetti *et al.*, 2000; Popescu & Lucchinetti, 2012). Recent years have witnessed an appreciation of GM pathology and it is now clear that GM disease is characterised by significantly less inflammation, but extremely severe demyelination and microglial reactivity (Calabrese *et al.*, 2010a; Geurts & Barkhof, 2008; Peterson *et al*, 2001; Pirko *et al*, 2007; Vercellino *et al*, 2005). GM damage has been documented in multiple brain regions including the cerebral cortex, thalamus, hypothalamus, basal ganglia, hippocampus, cerebellum and spinal cord (SC)(Calabrese *et al*, 2007; Geurts *et al*, 2007; Gilmore *et al.*, 2009; Kutzelnigg *et al.*, 2007; Kutzelnigg *et al.*, 2005; Papadopoulos *et al*, 2009; Peterson *et al.*, 2001; Vercellino *et al.*, 2005) and several studies have reported that severe GM lesions are already present in early MS stages when WM pathology is relatively limited (Calabrese *et al.*, 2007; Calabrese *et al.*, 2010a; Geurts *et al.*, 2007; Peterson *et al.*, 2001; Pirko *et al.*, 2007). GM disease is poorly detectable by MRI, but is associated with atrophy (Filippi *et al*, 2007;

Mahad *et al*, 2015). Indeed, GM atrophy is more closely linked to overall disability than lesion load and is now considered as a better predictor of neurological disability (Mahad *et al.*, 2015).

The introduction of more sensitive approaches for the identification of demyelination revealed the extent of cortical pathology in the forebrain (Bo *et al.*, 2003; Calabrese *et al.*, 2007; Lucchinetti *et al*, 2011; Peterson *et al.*, 2001; Reynolds *et al*, 2011). Subsequently studies of the cerebellum identified the cerebellar cortex as a major predilection site for demyelination, with on average 38.7% of cerebellar cortical area, but up to 92%, in progressive stage post-mortem tissues. Demyelination occurs in a band-like manner, affecting multiple folia (Kutzelnigg *et al.*, 2007; Kutzelnigg *et al.*, 2005). Cortical demyelination is independent of WM lesions, with extensive demyelinated regions often adjacent to areas free of WM lesions (Kutzelnigg *et al.*, 2007; Kutzelnigg *et al.*, 2005). The most extensively characterised function of the cerebellum is movement regulation and the modulation of co-ordination and balance. Movement disorder is a common symptom at clinical presentation, yet pathological processes underlying cerebellar dysfunction remain largely unidentified. In order to gain an insight into cellular mechanisms underlying cerebellar cortical atrophy and neurodegeneration, investigators have relied heavily on EAE, the most commonly used animal model for MS (Dang *et al*, 2015; Kipp *et al*, 2012; Robinson *et al*, 2014). EAE is generated by vaccination against myelin proteins or peptides derived from sequences of myelin proteins in susceptible rodent or non-human primate species. This results in neuroinflammation and clinical disease, exhibiting a CR, monophasic or CP profile depending on the protein/neuropeptide and host combination. EAE and MS are distinct diseases, nonetheless it is generally accepted that the different EAE variants represent different facets of MS.

Classical EAE generally manifests as an ascending paralysis, which is associated with SC disease, however, the cerebellum is also a site of disease predilection in the model. In genetically modified models, where SC injury is eliminated, ataxia is commonly observed showing that cerebellar disease is independent of SC disease (Batoulis *et al*, 2011). In the EAE model, extensive studies based principally on combined MRI and histology, have provided much insight into cerebellar degeneration over the disease course (MacKenzie-Graham *et al.*, 2012; MacKenzie-Graham *et al.*, 2006; MacKenzie-Graham *et al.*, 2009). These showed (1) significant whole cerebellar volume reduction by late disease relative to matched controls and a correlation between cerebellar cortical atrophy and disease duration (MacKenzie-Graham *et al.*, 2006). (2) Cerebellar atrophy was localised to the molecular layer (ML) and associated with a significant decrease in Purkinje cell numbers. There was a significant association between Purkinje cell loss and atrophy of the ML. However, lesions were observed in WM but not GM (MacKenzie-Graham *et al.*, 2012). (3) Finally, longitudinal studies beginning at the pre-onset stage showed progressive cerebellar volume loss over time and identified regions that were more sensitive to volume loss (MacKenzie-Graham *et al.*, 2009). These data are important because they validate the use of EAE for prospective studies and the identification of prognostic markers.

These studies, however, paid little attention to the DCN, another functionally significant region of the cerebellum (Diedrichsen *et al*, 2011; Dum & Strick, 2003). The DCN consists of a group of nuclei at the centre of the cerebellum associated with relaying information from the cerebellum to the brainstem and thalamus. These nuclei receive inhibitory (GABAergic) inputs from Purkinje neurons in the cerebellar cortex. Most output fibres of the cerebellum originate from these nuclei (Dum & Strick, 2003). The objective of this study was to identify changes in the DCN to an increasing inflammatory environment over the disease trajectory. This was performed in two EAE variants, namely the myelin

oligodendrocyte glycoprotein (MOG)-induced C57Bl/6 strain, which exhibits a CP clinical profile and the proteolipid protein (PLP)-induced SJL/J, which exhibits CR-EAE (Miller & Karpus, 2007). In both variants, the DCN (a) remains free from large scale inflammatory infiltration over the whole disease course, but (b) nevertheless exhibits hallmarks of neuroinflammation at relatively reduced levels, sufficient to expect functional disturbances.

Experimental Procedures

Materials

C57Bl/6 and SJL/J mice were obtained from the Animal Resource Centre (Western Australia). MOG_{35-55} peptide (MEVGWYRSPFSRVVHLYRNGK) and $PLP_{139-151}$ (HSLGKWLGHPDKF) were prepared by ModPep (Melbourne, Vic., Australia) at $\geq$ 96% purity. For the preparation of emulsions, complete Freund's adjuvant (CFA) was obtained from Sigma-Aldrich (Saint Louis, MO, F5881) and *Mycobacterium tuberculosis* from Beckton Dickinson (Franklin Lakes, NJ, 231141). The toxic protein from *Bordetella pertussis* was obtained from Sigma-Aldrich (P7208). For immunohistochemistry (IHC), primary antibodies included monoclonal mouse anti-glial fibrillary acidic protein (GFAP) from Merck Millipore (Billerica, MA, MAB360), polyclonal rabbit anti-myelin basic protein (MBP) from DAKO (Glostrup, Denmark, A0623), mouse monoclonal anti-CD3 (DAKO, A0452), polyclonal rabbit anti-ionised binding adapter molecule 1 (Iba1) from WAKO Chemicals (Richmond, VA, 019-19741); polyclonal goat anti-Iba1 from Novus Biologicals (Centennial, CO, NB100-1028SS); monoclonal rabbit anti-TMEM119 from abcam (Cambridge, UK, ab209064); monoclonal mouse anti-PLP from Merck Millipore (MAB388); and monoclonal mouse anti-hypo-phosphorylated neurofilament (NF) (Covance, Princeton, NJ, SMI32R). Secondary antibodies included Alexa 488, Alexa 546, Alexa 594 and Alexa 647 conjugated to IgG against the appropriate animal host from Invitrogen (Carlsbad, CA). Amplification was achieved using biotinylated horse-anti-

mouse (Vector Laboratories Inc., Burlingame, CA, BA-2000) and biotinylated goat-anti-rabbit (Vector Laboratories Inc., BA-1000) alongside streptavidin-Alexa 488 (Invitrogen, S11223) and streptavidin-Alexa 555 (Invitrogen, S32355). Nuclei were stained using 4', 6 diamidino-2-phenylindole (DAPI) from Sigma-Aldrich (D9564). For cryostat sections, tissue was embedded using optimum cutting temperature (OCT) compound from Sakura Finetek (Torrance, CA, 4583) and coverslips were mounted using fluorescent mounting medium from DAKO (S302380). Alto stainless steel 1 mm coronal matrices were obtained from AgnTho (Lidingö, Sweden, 69-2175-1). The TUNEL kit was obtained from Boehringer Mannheim GmbH (Mannheim, Germany, 11684795910).

Mice and EAE induction

EAE was induced with MOG_{35-55} peptide in C57Bl/6 mice (Pham *et al*, 2009) and with $PLP_{139-151}$ peptide in SJL/J mice (Miller & Karpus, 2007). Female mice only, aged at least 9 weeks old and weighing a minimum of 21 g were used for experimentation. They were housed in the specified pathogen free area of the La Trobe Animal Research and Teaching Facility under standard conditions. All animal experiments were performed in accordance with the National Health and Medical Research Council regulations and approved by the institutional animal ethics committee. EAE was induced by a single subcutaneous injection into each inguinal region, of an emulsion containing 100 µg of neuropeptide in 50 µL of phosphate buffered saline (PBS; 7.68 mM Na_2HPO_4, 2.67 mM NaH_2PO_4, 154 mM NaCl, pH 7.4) emulsified in an equal volume of CFA supplemented with 4 mg/mL of *M. tuberculosis*. Immediately following neuropeptide injections, an intraperitoneal injection of 350 ng of pertussis toxin in 300 µL of PBS was administered. This was repeated two days thereafter (2 days post-injection; DPI). Control animals (vehicle only; VO) received the above, except that neuropeptide was substituted with PBS. Mice were weighed on 0, 2, 7 and 9 DPI, after which weighing was performed daily. Disease progression was

monitored using a clinical scoring (CS) system: 0 – no observable disease, 1 – limp tail, 2 – hind limb weakness, 3 – paralysis of one hind limb, 4 – paralysis of both hind and one forelimb, 5 – moribund (Dang *et al.*, 2015). Where intermediate symptoms were observed the value of 0.5 was added to the score.

Tissue preparations, histology and immunostaining

Mice were taken at a low CS (0.5 - 2.0), or high CS (2.5 - 3.5) alongside normal and VO mice with a minimum of three mice per group. Animals were killed and transcardially perfused first with 10 mL of PBS, followed by 4% w/v paraformaldehyde in PBS. The brain was removed and cut into quarters using a brain matrix. The two cerebellar quarters were then embedded in either paraffin wax for histological staining with haematoxylin and eosin (H&E) or IHC, or OCT for cryostat sectioning and IHC. Sections were cut at 7 μm thick in the sagittal plane and H&E staining was performed on 1 out of every 10 slides and used as a reference for further IHC staining. For IHC, antigen unmasking was performed using citrate solution (113.93 mM $Na_3C_6H_5O_7$, pH 6) prior to blocking for 1 hour (with PBS containing 3% horse serum and 0.3% Triton X-100). Incubation with primary antibody was performed overnight at 4 °C, followed by incubations with secondary antibodies for 1 hour at room temperature. Where required, amplification was achieved using the appropriate biotinylated antibody and fluorescent streptavidin conjugate. Finally, 0.001% 4′,6-diamidino-2′-phenylindole, dihydrochloride (DAPI) in PBS was applied to sections for 5 min prior to mounting with fluorescent mounting medium (Dako, S3023). TUNEL staining was performed as per the manufacturer's instructions, in combination with anti-CD3 or anti-NF protein. Images were captured using the AxioObserver Z1 epifluorescent microscope (Zeiss, Oberkochen, Germany) or the Nikon Ti Eclipse inverted microscope (Nikon, Minato, Japan) and annotated using the programs Zen Blue (Zeiss), NIS Elements (Nikon) and ImageJ (NIH). In all immunostaining experiments n = three per group with

triplicate sections. Negative controls included absence of primary antibody or biotinylated antibody and normal and VO mice were included in each round. For TUNEL staining, positive controls included mouse breast tumour tissue and DNAse I treated normal mouse cerebellum.

Mouse Atlas Construction and mapping of lesion topography

Images of H&E-stained slides were taken at 6 x magnification using a Nikon Ti Eclipse inverted microscope (Nikon Corporation, Chiyoda, Tokyo, Japan) and stitched together using NIS Elements (Nikon) to give a high-resolution single image of each stained section. WM lesions were mapped using GIMP (GNU image manipulation program, https://www.gimp.org) onto traces of the mouse cerebellum taken from The Mouse Brain in Stereotaxic Coordinates (Franklin & Paxinos, 2008) using Adobe Illustrator and compiled using the free rendering program Blender (https://www.blender.org), to produce a three-dimensional image in the sagittal plane of the cerebellum (Fig. 3-1).

Neuron counting

Cerebellar tissue was taken from normal, VO and high CS (2.5+) EAE induced mice and embedded in paraffin. Seven cresyl violet stained sections of the fastigial and interposed nuclei (Supp. 3-1) were selected from the region between 0.60 mm to 1.32 mm lateral from the midline and imaged using an Olympus microscope (CH-2, Olympus, Japan) with a USB camera (MD500L, AmScope, Irvine CA, USA) at 10 x magnification. Neurons were manually counted by a partially blinded researcher that was not involved with the experimentation, handling of tissues or collection of data.
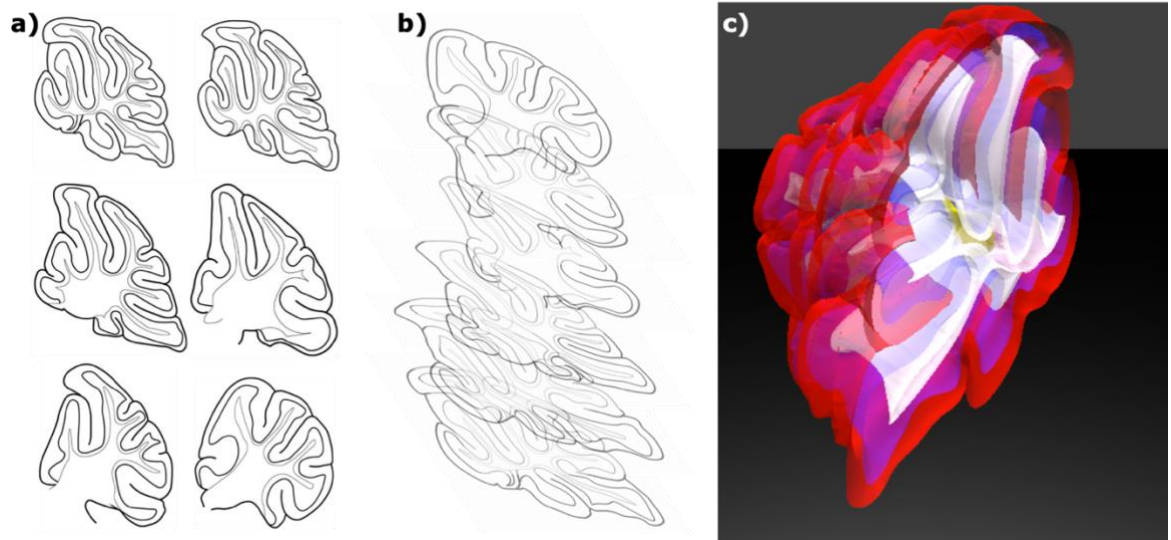
Fig. 3-1 Creating the three-dimensional map of the mouse cerebellum. Cerebellar traces were made from sagittal sections of the Mouse Brain Atlas (Franklin & Paxinos, 2008) (a). Inflammatory lesions across all experimental mice used were recorded on these traces before being aligned and connected using the program Blender (b and c) to create a three-dimensional map of cerebellar lesion topography in the mouse.

Results

Similar lesion topography is observed in the cerebellum of C57Bl/6 and SJL/J EAE variants.

It is well established that disease development along the neuraxis is asynchronous in EAE. In the commonly used variants, the earliest symptom is optic neuritis, first evident from 10 - 12 DPI (corresponding approximately to CS 0 to 0.5). This is followed by ambulatory difficulties, characteristic of SC inflammation, from 12 - 14 DPI (approximately CS 1.0 to 2.0) (Kuerten *et al*, 2008). Subsequently, the disease takes a CR course in $PLP_{139-151}$ induced SJL/J mice (Miller & Karpus, 2007), but can exhibit CP, CR, or monophasic clinical profiles in C57Bl/6 mice within a single cohort of induced animals (Berard *et al*, 2010). Cerebellar inflammation has been documented in both variants, but the spatiotemporal pattern of disease evolution in the DCN has been mostly ignored. This was achieved in this study by sampling EAE-induced mice at two disease stages, namely CS $\geq$ 0.5 $\leq$ 2.0 (low CS) and $\geq$ 2.5 $\leq$ 3.5 (high CS), with VO mice (taken at times corresponding to low and high CS in experimental mice) as controls.

MOG_{35-55} induced cerebellar inflammation in C57Bl/6 mice.

Locations of reproducible lesion topography are shown in Fig. 3-2a, b, c. Severe cerebellar inflammation was already detectable at low CS, manifested by highly inflamed blood vessels and medium to large perivascular lesions (Fig. 3-2d, e, f, g). These lesions were almost exclusively located in WM, with rare evidence of GM disease activity. We identified two defined regions where lesions were reproducibly located in all mice examined. The first was the ventrocaudal region, in the 8th and 9th folds (Fig. 3-2d). The salient feature of this region is the absence (or extreme thinness) of the cortical layers (ML and GL), resulting in apparently direct contact between meninges and WM. From there, lesions appeared to spread throughout the ventral WM circumventing, but not penetrating the DCN (Fig. 3-2e). These lesions appeared to be limited to the caudal region of the ventral cerebellum, with

more rostrally located regions, for example the 3rd fold, exhibiting inflammation less frequently (Fig. 3-2f). The other regions reproducibly involved were the WM areas within the 4th/5th folds (Fig. 3-2g). Lesions in this region appeared to originate from meningeal blood vessels entering the cerebellum from the dorsal aspect. Of interest was the observation that while traversing the ML, blood vessels were associated with minimal inflammation, but upon reaching the GL the same blood vessels were associated with severe inflammation (Fig. 3-3a, b).

Mice at high CS exhibited lesions in the same regions as at low CS. More diffuse inflammation was observed, but this inflammation appeared less florid (Fig. 3-2h, i, j, k) particularly in the ventrocaudal region between the 8th and 9th folds (compare Fig. 3-2d versus Fig. 3-2h) and the WM surrounding the DCN (compare Fig. 3-2e versus Fig. 3-2i). The overall lesion load at high CS also appeared less severe than at low CS, suggesting that the peak of cerebellar inflammation precedes that of the SC.

Fig. 3-2 H&E-stained sections showing regions of reproducible cerebellar WM lesion formation. Prominent WM lesions are found in regions (a) 0.6 mm, (b) 1.08 mm and (c) 1.44 mm laterally from the midline in the sagittal plane. Both C57Bl/6 (d-k) and SJL/J (l-s) mice show reproducible lesion topography (arrowheads) in a number of WM regions: (d, h, l, p) between folds 8 and 9 where the meningeal layers rest against the WM. (e, i, m, q); In WM surrounding the DCN, inflammation is severe while the DCN is spared. (f, n, j, r); More rostrally, inflammation is seen where the 2nd, 3rd or 4/5th fold meet the base of the cerebellum. WM within the numerous folds presented moderate to severe inflammation, with (g, k, o, s) fold 4/5 frequently seen to be inflamed.
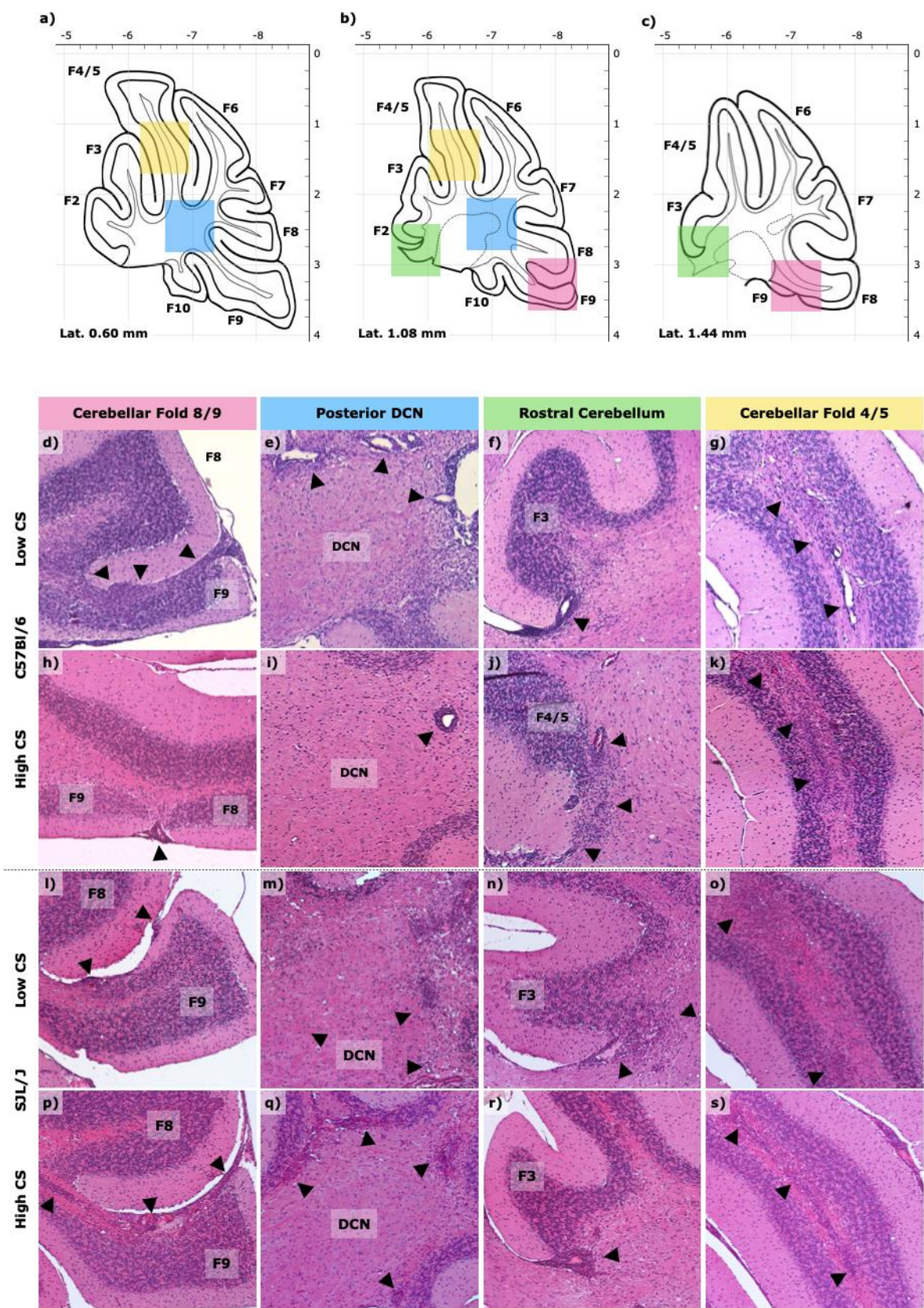
PLP$_{139-151}$ induced cerebellar inflammation in SJL/J mice.

Using a similar approach, lesion development was mapped in the PLP$_{139-151}$ induced SJL/J variant. Sampling was again performed at low ($\geq 0.5 \leq 2.0$) and high ($\geq 2.5 \leq 3.5$) CS (n = 3). In one out of three low CS animals very severe lesions were present (Fig. 3-2l, m, n, o) while minimal disease activity was detectable in the other two. At high CS lesions of moderate to high severity were identified in two out of three mice (Fig. 3-2p, q, r, s), but none in the remaining animal. This suggests an unpredictable timing of lesion development in the cerebellum relative to SC, in the SJL/J EAE variant. On the other hand, similarly to the C57Bl/6 variant, inflammatory infiltration appeared to originate from between the 8th and 9th folds and progress in a caudorostral direction throughout the WM, circumventing the DCN (Fig. 3-2l, m, p, q). Lesions were also reproducibly observed in the rostral aspect of the cerebellum at the base of the 3rd fold (Fig. 3-2n, r). Other regions where lesions were identified included the 4th/5th folds, appearing to originate from the dorsal aspect of the cerebellum (Fig. 3-2o, s). In sharp contrast with C57Bl/6 mice, however, GM lesions were found in the cortical folds of SJL/J mice within both the ML and GL (Fig. 3-3c, d).

3-D reconstruction of lesion topography in the MOG$_{35-55}$-C57Bl/6 and PLP$_{139-151}$-SJL/J induced EAE variants.

3-D reconstruction (Fig. 3-4) was used to demonstrate the relationship between WM inflammation and the DCN. Data showed that over the complete disease course in the C57Bl/6 mice lesions were almost exclusively identified in WM in every mouse examined (Fig. 3-4e, f). In the SJL/J strain some mice did not exhibit cerebellar inflammation despite the observation of a CS and lesions were found in both WM and GM (Fig. 3-4g, h). On the other hand, lesion topography was remarkably similar in the two mouse strains, but the DCN was always spared in every mouse examined.
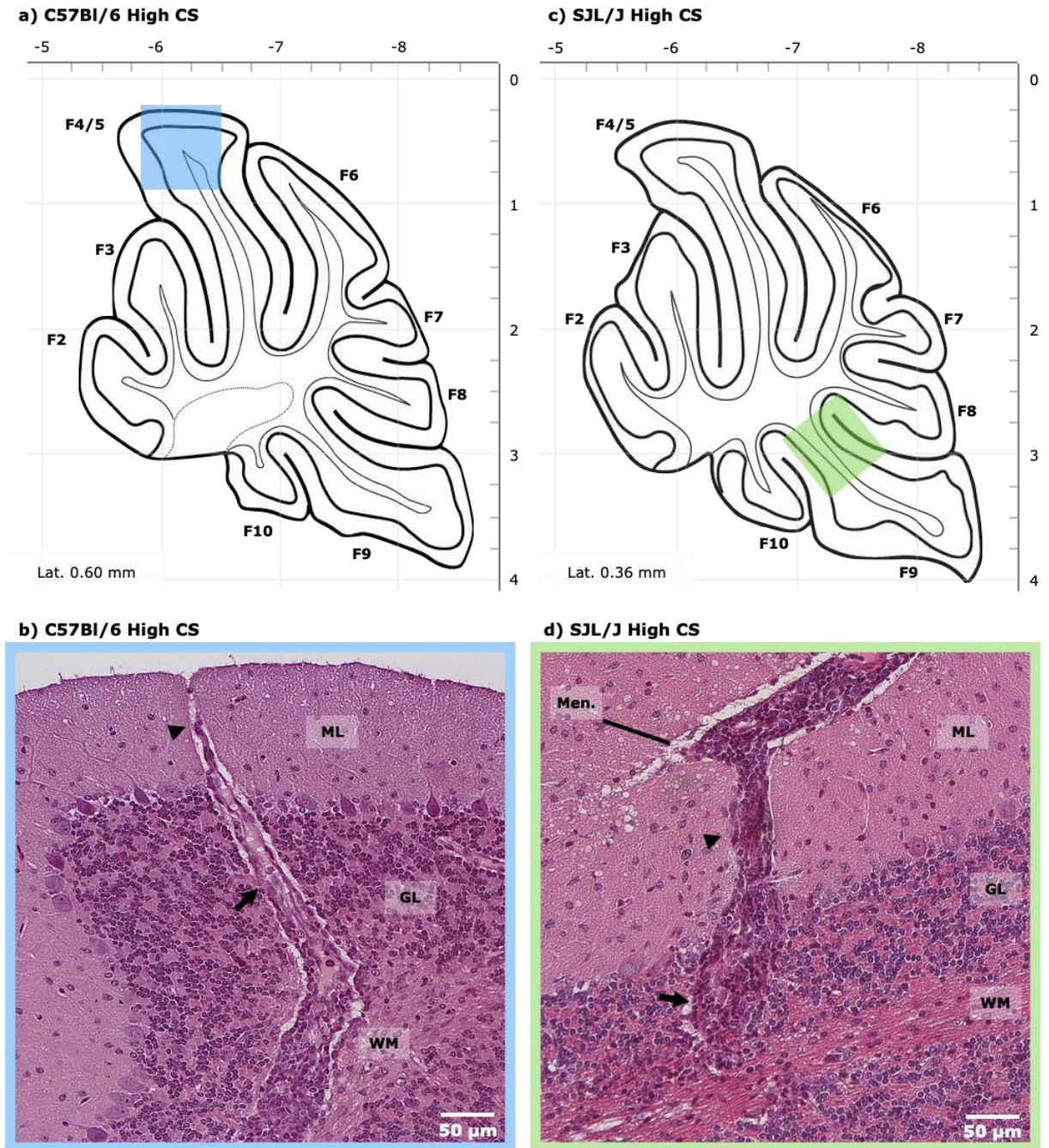
Fig. 3-3 Cortical lesions are more severe in SJL/J mice. (a, b) In the C57Bl/6 mouse strain, inflammation of blood vessels is mild in the ML (arrow heads) and GL (arrows) relative to (c, d) SJL/J. ML - molecular layer, GL - granular layer, WM - white matter, Men. - meninges.

Bregma Coordinates

Cerebellum

a) **Cortical Surface**   b) **Granular Layer**   c) **White Matter**   d) **Deep Cerebellar Nuclei**

Lat 0.48 mm
Breg -6.75 mm

Lat 1.56 mm
Breg -7.0 mm

e) **C57Bl/6 Low CS**   f) **C57Bl/6 High CS**   g) **SJL/J Low CS**   h) **SJL/J High CS**
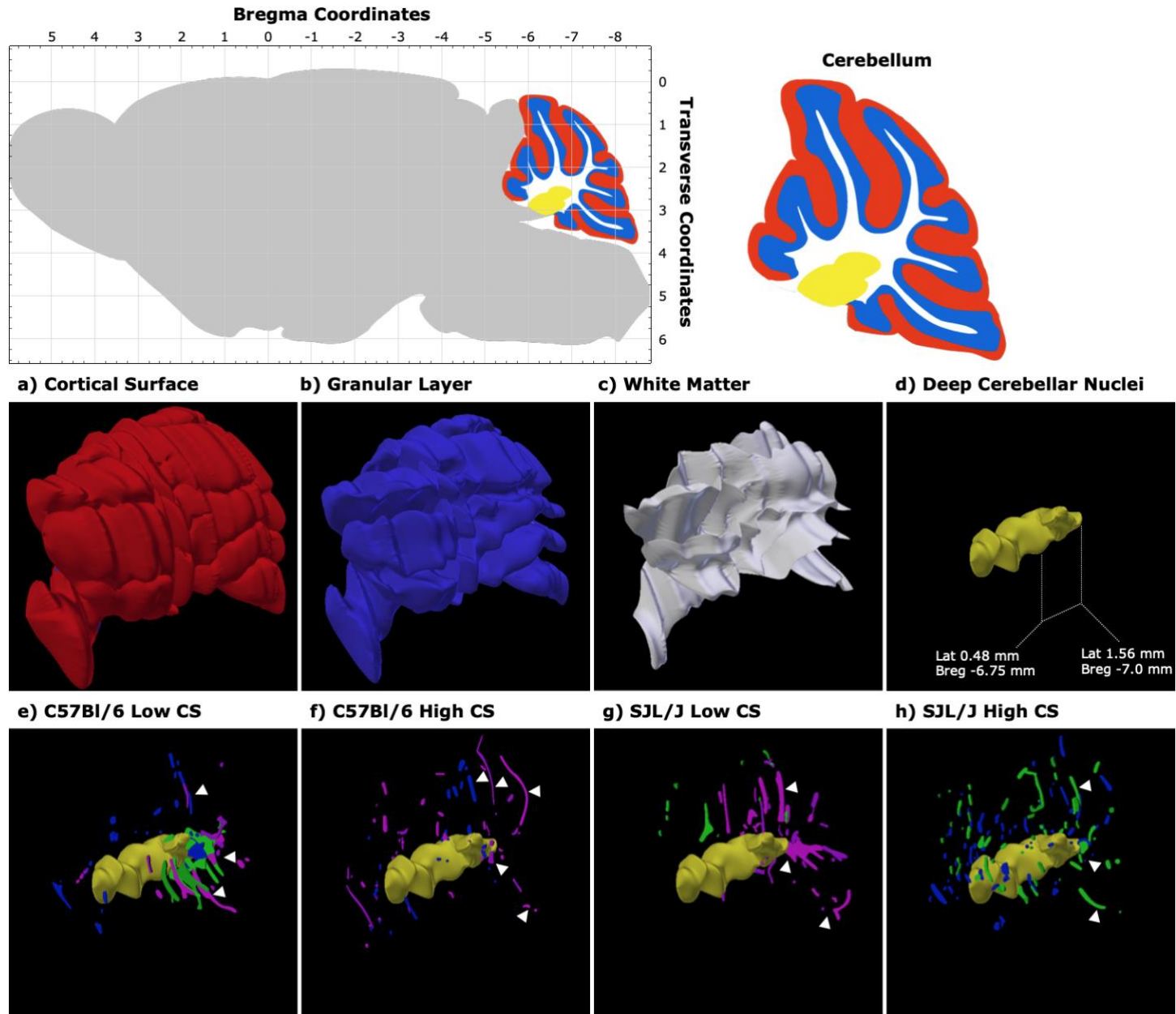
Fig. 3-4 The three-dimensional model used to map out lesion locations can be split into (a) the cortical surface, (b) the GL, (c) the WM and (d) the DCN. Lesions have been recorded for each mouse strain with a separate colour used for each mouse (i.e. blue, green and magenta). C57Bl/6 mice showed higher overall lesion load at (e) low relative to (f) high CS, most notably in a region posterior to the DCN, within the WM of fold 4/5 and between folds 8/9 (arrowheads). Severe inflammation was observed in (g) 1 out of 3 SJL/J low CS mice, with little to no inflammation seen in the other two mice. Similar to (f) C57Bl/6 high CS, (h), 2 out of 3 SJL/J high CS mice had a severe lesion load.

Evidence of hallmarks of neuroinflammation in the DCN, despite lack of overt inflammation.

The highly inflammatory environment surrounding the DCN suggests that despite no evidence of inflammatory infiltration, this region is likely to experience severe disturbances. Examination of hallmarks of neuroinflammation was performed by immunochemical identification of T lymphocyte infiltration, microglial reactivity, axonal integrity, stress markers and demyelination. T lymphocyte infiltration was detectable at low levels within the DCN of almost all mice examined, irrespective of CS in both EAE variants (Fig. 3-5). This was manifested by the presence of single CD3+ T cells dispersed throughout the GM, but often in close association with neuronal cell bodies (Fig. 3-5a, b, d, e). However, in mice where severe inflammation surrounded the DCN, small collections (2-10) of CD3+ T cells were found at the WM to GM demarcation, suggesting that they originated from WM inflammation (Fig. 3-5c, f). Large-scale CD3+ T cell infiltration, however, was never detectable in the DCN of either EAE variant, either at low or high CS.

a) C57BL/6: Low CS - DCN

d) SJL/J: Low CS - DCN

b)

b) inset

c)

e)

e) inset

f)

DAPI   Neurofilament   CD3
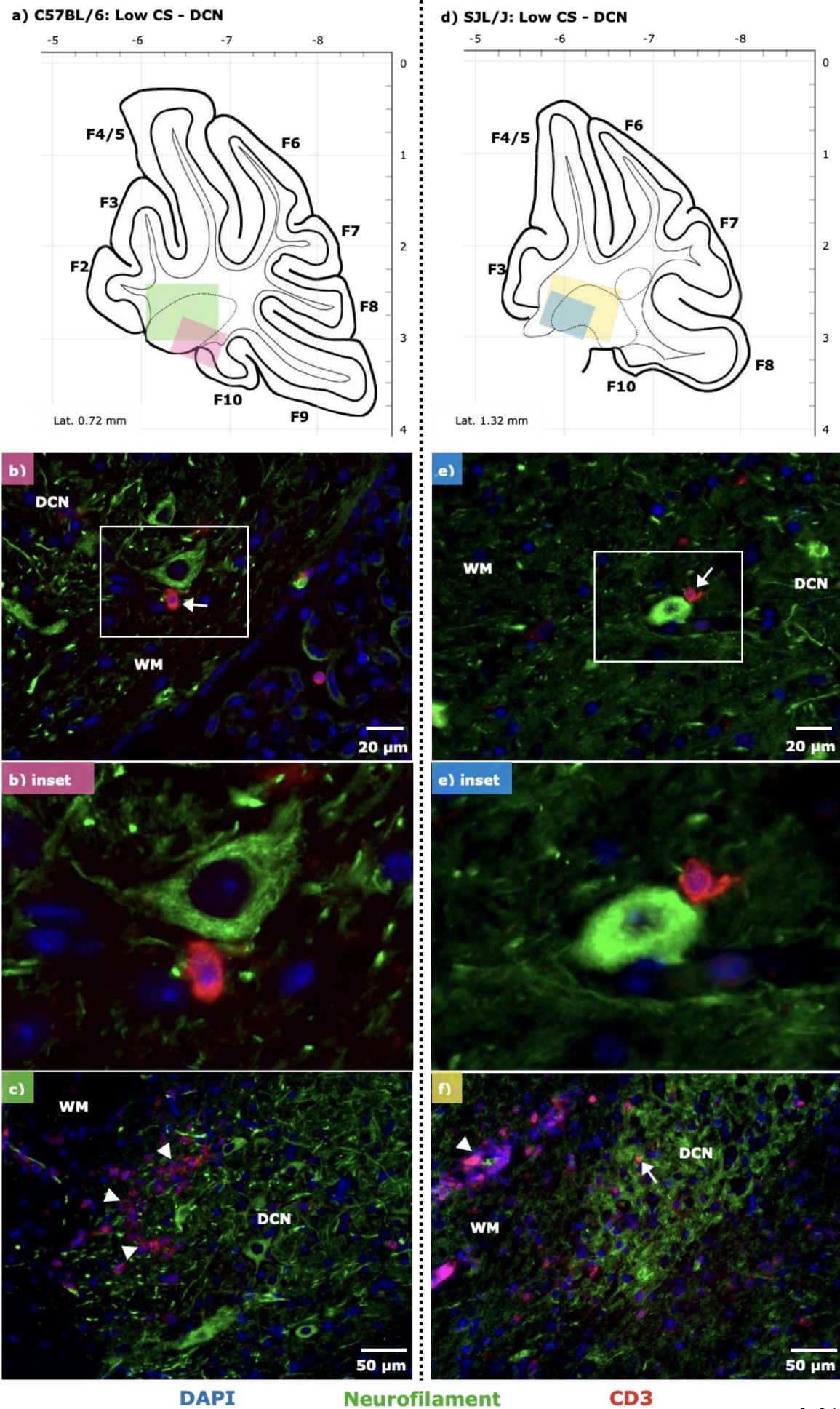
Fig. 3-5 CD3+ T cell infiltration into the DCN. (a, b, d, e). Individual CD3+ cells (arrows) are seen in the DCN adjacent to NF+ neurons in both strains. (c, f) In both mouse strains severe inflammation (arrowheads) consisting of CD3+ T cells were seen in WM surrounding, but not extending into the nearby DCN. WM - white matter, DCN - deep cerebellar nuclei.

Surprisingly, Iba1+ macrophage-like reactivity was very pronounced in the DCN of EAE-induced mice (suggestive of a highly inflammatory environment) relative to controls (Fig. 3-6a, d). This was true of both EAE variants, where levels of microglial reactivity appeared equivalent in the DCN and in the surrounding WM at low (Fig. 3-6b, e) and high CS (Fig. 3-6c, f). These levels of microglial reactivity, as well as of CD3+ T cells were comparable to those detectable in cortical regions (Supp. 3-2). Whether these reactive, Iba1+ macrophage like cells are derived from CNS resident microglia or peripheral monocytes is unclear. To further investigate this, double staining was performed using Iba1 combined with TMEM119, a relatively recently discovered marker of CNS tissue resident microglia that is absent on peripheral monocyte derived macrophages (Bennett *et al.*, 2016; Satoh *et al*, 2016). In C57Bl/6 normal, VO and EAE with low cerebellar inflammation groups, Iba1+ cells (Fig. 3-7a, c) are positive for TMEM119 (Fig. 3-7b, d). However, as Iba1+ amoeboid-like cells become more prolific in EAE with high cerebellar inflammation (Fig. 3-7e, g), TMEM119 is no longer seen on Iba1+ macrophages (Satoh *et al.*, 2016). Recent studies have suggested that TMEM119 may be a marker of homeostasis that is down regulated in proinflammatory environments similar to that observed in the C57Bl/6 EAE variant (Fig. 3-7f, h). As such, while the vast majority of macrophages-like cells are identifiable as microglia-derived in stages of lower cerebellar inflammation, the loss of TMEM119 expression in more florid lesions limits any conclusions as to the proportion of locally and peripherally derived macrophages at this time.

Demyelination in the DCN also proved difficult to assess in both the C57Bl/6 and SJL/J variants at low and high CS (Supp. 3-3), because this region is unevenly myelinated in normal animals. Therefore, no qualitative difference in myelin levels between these and experimental animals could be identified in the DCN. Inflammatory demyelination has been found to impair axonal integrity in areas beyond the immediate lesion boundary. NF staining was used to assess axonal health in the DCN and surrounding regions near to WM lesions aside the DCN. However, axons in the DCN are frequently positive for NF in normal mice (Supp. 3-4a, b, c), with no obvious increase in C57Bl/6 EAE variant mice with low (Supp. 3-4d, e, f) or high cerebellar inflammation (Supp. 3-4g, h, i), suggesting that this marker is not useful in this context.

Fig. 3-6 Images at 5 x magnification in both C57Bl/6 and SJL/J mouse strains show Iba1+ staining cells in the DCN and adjacent WM, which is upregulated in (b, e) low CS and (c, f) high CS mice relative to (a, d) controls. Images at 40 x magnification (inset) show reactive morphology of Iba1+ cells in the DCN in both strains at both (b, e) low and (e, f) high CS. Note paucity of GFAP+ staining in the DCN relative to surrounding WM.

DAPI   Iba1   TMEM119
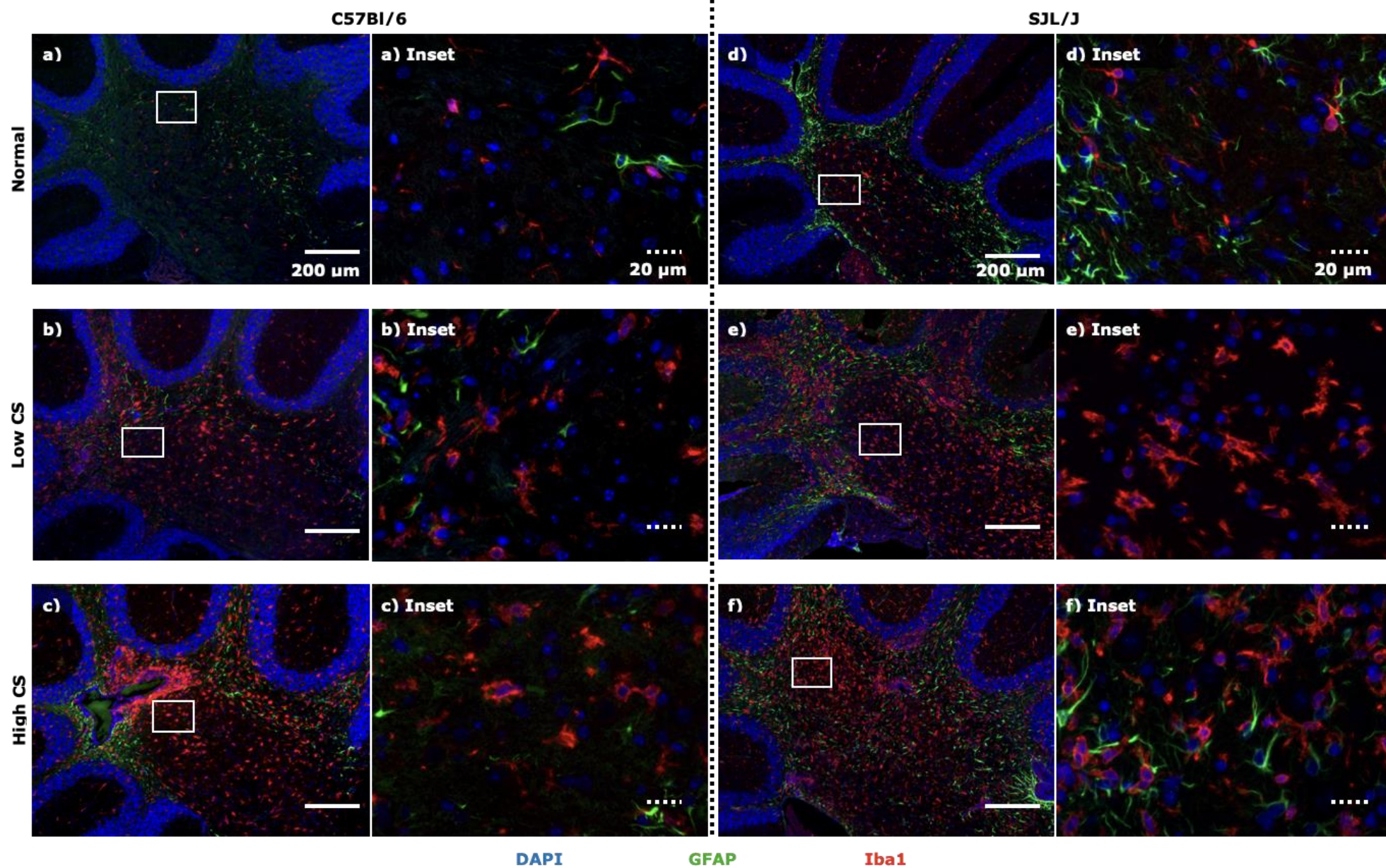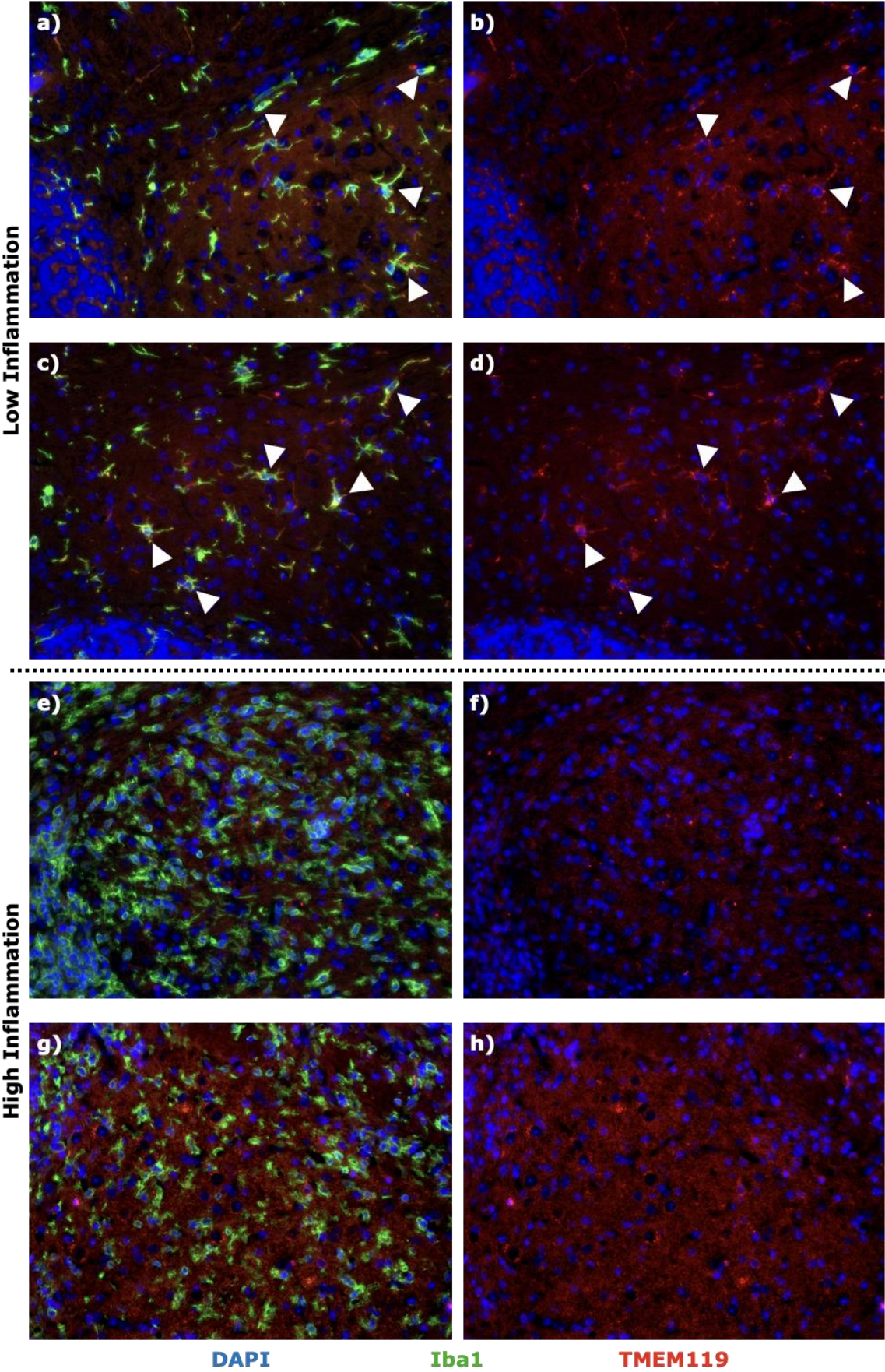
Fig. 3-7 Iba1+ (green; a, c) staining cells that also stain faintly for TMEM119 (red; b, d, arrowheads) are observed in the DCN and surrounding WM of C57Bl/6 mice showing low cerebellar inflammation. In mice showing more severe cerebellar inflammation Iba1+ cells (e, g) become more numerous and macrophage like, though TMEM119 is mostly absent (g, h).

To further explore the effect of the presence of CD3+ cells and the basis of microglial reactivity, a TUNEL assay was performed combined with immunostaining with anti-NF protein, and in conjunction with anti-CD 3. TUNEL+ cells were detectable within the DCN (Fig. 3-8a, c) and adjacent WM (Fig. 3-8b, d) of both mouse strains (C57Bl/6 at low CS, SJL/J at high CS) while they were undetectable in control animals. TUNEL+ cells were more frequently seen in WM than in the DCN and (Fig. 3-8d-h) occasionally colocalised with CD3+ cells, though the identity of TUNEL+ CD3- cells is unknown. Finally, αB-crystallin, a commonly used marker of neuronal stress (Ousman *et al*, 2007) was investigated to gain further insight into the effect of the changing environment on neuronal health. No clear difference was seen with apparently similar numbers of αB-crystallin+ cells frequently observed in normal (Supp. 3-5a, b, c), low CS (Supp. 3-5d, e, f) and high CS (Supp. 3-5g, h, i) EAE groups.
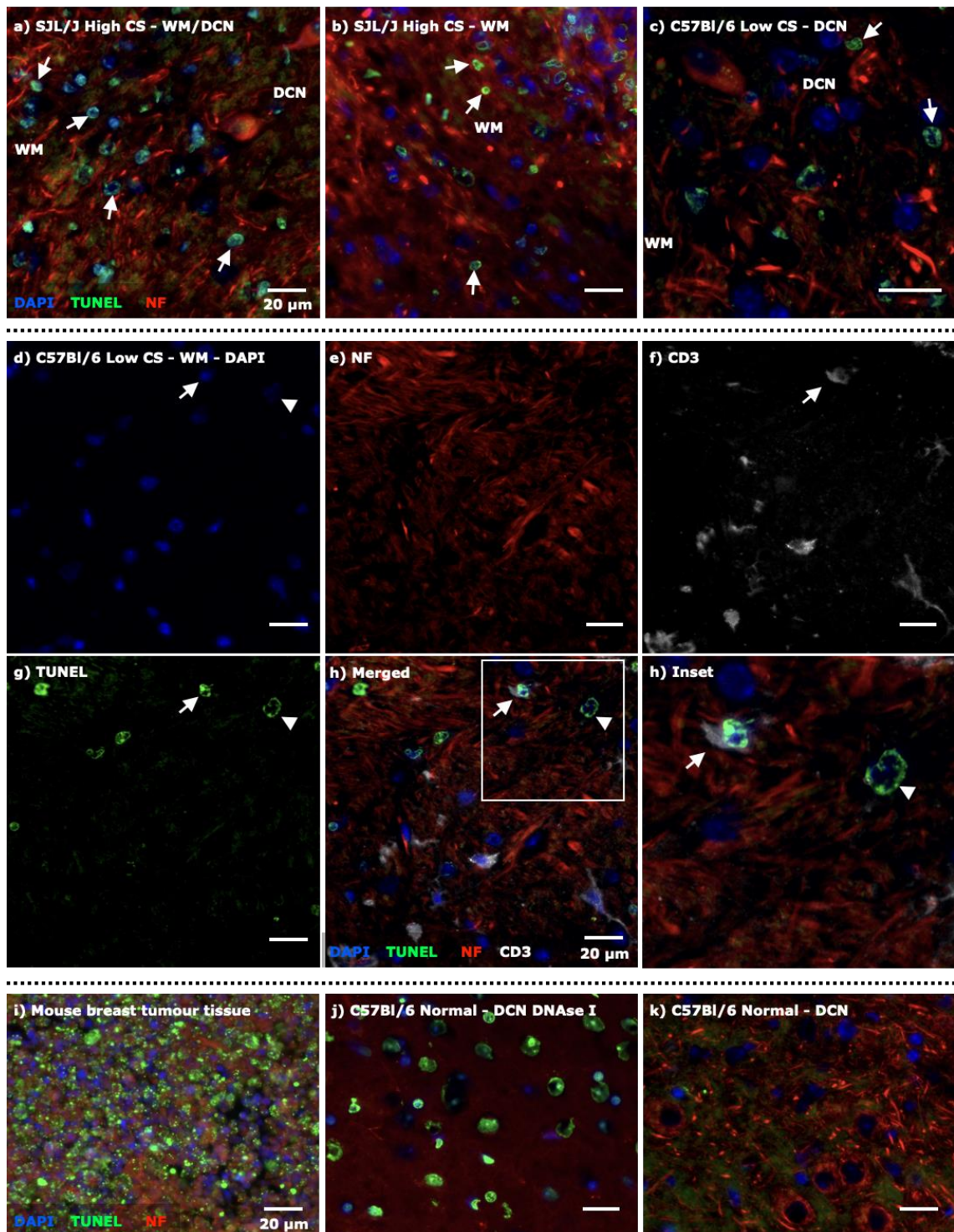
Fig. 3-8 TUNEL+ cells were seen in both mouse strains (a, c) in the DCN and (b, d) the adjacent WM. (d-h) TUNEL+ cells (arrowheads) rarely coincided with CD3+ cell (arrows). (d) DAPI, (e) NF, (f) CD3, (g) TUNEL, (h) merged and inset. Control tissues included (i) tumour tissue, (j) normal mouse cerebellar tissue treated with DNAse I and (k) normal mouse cerebellar tissue. DCN - deep cerebellar nuclei, WM - white matter, TUNEL - terminal deoxynucleotidyl transferase dUTP nick-end labelling, NF - hypo-phosphorylated neurofilament.

In view of the difficulties of identifying hallmarks of neuroinflammation using standard markers, neuronal populations of the DCN regions closest to inflammatory WM lesions were investigated with experimental groups consisting of VO (n = 6) and high CS EAE C57Bl/6 mice (CS 2.5+; n = 12). After sectioning and imaging, the high CS EAE cohort was then separated into two groups, the first consisting of high CS EAE mice exhibiting no/low cerebellar inflammation (n = 6) and a second high CS EAE group showing extensive cerebellar inflammation (n = 6). Sections of the DCN near to where inflammation was observed (fastigial, and interposed nuclei located between approximately 0.60 mm and 1.32 mm laterally from the midline in the sagittal plane) were stained with cresyl violet and an estimate of the neuronal population made by a blinded researcher from seven sections taken at regular intervals in this region (Supp. 3-1). In all, the total number of neurons in these regions was found to be significantly less in both low and high cerebellar inflammation EAE (CS 2.5+) groups than VO controls (both $p < 0.001$, Fig. 3-9a). When separated into counts per section, the largest contributor to this difference was observed in sections containing the interposed nuclei located approximately between 0.84 mm to 1.32 mm for both high CS EAE with no/low cerebellar inflammation (0.84 mm $p = 0.04$, 0.96 mm $p = 0.001$, 1.08 mm $p < 0.001$, 1.20 mm $p < 0.001$, 1.32 mm $p = 0.002$, Fig. 3-9b) and high CS EAE with extensive cerebellar inflammation (0.84 to 1.32 mm $p < 0.001$, Fig. 3-9b).

a) Total neurons counted in medial DCN

b) Neurons per Section
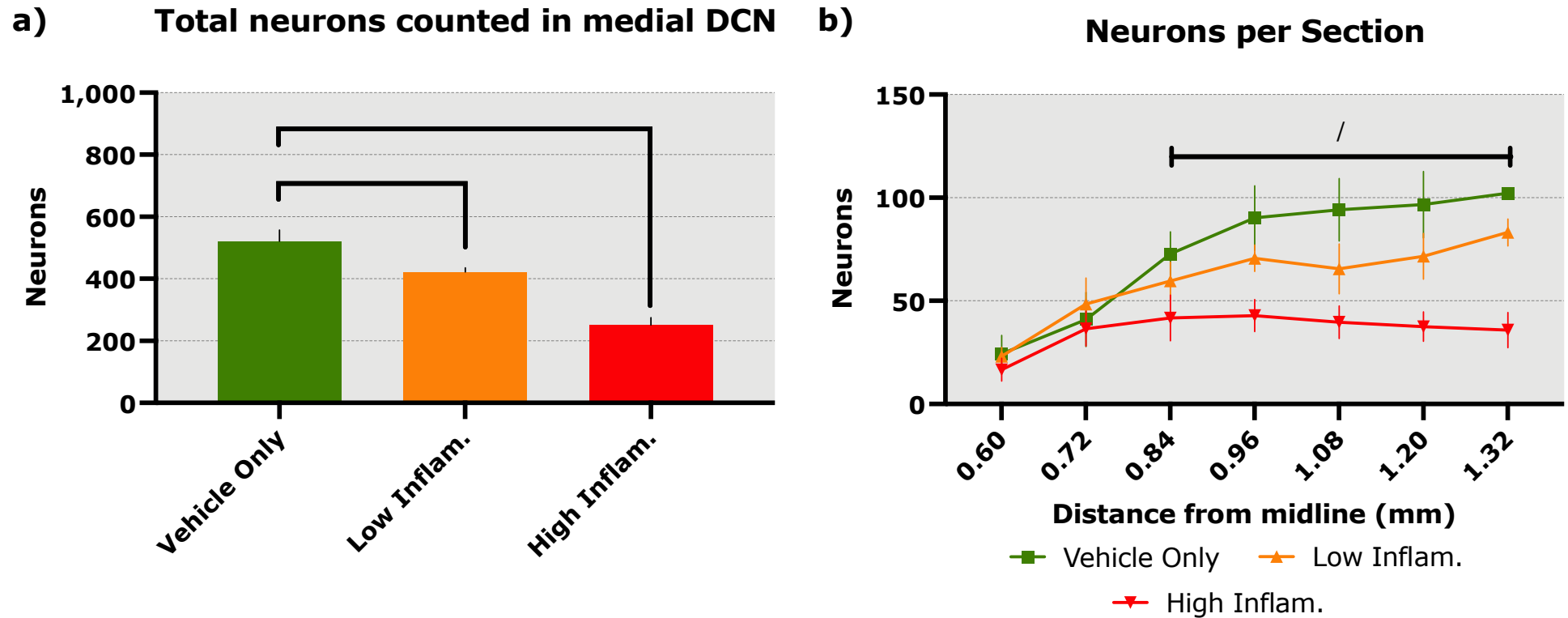
Fig. 3-9 (a) Fewer cresyl violet stained cells were counted in both high CS (2.5+) EAE groups with (orange) low cerebellar inflammation (p < 0.001) and (red) high cerebellar inflammation (p < 0.001). (b) Regions of the fastigial and interposed DCN were surveyed with sections selected at approximated 0.12 mm intervals beginning at 0.60 mm and ending at 1.32 mm from the midline in the sagittal plane. A significant reduction in cresyl violet stained cells was seen in the regions closest to large reproducible WM inflammation corresponding to a region between 0.84 mm to 1.32 mm. Low cerebellar inflammation (orange); 0.84 mm p = 0.04, 0.96 mm p = 0.001, 1.08 mm p < 0.001, 1.20 mm p < 0.001, 1.32 mm p = 0.002. High cerebellar inflammation; 0.84 to 1.32 p < 0.001). Statistical tests: (a) One-way ANOVA using Dunnet multiple comparison test; (b) Two-way ANOVA using Dunnet multiple comparison test. n = 6, error bars represent 95% CI.

Discussion

Since work by Kutzelnigg *et al.* (2007) identified cerebellar cortical demyelination as an early and significant pathological feature in MS, investigators have sought to validate the EAE model to obtain proof-of-concept for MS pathology of this region. The focus has been on the use of imaging approaches in murine variants, (MacKenzie-Graham *et al.*, 2012), which have uncovered volume loss in early and late stage disease, preferentially in the molecular and Purkinje cell layers and predilection of WM for lesion development. These findings bear remarkable similarities with hallmarks of MS cerebellar pathology (Geurts *et al.*, 2007). The above investigations, however, have neglected the DCN which is a functionally significant region of the cerebellum. Almost all cerebellar cortical projections travel to the DCN (mostly originating from inhibitory Purkinje cells) and the DCN is the primary source of signals leaving the cerebellum (White & Sillitoe, 2013); hence our investigations of these regions in two commonly used murine EAE variants. The variants selected (C57Bl/6 or SJL/J EAE) exhibit different clinical profiles (CP or CR) which was used to test the generality of the findings.

Spatiotemporal mapping of cerebellar disease revealed both differences and similarities between variants. A major difference consisted in the occurrence of GM lesions in SJL/J mice, not seen in C57Bl/6 mice. These were located particularly in the ML and GL of SJL/J mice where florid lesions were more commonly observed. An additional difference was the timing of the peak of cerebellar inflammation relative to SC disease (evaluated in terms of CS). Data showed that in C57Bl/6 mice, the peak of cerebellar inflammation preceded that of the SC, because the most intense inflammation was detected in low CS mice, while inflammation at high CS appeared less intense. However, the above did not appear to be the case for SJL/J mice where (a) cerebellar lesions were not detected in all mice and (b) there was no relationship between severity of inflammation and disease duration in the

cerebellum. This may be related to the fact that the disease exhibits a CR course in the SJL/J mice (Miller & Karpus, 2007) and, therefore, if disease develops independently in different CNS regions as suggested by this study, there will always be a disconnect between SC and cerebellar inflammation. Overall, however, in both variants, the different timing of SC and cerebellar disease is consistent with data from genetically modified EAE models.

On the other hand, despite differences in neuroantigen/mouse strain combination, there were striking similarities between the two variants in terms of progression of inflammatory infiltration and reproducibility of lesion topography. In both variants, in all mice that exhibited cerebellar inflammation lesions were observed in the caudal regions (8th and 9th folds) as well as in the dorsal aspect (4th/5th folds). Taken together, these observations raise the interesting possibility that these regions are associated with higher sensitivity to inflammatory infiltration though the nature of this shared predisposition is currently unclear. The most interesting common observation was that of apparent resistance of inflammatory infiltration in the DCN, whereby in both variants aggressive progression of inflammation circumvented, but did not deeply penetrate the DCN. Thus, even where CD3+ cells appeared to originate from WM inflammation, infiltration into the DCN was mild. No clear pattern to CD3+ cell invasion was apparent, however CD3+ cells were frequently seen directly opposed to large neurons within the structure, though whether this is coincidental due to the densely packed somal bodies in the DCN is unclear.

This absence of large-scale infiltration was in contrast with the high level of microglial reactivity, characterized by increased detectability, highly enlarged cell bodies and complex branching, which in both variants appeared equally severe in the DCN and surrounding WM. Iba1+ microglia or monocyte derived macrophage reactivity was, however, consistent with the presence of single CD3+ cells frequently found in close proximity to neuronal cell

bodies and TUNEL+ cells, which were undetectable in controls. TUNEL+ cells were not frequently coincident with CD3+ cells, thereby suggesting that dying cells were the neuronal and/or glia cells of the DCN and nearby WM. Determination of the functional damage to the DCN is outside the scope of this investigation, but evidence of hallmarks of neuroinflammation above control levels are suggestive of severe consequences on the refinement of cortical cerebellar inputs and their relay. Indeed, this appears to manifest as neuronal loss, more pronounced in regions proximal to the sites of highest WM inflammation.

While findings were broadly consistent between the variants, several issues bode further investigation. While most macrophage-like cells appear to be derived from CNS resident microglia as suggested by the presence of TMEM119, this marker was not seen in highly the highly inflamed cerebellum. The purinergic receptor, P2RY12 is frequently used to distinguish microglia derived macrophages from those of peripheral origin are also expressed in homeostatic conditions but is also down regulated during inflammatory episodes (Mildner *et al*, 2017; Zrzavy *et al*, 2017), whereas the relative expression of CD45 (high or low) combined with fluorescence activated cell sorting requires tissue homogenisation and the loss of regional context. This greatly limits the value of these techniques for this region to determine relative contributions to the population of macrophage-like cells. Secondly, while markers such as NF and αB-crystallin have been useful as a marker of pathology or stress in the EAE SC, high expression in controls make their value rather limited in the DCN. Future studies should consider the use of markers specific to macrophage-like cell based pathology such as markers of synaptic stripping (synapsin I, synaptophysin and PSD-95), presence of reactive oxygen/nitrogen species (iNOS, p22-phox and E06), or neuronal stress/damage (APP) that may be mediated by this cell type and has been observed in MS DGM tissue (Haider *et al*, 2014; Zhu *et al*, 2003;

Ziehn *et al*, 2010). Lastly, cresyl violet was chosen for its capability to stain the broadest swath of neurons in this diverse structure, with results suggesting that nearby WM inflammation is associated with a reduced neuronal population. However cresyl violet is not a neuron-specific marker and it cannot be ruled out that non-neuronal cells may have been unintentionally included in neuronal counts. As such, determining whether a specific sub-population of neurons is lost will require the use of a multiplex IHC staining protocol or similar technique to separate the approximately six different neuronal populations present in the DCN (Uusisaari & Knöpfel, 2013). Recent studies using MS tissue have found that specific sub-populations of neurons may be at greater risk from inflammatory demyelination (Zoupi *et al*, 2021) further supporting the individual counting of neuron populations.

Conclusions

This study focused on the DCN but highlights the remarkable resistance of defined cerebellar GM regions not only to major inflammatory infiltration, but also to migration of inflammatory cells from adjacent WM, despite the absence of physical barriers between compartments. Given the reproducibility of lesion topography demonstrated here, the basis of the restricted ability of inflammatory cells to progress from WM to DCN should be further explored in longitudinal studies, as it would provide valuable insight into the development of differential microenvironments in different CNS regions. Furthermore, future electron microscopy will likely give some insight as to the impact inflammatory processes have on nearby GM that appears relatively normal under standard histological techniques as well as the nature of the apparent CD3+/neuron interaction. Since the cerebellum is a highly clinically relevant CNS region to MS, this study further supports the use of the EAE model for the evaluation of GM-specific therapeutic approaches.

Supplementary Figures

| Vehicle Only | EAE ~ Low Inflam. | EAE ~ High Inflam. |
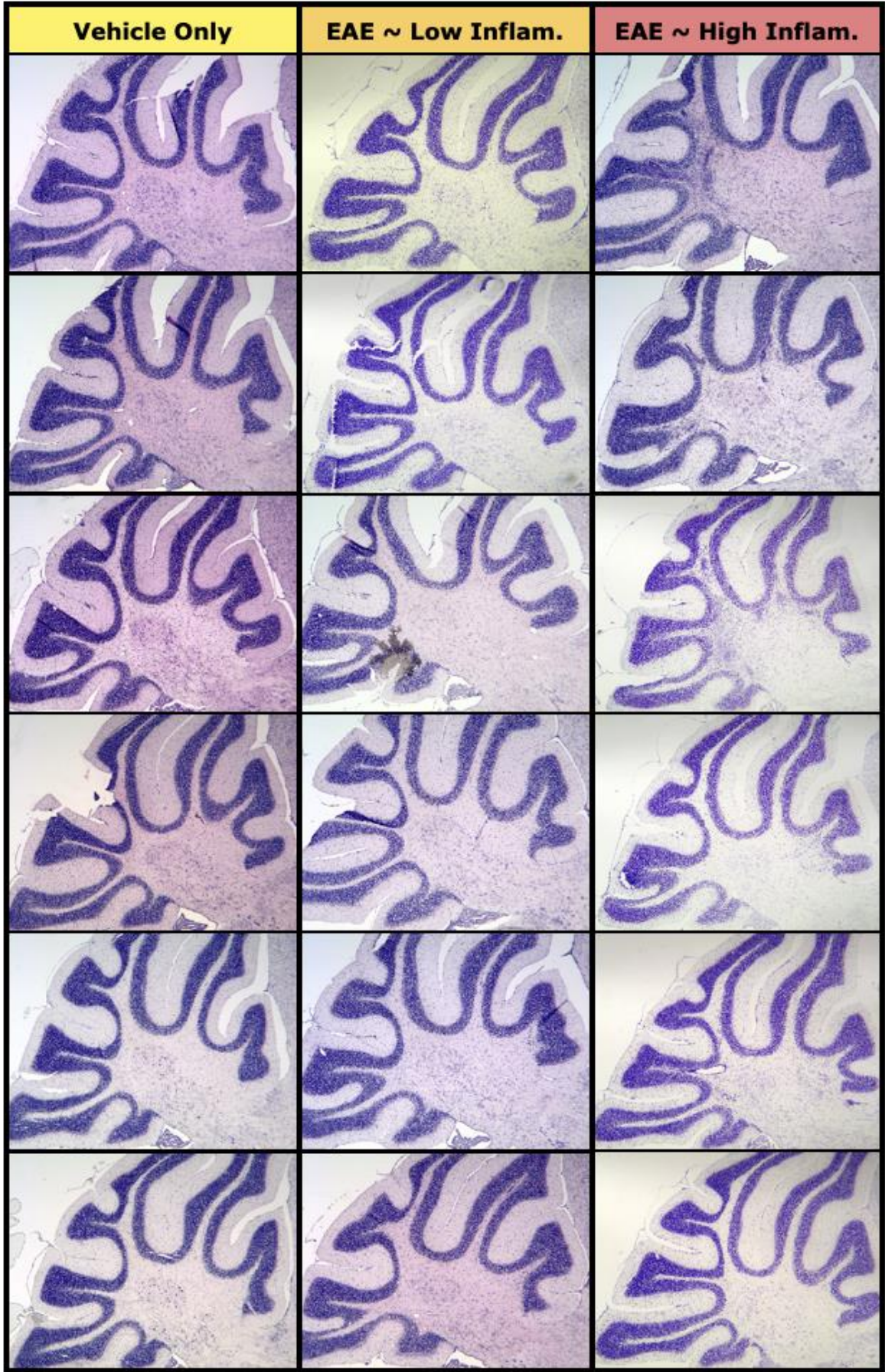
Supp. 3-1 Cresyl violet stained sagittal cerebellar sections were matched with others before selecting sections to count. One such set of matched sections is presented as an example consisting of VO controls and high CS EAE mice (CS 2.5+) that were separated into groups dependent on the extent of cerebellar inflammation, EAE with no/low inflammation and EAE with high inflammation (n = 6).

a) C57Bl/6 - Cerebellar Cortex - Low CS
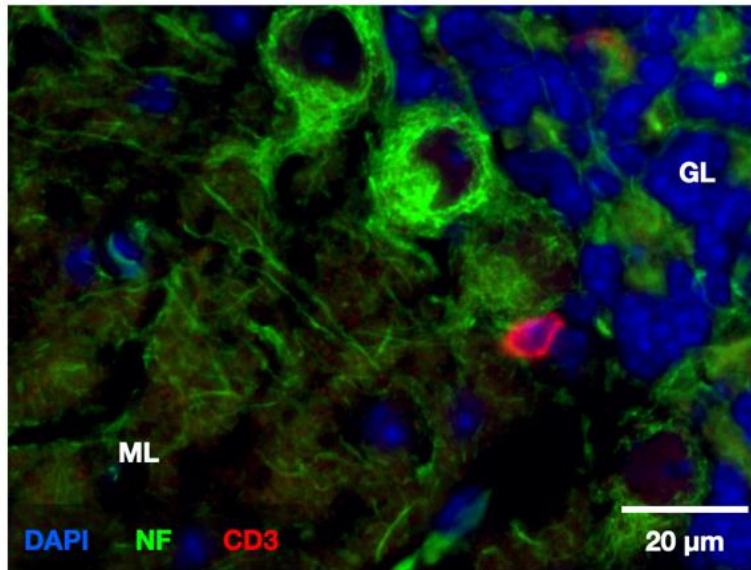
b) SJL/J - Cerebellar Cortex - Low CS

SJL/J - Cerebellar Cortex

c) Low CS

d) High CS

e) Normal
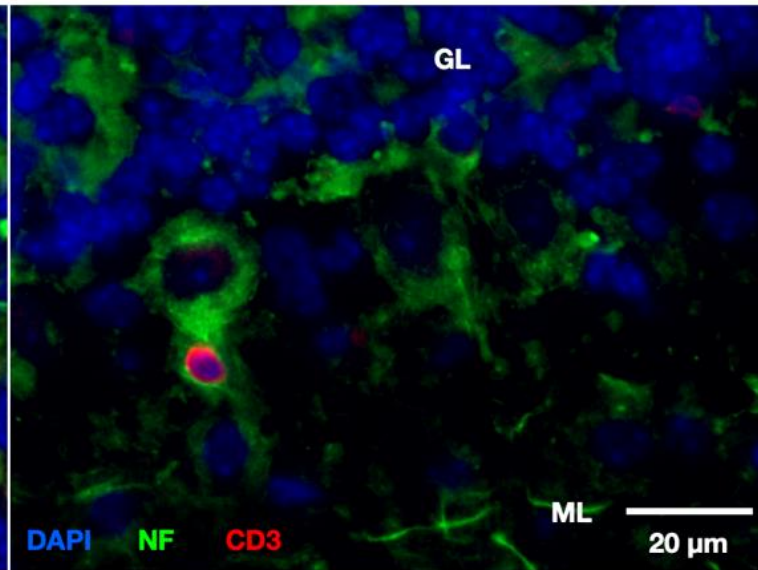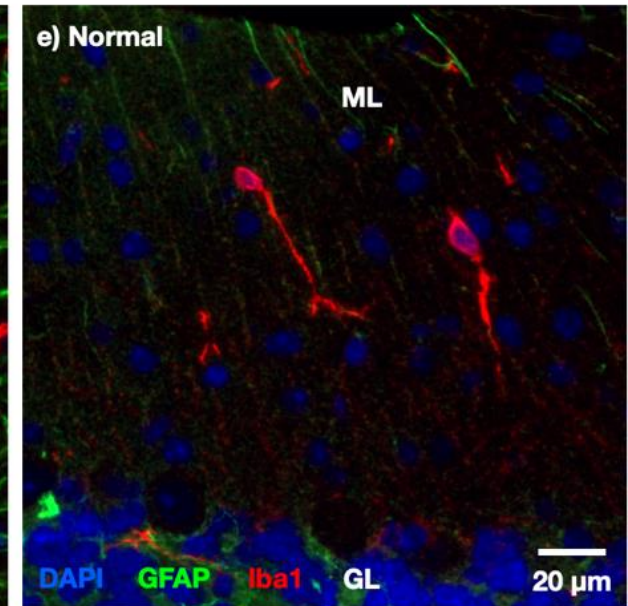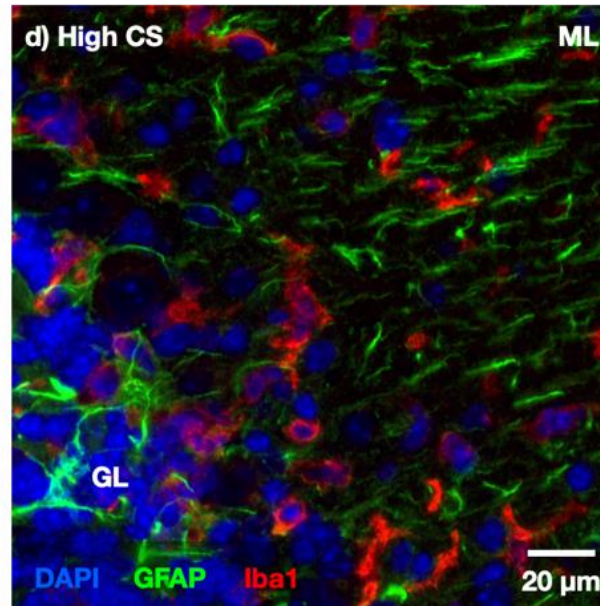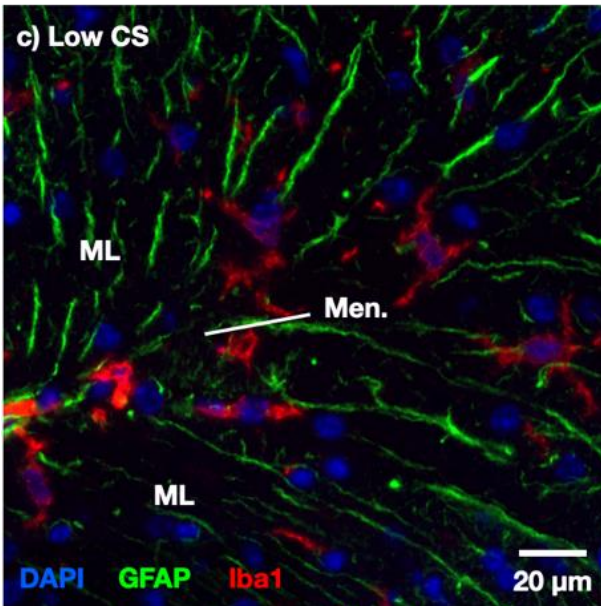
Supp. 3-2 The cerebellar cortex shows similar pathology to the DCN. (a, b) Single CD3+ cells are observed in the cerebellar cortex adjacent to NF+ Purkinje neurons in both mouse strains. Both (c) low CS and (d) high CS Iba1+ cells exhibit reactive morphology relative to (e) normal controls. GL - granular layer, ML - molecular layer, Men. - meninges, NF – hypo-phosphorylated neurofilament, GFAP - glial fibrillary acidic protein, Iba1 - ionised binding adapter molecule 1.

Supp. 3-3 Myelin staining in the C57Bl/6 and SJL/J cerebellum. C57Bl/6 and SJL/J (a, e) normal and (b, f) VO animals exhibit uneven myelination in the DCN, while WM myelination is abundant. (c, d) WM lesions are more florid in C57Bl/6 (arrow heads) at a low CS, however changes in DCN myelin are difficult to evaluate due to paucity of myelination in this region even in control animals. (g, h) Lesions in the WM adjacent to the DCN is evident (arrow heads) in SJL/J mice, but the DCN is difficult to assess as in (c, d). MBP - myelin basic protein, PLP - proteolipid protein, DCN - deep cerebellar nuclei.

DAPI   Neurofilament
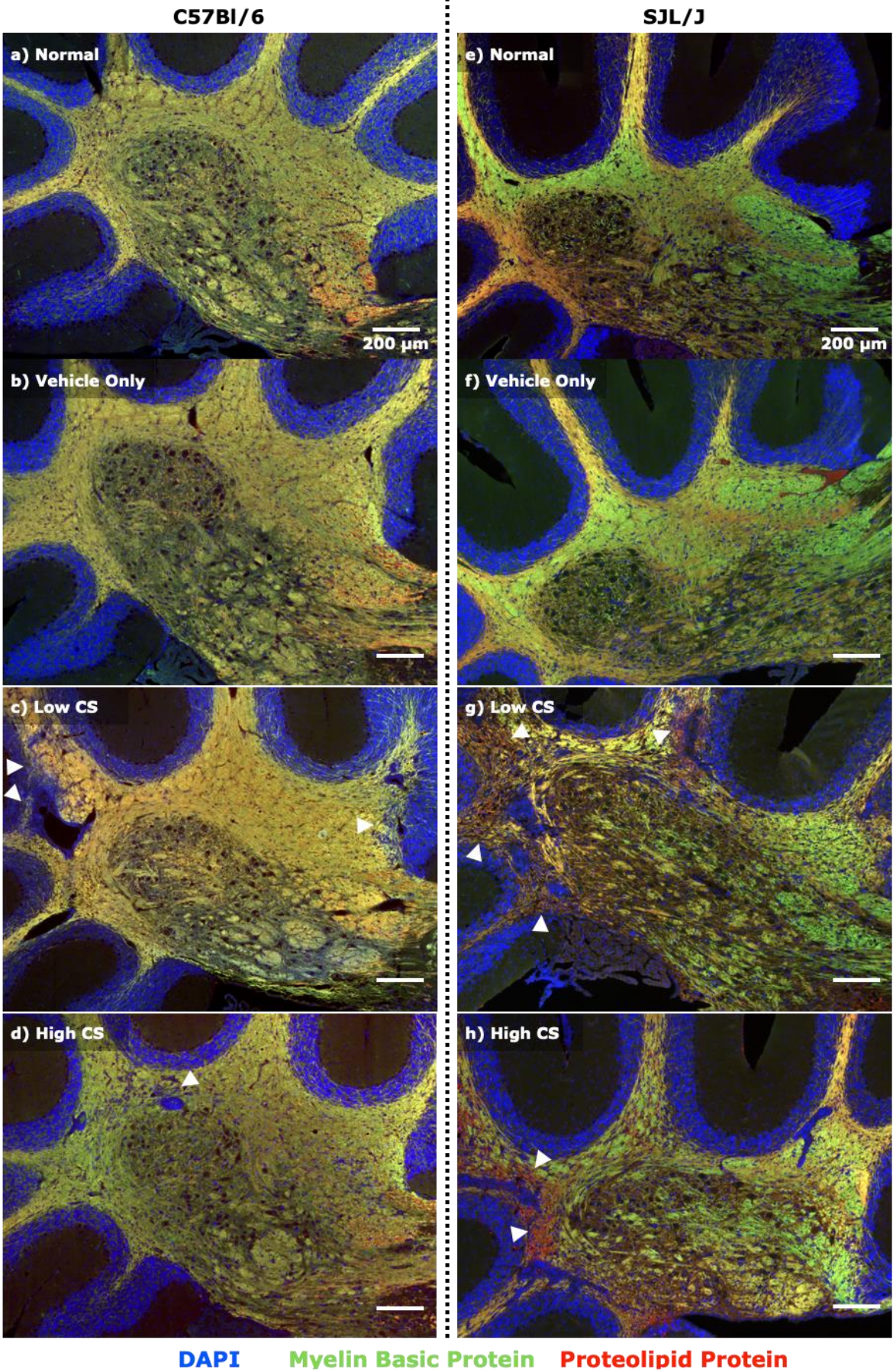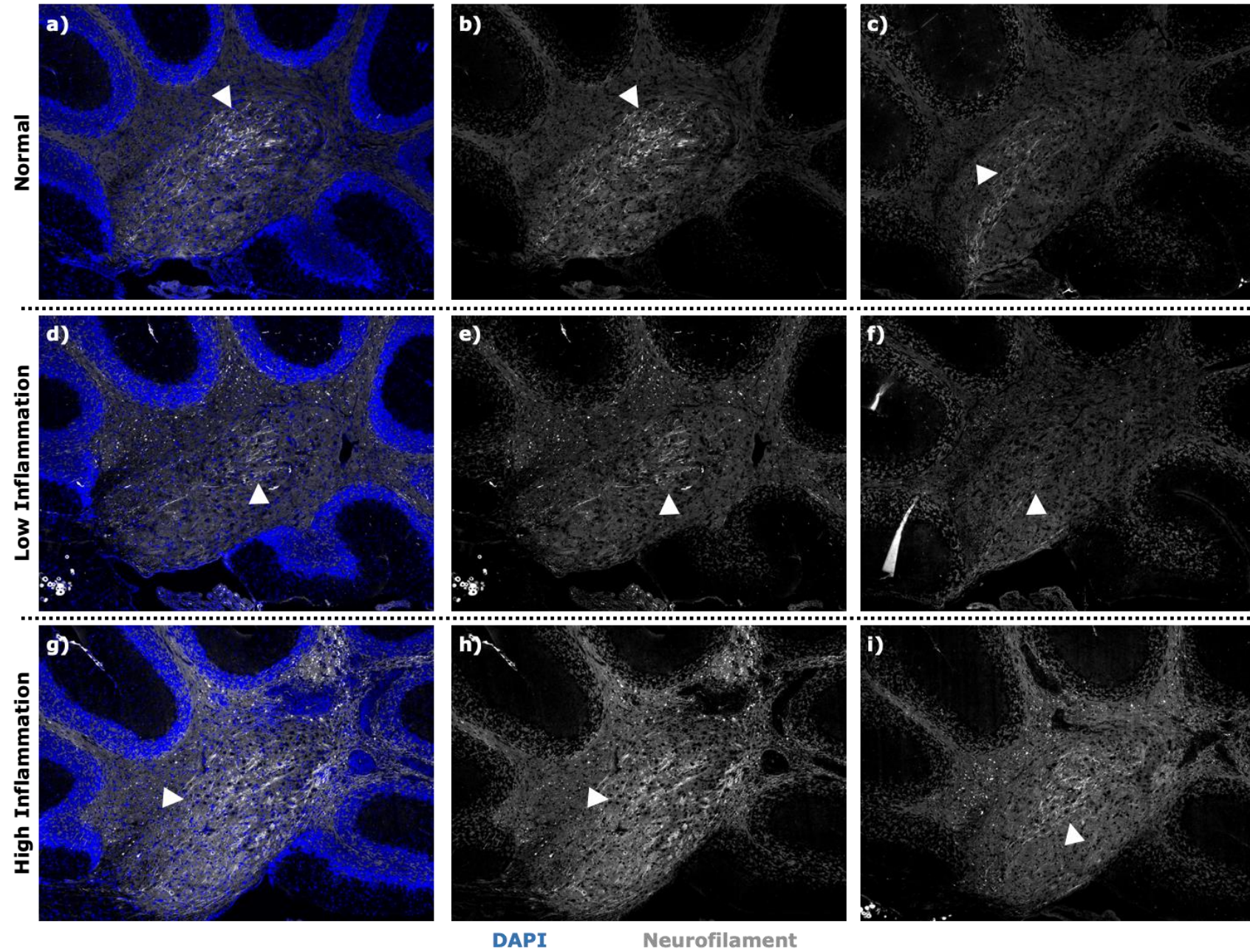
Supp. 3-4 NF (grey) IHC staining in C57Bl/6 mice. NF staining is seen most intensely, though highly variable in the DCN in normal C57Bl/6 mice with low but consistent staining in the surrounding WM (a, b, c). In high CS EAE (CS 2.5+) mice showing either low cerebellar inflammation (d, e, f) or high cerebellar inflammation (g, h, i), NF staining is not significantly different to that seen in normal controls.

Supp. 3-5 αB-Crystallin (green) IHC in C57Bl/6 mice. Cell bodies positive for αB-crystallin are frequently seen in the cerebellum in normal (a, b, c), low CS EAE (d, e, f) and high CS (g, h, i) groups in and around the DCN with no clear differences between the groups.

DAPI   **αB-Crystallin**
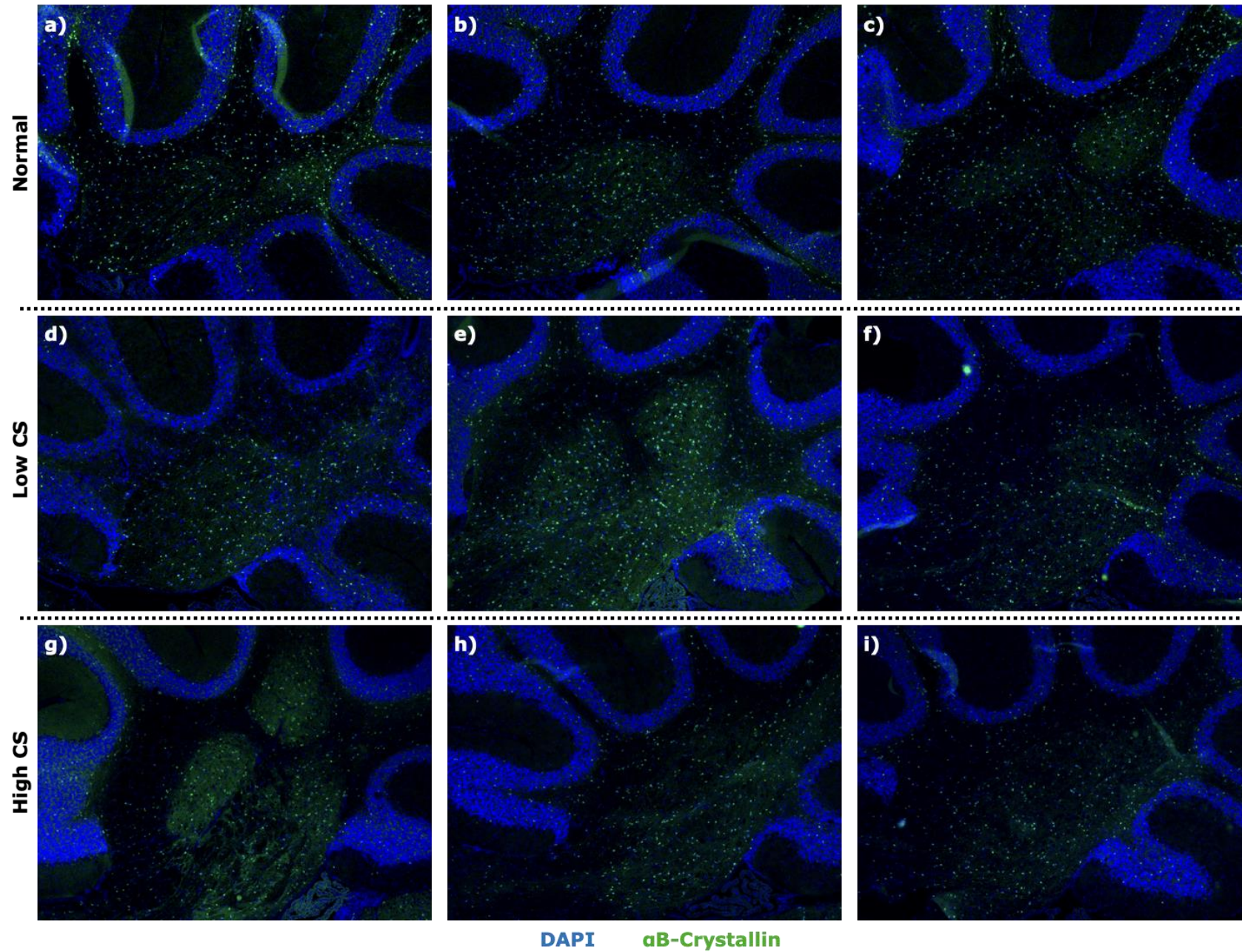
Chapter 4 Rotarod assessment as a measure of cerebellar disease in EAE.

<u>Introduction</u>

While the focus of MS pathological investigations has been on the brain because of the association of symptoms with cortical atrophy and lesions in the WM, cortical GM and deep GM, cerebellar disease also has profound consequences on the quality of life of people with MS. EAE however, has been most intensively used to elucidate mechanisms of neuroinflammation in the SC due to the predilection of this CNS region for lesion development, the relative anatomical simplicity of the SC, ease of access relative to other CNS structures supported by the convenience of the CS system to evaluate disease severity and progression. Furthermore, as MRI technology improves SC pathology is becoming increasingly recognised in MS. On the other hand, cerebellar disease has long been known to be of significance in MS but has been grossly understudied relative to brain pathology. Approximately 48% of patients with early MS showing impaired balance (Cameron & Nilsagard, 2018; Cattaneo *et al*, 2021) and up to 80% experience some form of ataxia throughout the course of the disease (Wilkins, 2017). More recently, the role of the cerebellum in cognition in MS has been recognised, particularly with the evidence that patients with cerebellar motor dysfunction have a different cognitive profile than those without such dysfunction. This evidence is also corroborated by data generated from functional MRI and information processing tasks. The precise nature of cerebellar involvement in cognition is yet to be determined, however the implications of these findings is that early evidence of cerebellar symptoms is suggestive of concurrent onset of disease activity in multiple CNS regions (Weier *et al*, 2015).

As touched on in Chapter 1, a number of pathological hallmarks seen in the cerebellum are not dissimilar to those found in the brain such as WM/GM lesions, non-inflammatory

cortical demyelination and atrophy. Some of this pathology is believed to long precede cortical damage in the brain. As such, studying the development of EAE in the cerebellum may shed light on early disease processes that are not investigable in people with MS potentially enabling earlier diagnosis, assisting in the development of measures more sensitive than the current EDSS scale to quickly gauge patient responsiveness to therapeutics as well as providing a more clinically relevant region than the SC to evaluate promising drug candidates.

The rotarod performance test is a validated measure of balance and coordination associated with cerebellar functionality in rodent species. The key outcome measure is the time taken for the mouse to fall (or cling to the rod doing full rotations without moving the feet) from a rod that is either accelerating or rotating at a static speed, requiring considerable coordination and balance. While patients do not undergo a direct analogue of the rotarod, wearable gyroscopic devices are used alongside tests measuring walking time, speed and balance and have been linked to GM/WM lesion volume and atrophy (Shanahan *et al*, 2017). The rotarod test on mice has been found to be sensitive to physical trauma associated with a loss of balance in humans such as a traumatic brain injury, as well as pharmacological interference such as inebriation. Furthermore, this test is routinely used to investigate potential therapeutics and their impact on the recovery of motor function, coordination and balance.

In this study, the rotarod test was applied to determine its suitability to detect pre-clinical deficits in balance and coordination and if this was associated with cerebellar disease described in Chapter 3. A standard protocol was first evaluated, with refinements made thereafter to more accurately determine the point of onset of disease as well as to limit other extraneous variables such as learning and ceiling effects.

Results

The rotarod was used to examine the relationship between impaired balance and cerebellar pathology identified in Chapter 3. The latency (time to fall from the rotarod) was the main outcome measured as the average time mice were able to remain on the rotarod, with the aim of identifying the earliest time point over the disease course when a significant difference between EAE and controls (normal and VO) was observed. To achieve this, three protocols were trialled with optimisations made where needed, relating to frequency of training and testing the mice received and the maximum speed the accelerating rod reached. Optimisations were made to more accurately determine when a loss in rotarod performance could be observed, address concerns that learning effects may mask a drop in functional capacity and to address the ceiling effect where maximum performance cannot be properly determined (Table 4-1). Furthermore, weight and CS were monitored for EAE mice tested on the rotarod and compared with the disease progression of control mice to ensure the procedure itself had no effect on the disease course.

Protocol	Training	Assessment	Results	Problems
1	Two Sessions DPI -1 and 6	Two Sessions on DPI 8 and 14 5 – 40 RPM	Performance dropped from DPI 8 to DPI 14 in the EAERota+ versus NormRota+ and VORota+.	NormRota+ controls improved from one test to the other indicating more training is required. More frequent tests are required to determine when performance begins to drop.
2	Five Sessions DPI -4 to 0	Daily from DPI 5 5 – 40 RPM	Time spent on rotarod dropped at the same time that EAERota+ mice developed a clinical score.	All groups regularly reached the maximum possible time/RPM for the rotarod test.
3	Five Sessions DPI -4 to 0	Daily from DPI 5 5 – 60 RPM	Time spent on rotarod dropped at the same time that the EAERota+ mice developed a clinical score.	No drop in performance was observed prior to ascending paralysis in EAERota+.

Table 4-1 Summary of details, results and ensuing issues involved in optimising each rotarod protocol tested.

Protocol 1

Conditions are described in Chapter 2 - Protocol 1 and Table 4-1. Body weight remained

steady in normal and VO groups that were rotarod rod assessed (NormRota+ and VORota+

respectively) throughout the course of the experiment with no significant change detected

(Fig. 4-1a). Similarly, both EAE induced mice trained and tested on the rotarod

(EAERota+) and those that were not (EAERota-) showed significant decrease in weight

relative to both NormRota+ and VORota+ on DPI 14 as well as the development of

ascending paralysis (Fig. 4-1a). However, EAERota- mice were found to be significantly

heavier than EAERota+ at DPI 9 (p = 0.04) suggesting that post induction weight gain may

be impacted by testing itself or stress resulting from handling. However, training and testing

phases did not appear to have a significant impact on the disease course of EAE, with

EAERota+ not showing a significantly different progression in CS relative to the EAERota-

group (Fig. 4-1b). EAERota- mice do show a trend of earlier onset of disease at DPI 13 but

this did not reach significance. At DPI 8 all groups (NormRota+, VORota+ and EAERota+)

showed a comparable performance in time to fall (Fig. 4-1c). When tested again at DPI 14,

EAERota+ had a significantly worse performance with average time to fall being under

half that seen in the control groups (NormRota+ and VORota+; both p < 0.001). This drop

in performance was also verified when comparing average fall time between 8 and 14 DPI

for EAERota+ (p = 0.002), though the NormRota+ group had an improved average (p =

0.03).

Overall, we see a drop in rotarod performance in the second (DPI 14) relative to the first

(DPI 8) day of testing, though this cannot be solely attributed to cerebellar damage due to

mice also showing signs of ascending paralysis due to SC inflammation (Fig. 4-2).

Interestingly, a slight improvement is seen in the NormRota+ mice from DPI 8 to 14,

though this is not seen in the VORota+ group.

a) Weight (%) During Rotarod Assessment (P1)
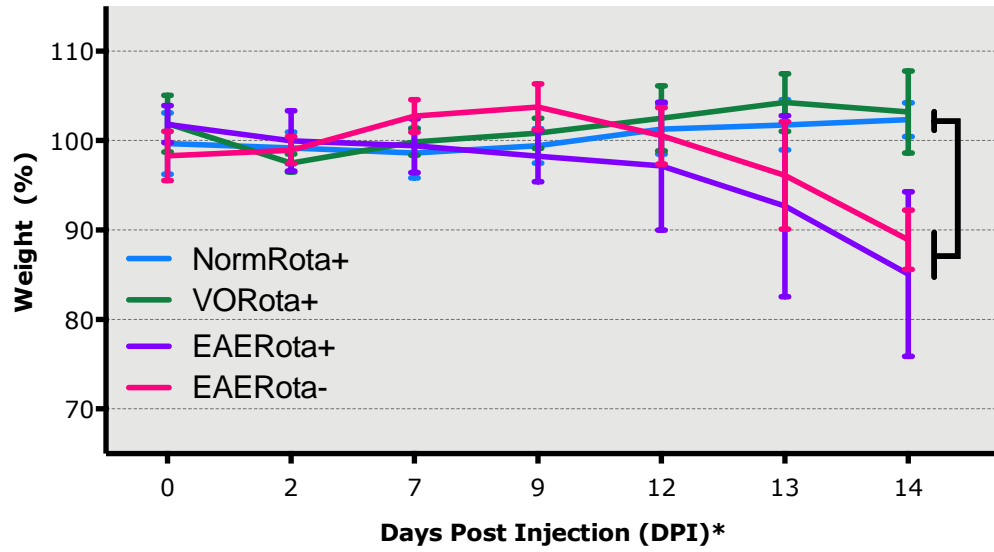
b) Clinical Score During Rotarod Assessment (P1)
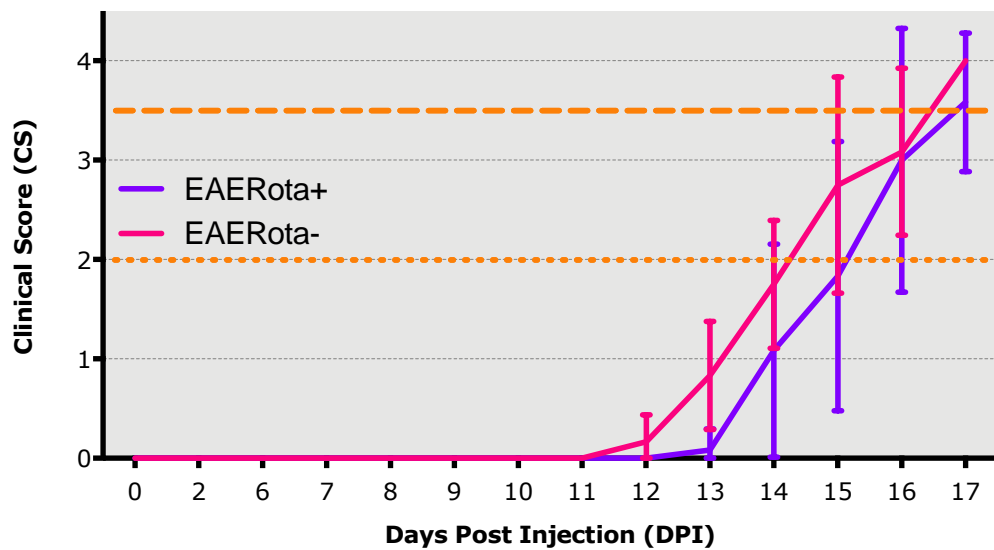
c) Rotarod Performance (P1)
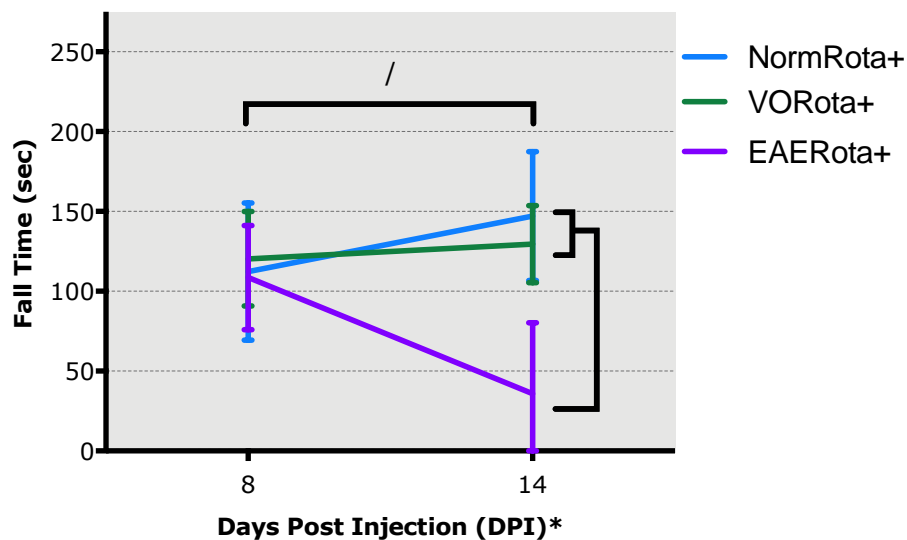
Fig. 4-1 Data for rotarod protocol 1. (a) Weight measurements are shown as a percentage difference from an average of the first three measurements taken for NormRota+ (blue), VORota+ (green), EAERota+ (purple) and EAERota- (pink). (b) Average CS data for EAERota+ (purple) and EAERota- (pink). (c) Average group rotarod performance recorded as time to fall or three full rotations clasping the rod in a row. Statistical tests: (a) Repeated measures two-way ANOVA, no sphericity assumed (Geisser-Greenhouse correction) using Tukey multiple comparison test; (b) Mann-Whitney test with multiple comparisons using Holm-Šidák method; (c) Repeated measures two-way ANOVA, no sphericity assumed (Geisser-Greenhouse correction) using Tukey multiple comparison test. n = 5, error bars represent 95% CI, *NormRota+ were not injected but training and assessment occurred on days as if they had been.

Fig. 4-2 SC inflammation in C57Bl/6 mice at CS 1.5. Even at a low CS, light to moderate meningeal inflammation is seen (arrow heads) at the (a, b) cervical and (c, d) thoracic regions. More severe inflammation is observed in the meninges and underlying WM at the (e, f) lumbar and (g, h) sacral regions.

C57Bl/6 ~ CS 1.5
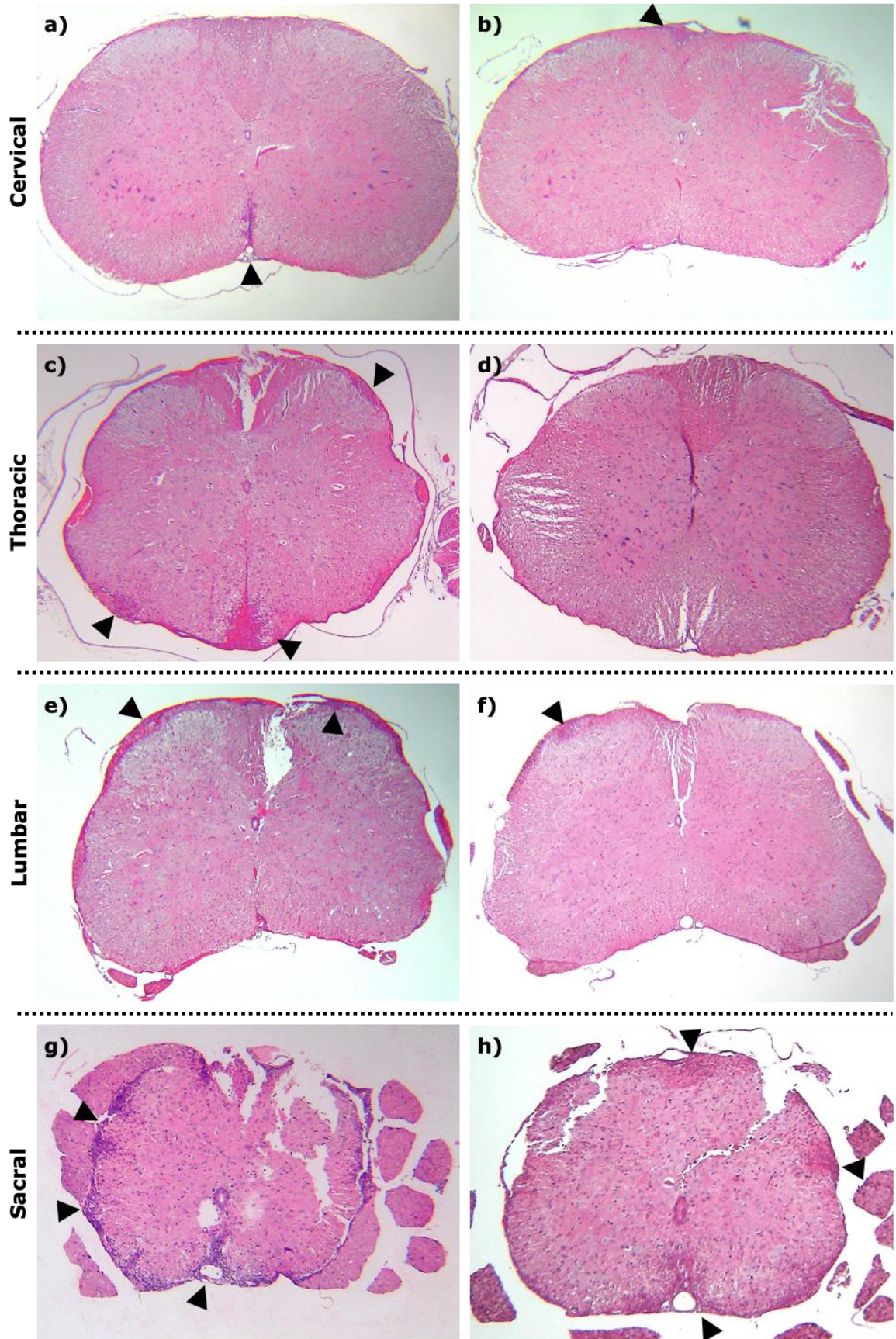
Protocol 2

The second protocol was modified to include an increased number of training days with a more gradual increase to maximum RPM to limit learning effects on the results (Chapter 2 - Protocol 2; Table 4-1)[1]. Testing frequency was also increased from just two days (DPI 8 and 14) to daily starting at DPI 5, to provide a more accurate measure of when a drop in rotarod performance is first observed.

Both EAERota+ and EAERota- groups showed weight loss alongside onset of clinical disease beginning at 12/13 DPI (Fig. 4-3a). However, as with protocol 1, EAERota- showed a significantly increased weight gain post induction relative to EAERota+ at DPI 7 (p = 0.03), though the difference observed at DPI 9 (p = 0.06) and DPI 12 (p = 0.10) did not reach significance. As in protocol 1, there did not appear to be any significant difference in either day of onset (DPI 11/12) or rate of disease progression in protocol 2 (Fig. 4-3b). Surprisingly, rotarod performance between EAERota+ and VORota+ showed no significant difference in time to fall despite the EAERota+ beginning to show signs of disease (CS 0.5 ~ 1.5) at DPI 11, 12 and 13 (Fig. 4-3c).

While a drop in average rotarod performance was expected alongside onset of ascending paralysis, there was no evidence of any loss in performance prior to this time point that may be indicative of impending weakness/paralysis. This can be explained in part by the ceiling effect observed whereby mice regularly reached the maximum possible time on the rotarod when the maximum speed was 40 RPM. This suggests that no accurate upper limit to measure peak performance had been reached. Furthermore, removing mice from analysis when it was deemed unethical to test them on the rotarod when CS above 1.5 was identified,

---

[1]All experiments performed using protocol 2 occurred during a period where mice were living in perpetual daylight due to a maintenance error in the LARTF. Despite the expected increase in stress from being in constant light, the disease course was not significantly altered relative to standard EAE conditions.

combined with outliers in terms of onset and rate of disease make statistical comparisons challenging with such small group sizes (n = 5).

Fig. 4-3 Data for rotarod protocol 2. (a) Weight was monitored throughout the experiment and presented as a percentage change from the average of the first three measurements for NormRota+ (blue) and EAERota+ (purple) and for EAERota- (pink). (b) Comparison of CS progression in EAERota+ (purple) relative to EAERota- (pink). (c) Average time to fall off the rotarod was measured for both NormRota+ (blue) and EAERota+ (purple) mice. Statistical tests: (a) Repeated measures two-way ANOVA, no sphericity assumed (Geisser-Greenhouse correction) using Tukey multiple comparison test; (b) Mann-Whitney test with multiple comparisons using Holm-Šidák method; (c) Repeated measures two-way ANOVA, no sphericity assumed (Geisser-Greenhouse correction) using Tukey multiple comparison test. n = 5, error bars represent 95% CI, *NormRota+ mice were not injected but training and assessment occurred on days as if they had been.

a) Weight (%) During Rotarod Assessment (P2)
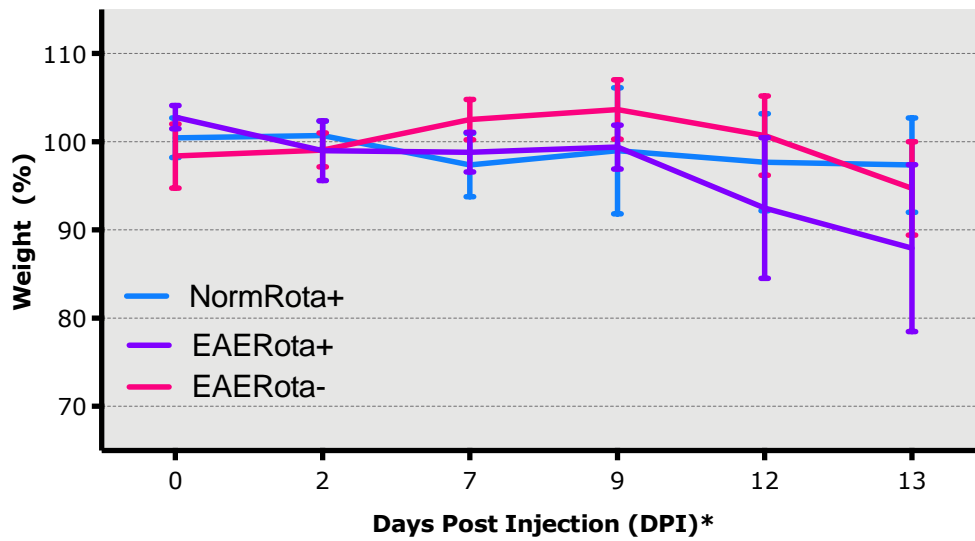
b) Clinical Score During Rotarod Assessment (P2)
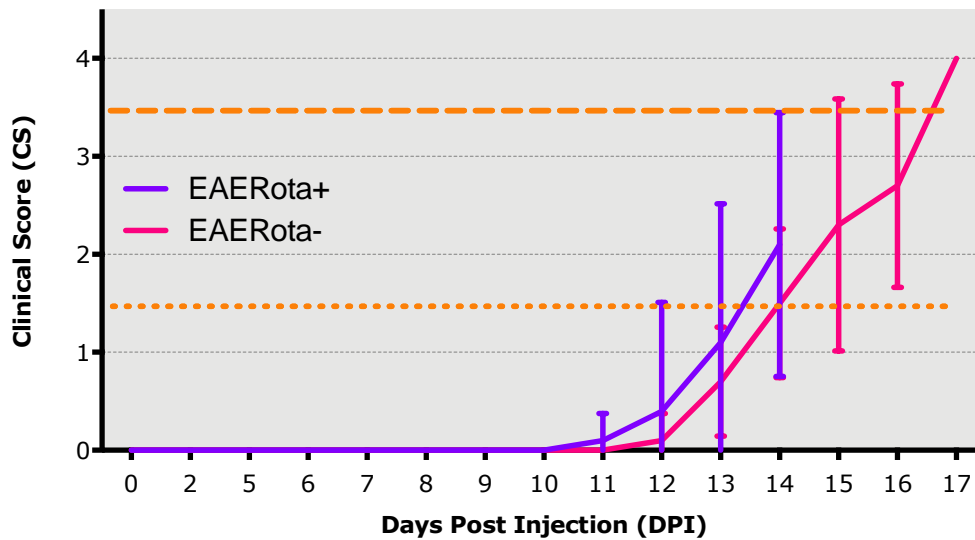
c) Rotarod Performance (P2)
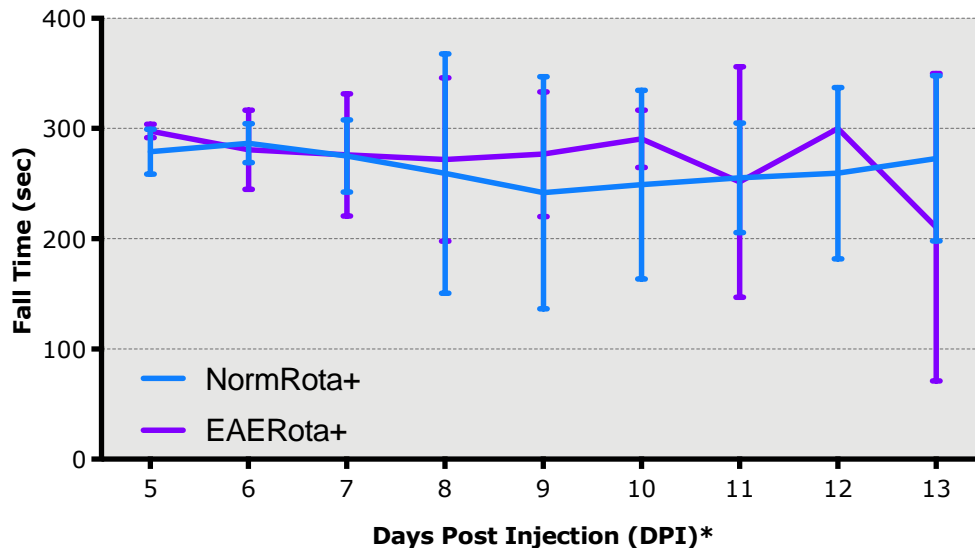
Protocol 3

Despite the more extensive training and assessment program coupled with an increased max RPM (Protocol 3; Table 4-1), NormRota+ weight remained steady throughout the test (Fig. 4-4a). Similar to protocols 1 and 2 (Fig. 4-1a; Fig. 4-3a) EAERota- groups trended towards increased weight gain post induction/prior to onset of disease. However, this difference was not as high relative to protocol 1 and 2, with significant differences only seen between VORota+ on DPI 7 and 9 (p < 0.001) and no significant difference relative to EAERota+ (DPI 7 p = 0.10 and DPI 9 p = 0.15). As the ascending paralysis begins on DPI 11/12, a loss of weight is seen in the EAERota+ group relative to VORota+. This trend begins at DPI 12 (p = 0.06) and continues at DPI 13 and 14 (p < 0.001 for both days). Similarly, between VORota+ and EAERota- groups this difference does not reach significance immediately (DPI 12 ~ p = 0.16, DPI 13 ~ p < 0.001, DPI 14 ~ p < 0.001), possibly as a consequence of the increased post induction/pre-clinical weight gain. No significant difference is seen between EAERota+ and EAERota- groups at any time point with the post induction weight gain trend at DPI 7 (p = 0.10) not reaching significance. The possible increase in stress from the increased maximum speed of rotarod protocol 3 (40 RPM vs 60 RPM) did not appear to significantly alter the disease course of EAE with no significant differences in the onset, rate of progression and maximum CS seen between the EAERota+ and EAERota- groups (Fig. 4-4b). In protocol 2 mice from both rotarod tested groups (NormRota+ and EAERota+) regularly reached the maximum latency of 300 seconds (Fig. 4-1c; Fig. 4-3c). With a maximum speed of 60 RPM mice typically reach a latency of between 150 and 250 seconds with relatively few incidences of mice reaching 300 seconds (Fig. 4-4c). When comparing VORota+ and EAERota + groups, no significant differences in performance are seen until 12 DPI (p = 0.03) and again at 15 DPI (p = 0.02). While this drop in performance is observable from 12 DPI to 15 DPI, as mice reach CS > 1.5, these mice are no longer placed upon the rotarod leading to reduced numbers per group making statistical comparison post-onset challenging.

a) Weight (%) During Rotarod Assessment (P3)
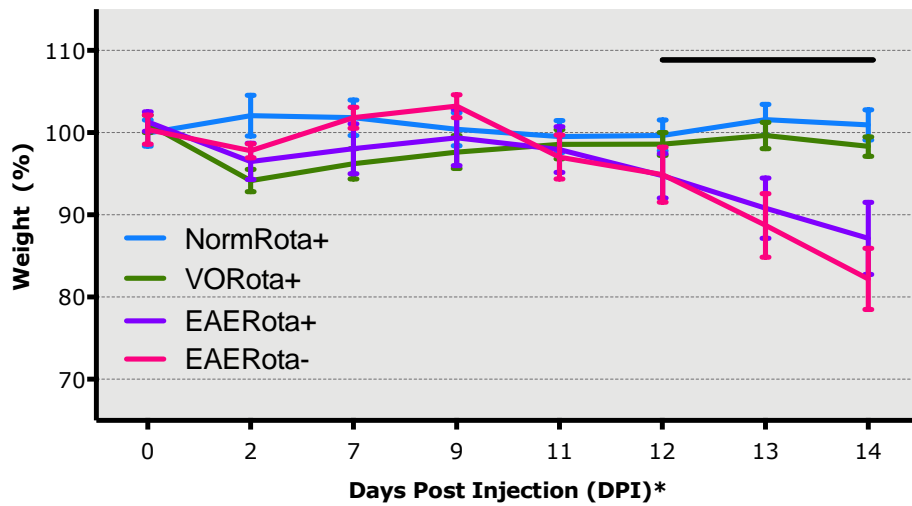
b) Clinical Score During Rotarod Assessment (P3)
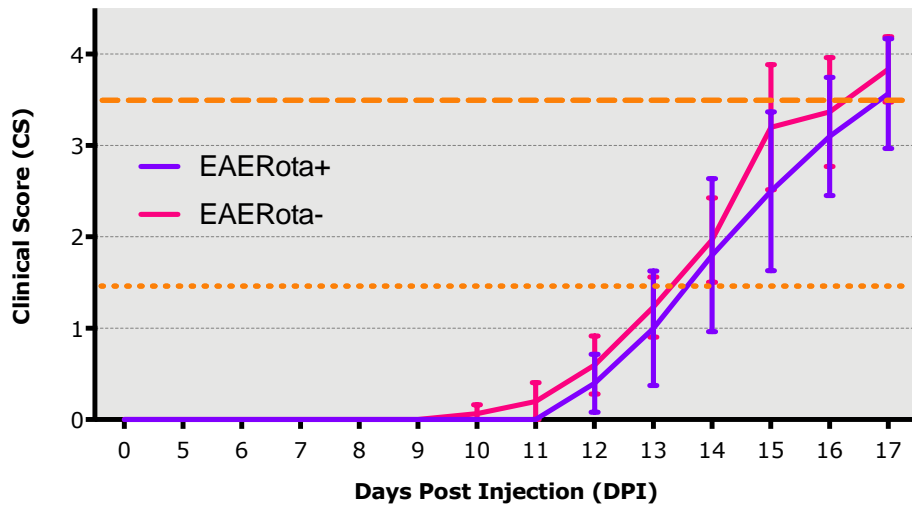
c) Rotarod Performance (P3)
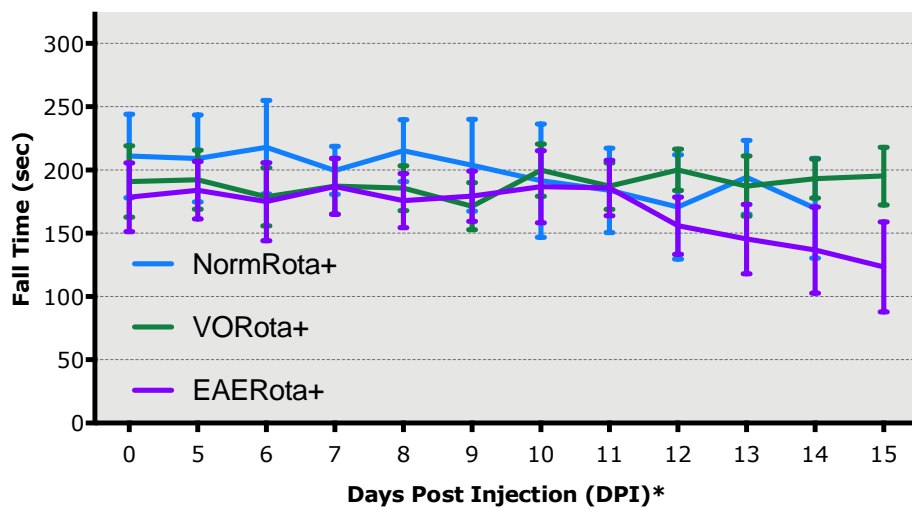
Fig. 4-4 Data for rotarod protocol 3. (a) Weight was recorded for NormRota+ (blue), VORota+ (green) and EAERota+ (purple) and EAERota- (pink). (b) CS progression over the course of the experiment was recorded for EAERota+ (purple) and compared with EAERota- (pink). (c) Time to fall was taken for NormRota+ (blue), VORota+ (green) and EAERota+ (purple) mice as a measure of rotarod performance. Statistical tests: (a) Mixed effects analysis, no sphericity assumed (Geisser-Greenhouse correction) using Tukey multiple comparison test; (b) Mann-Whitney test with multiple comparisons using Holm-Šidák method; (c) Repeated measures two-way ANOVA, no sphericity assumed (Geisser-Greenhouse correction) using Tukey multiple comparison test. NormRota+ n = 10, VORota+/EAERota+/EAERota- n = 15, error bars represent 95% CI, *NormRota+ mice were not injected but training and assessment occurred on days as if they had been.

Pre-clinical rotarod testing using protocol 3

Previous protocols did not show any drop in rotarod time to fall prior to the onset of ascending paralysis. Histology was performed on cerebellar and SC regions to investigate whether inflammation was observable in these structures despite rotarod performance being indistinguishable from controls. This was performed on DPI 11/12, just prior to first observable CS in previous protocols.

Mouse weight and rotarod performance scores were pooled for the EAERota+ groups up to and including DPI 11 (n = 7) where 4 mice were taken after rotarod assessment (Fig. 4-5). The remaining 3 mice were taken on DPI 12 after rotarod assessment. All mice showed no signs of ascending paralysis (CS 0) when taken on either 11 or 12 DPI (not pictured). Similarly, no significant differences were seen between either VORota+ or EAERota+ with rotarod groups with respect to weight changes over the course of the experiment (Fig. 4-5a). Fall time remained consistent for the EAERota+ group throughout the experiment with the average sitting between 150 - 200 seconds with no significant drop in performance seen on the final day (12 DPI; Fig. 4-5b).

This was supported by cerebellar histology performed on mice taken at DPI 11 and 12 with no inflammatory lesions observed throughout the cerebellum as assessed by H&E staining in all EAERota+ mice (not shown). No obvious inflammation was observed in the SC of pre-clinical mice taken at DPI 10 (Fig. 4-6)

a) Weight (%) during Rotarod Assessment (P3)
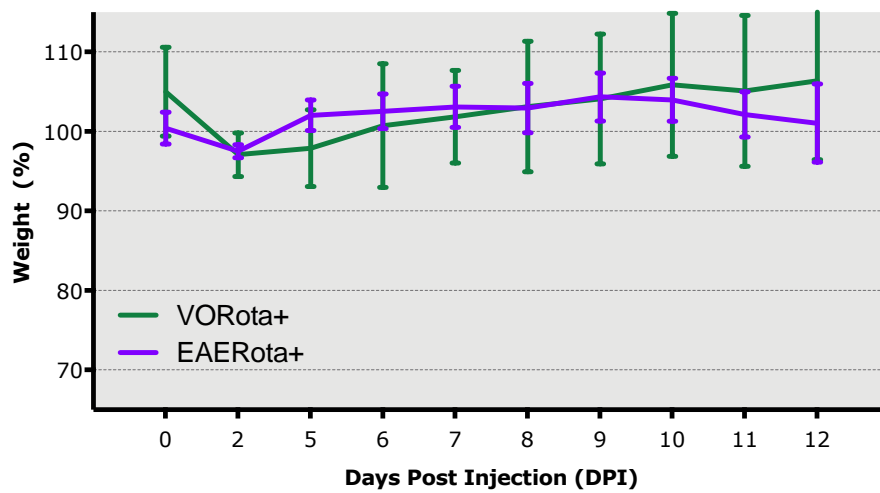
b) Rotarod Performance (P3)
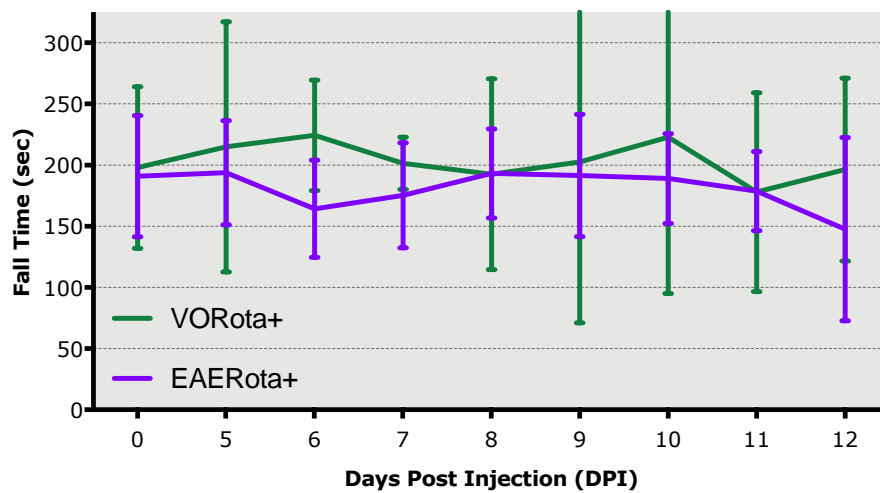
Fig. 4-5 Protocol 3 data for EAERota+ mice taken at CS 0 for pre-clinical analysis. (a) Weight monitoring data for VORota+ (green) and EAERota+ (purple) mice undergoing rotarod assessment. (b) Rotarod performance of VORota+ (green) and EAERota+ (purple) mice recorded as time to fall. VORota+ n = 3, EAERota+ n = 7 until 11 DPI, n = 4 on DPI 12. Statistical tests: (a) Repeated measures two-way ANOVA, no sphericity assumed (Geisser-Greenhouse correction) using Tukey multiple comparison test; (b) Repeated measures two-way ANOVA, no sphericity assumed (Geisser-Greenhouse correction) using Tukey multiple comparison test, error bars represent 95% CI.

C57Bl/6 ~ Pre-CS (DPI 11)
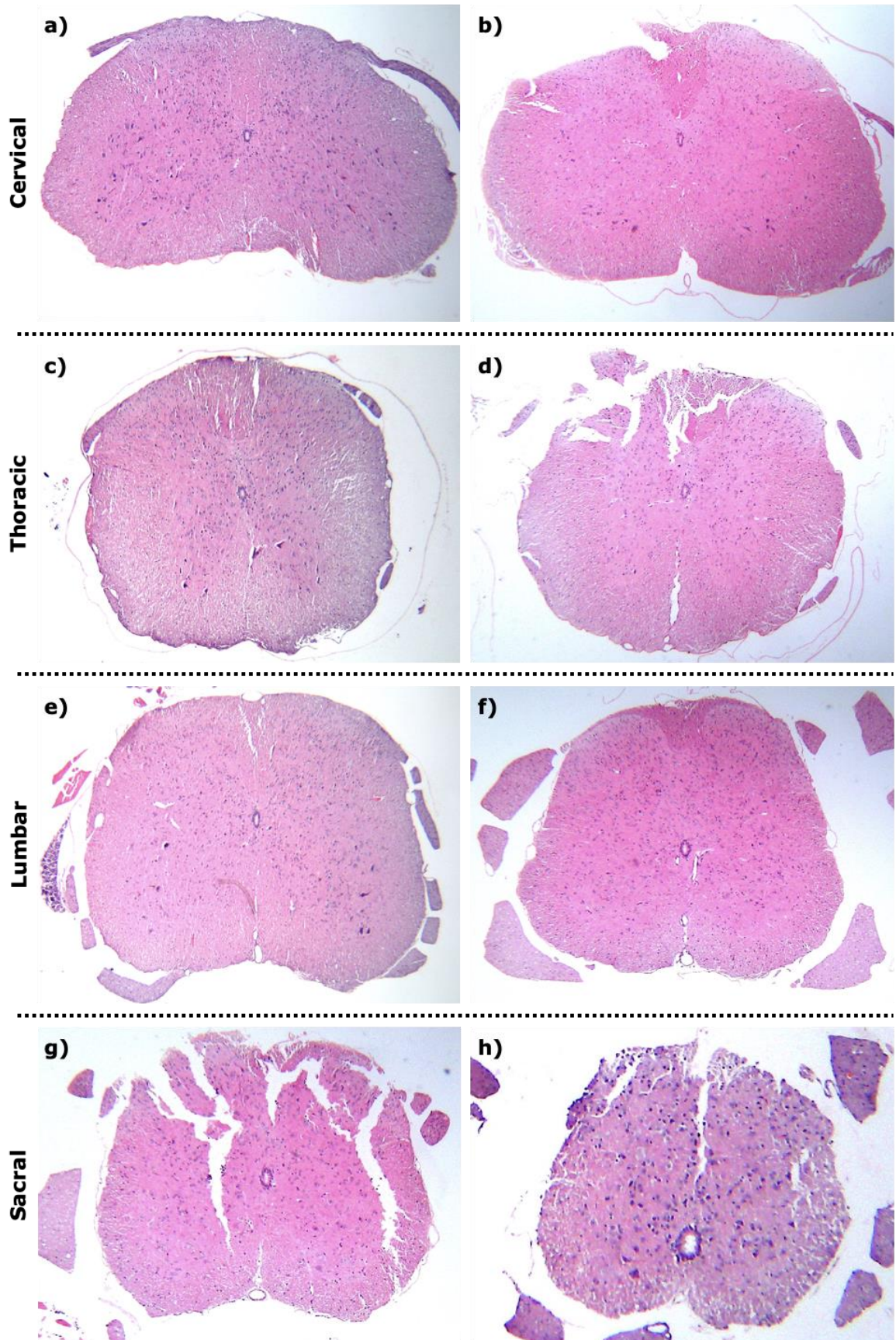
Fig. 4-6 Pre-clinical SC sections from C57Bl/6 at DPI 10. No evidence of meningeal or WM inflammation is observed at either the (a, b) cervical, (c, d) thoracic, (e, f) lumbar or (g, h) sacral regions.

Discussion

Symptoms of MS regularly include debilities relating to coordination, balance and cognition as a result of cerebellar pathology. Furthermore, in the early disease stages these often-subtle symptoms may potentially be written off as "having a bad day", whereby the patient may not present themselves to a clinic. To improve both treatment of these symptoms as well as aiding earlier diagnosis it is important to understand how a similar process develops in the EAE cerebellum. In Chapter 3 extensive florid lesions were observed very early in the disease process (CS 0.5 ~ 1.5). Given the early and severe accumulation of cerebellar pathology identified in C57Bl/6 mice, pre-clinical detection of this pathology was attempted using the rotarod test.

Careful attention was paid to standard measures for monitoring EAE, such as changes in weight as well as the onset and rate of CS progression, to ensure that alterations in training and testing protocols had no effect on disease initiation and development. Stress has been shown to alter the immune response producing a more, or less, severe response (Dhabhar, 2009). Harpaz *et al* (2013) found that chronic stress in the mouse model of EAE lead to a more severe disease course, where sources of stress included isolation, restraint, predator odour, cold water and illumination (Harpaz *et al.*, 2013). Studies investigating if a substantial stress response occurs due to the extensive handling associated with rotarod training and assessment are currently lacking. However as no discernible impact was observed in this study it suggests that the conditions associated with rotarod testing in this study do not equate to chronic stress in this particular EAE variant. However there was a consistent trend of reduced post-induction/pre-clinical score (DPI 7 ~ 10) weight gain in

the rotarod assessed groups (NormRota+, VORota+, EAERota+) relative to EAERota- mice that had not undergone any rotarod testing protocol. While this difference occasionally reached significance the actual difference in the weight was marginal and did not appear to have an impact on the overall health of the mice. More in-depth measurements of stress hormones, lesion number/volume, or combined rotarod testing with a test of anxiety-like behaviour such as the elevated plus maze would be of interest to more accurately gauge the subtler impacts of using tests requiring significant handling of the mice in a disease model that may be sensitive to stress.

Multiple iterations were made to the rotarod protocol used to train and assess the performance of the mice. The initial proof of concept (Chapter 2 - Protocol 1; Table 4-1) consisted of just two training (DPI -1 and 6) and assessment (DPI 8 and 14) sessions. As expected, this was enough to show a drop in performance from a low CS onwards, however it was not suitable to detect disease prior to the development of tail weakness/paralysis as the second test point typically occurred post recording of a CS. Furthermore, as the NormRota+ group was found to improve over the course of just two tests it was deemed necessary to provide a less steep learning curve during training and to increase the frequency of training (DPI -4 ~ 0) and testing (DPI 5+). Lastly, limits on the highest score a mouse should ethically be placed on the rotarod were initially set at CS 2 as the main focus was pre-clinical/early disease. In practice, it was found that even at low CS correlating to loss of tail tonicity (CS 0.5 ~ CS 1.5), likely unrelated to cerebellar pathology, a dramatic impact on rotarod performance was observed with mice frequently falling during the setup phase of the assessment when placed on the rotarod at a static speed of 5 RPM (data not shown). To address this, the maximum score allowed on the rotarod was reduced to CS 1.5 to ensure less unnecessary stress on the animals.

The increased training appeared to be successful in eliminating learning effects during the assessment phase of protocol 2 (DPI 5+). However this resulted in a ceiling effect whereby most mice reached the end of the test without falling off and the first drop in performance only occurred after the onset of ascending paralysis became evident. Furthermore, while protocol 1 showed a clear drop at the second timepoint, protocol 2 did not. This is believed to be in part due to a reduced maximum assessable CS excluding mice that would score lower on the test, thus driving up the average time to fall for the group. This effect, as well as that of noncompliant mice refusing to be assessed on the rotarod was also compounded by low group sizes (n = 5). To address this, a further modification was introduced, whereby protocol 3 retained the increased training and assessment frequency from protocol 2, but the maximum speed that the accelerating rotarod reached was increased from 5 ~ 40 RPM to 5 ~ 60 RPM. Very few mice managed to remain on the rod for the full duration the end of the test (300 seconds) giving a clearer view of each group's peak performance. Furthermore, the group size was increased (n = 5 to n = 15) to reduce the impact of outliers regarding time of disease onset and mice refusing to take the test. Despite these improvements, no drop in performance prior to the development of ascending paralysis was again evident. While a significant difference between the VORota+ and EAERota+ groups time to fall is seen at DPI 12 and 15, this significance is lost at DPI 13 and 14 as a consequence of removing mice from analysis that were deemed too sick to take part in the test.

In all, while it was found that rotarod training and testing did not appear to have a significant impact on the development of EAE, the accelerating rotarod test does not appear to detect either histologically silent cerebellar of pre-clinical SC pathology. This is supported by other recent EAE studies using a variety of protocols where any drop in time to fall inevitably occurs alongside the onset of ascending paralysis (van den Berg *et al.*, 2016). On

one hand this may be due to an absence of pre-clinical cerebellar functional impairment, meaning that the rotarod has nothing to detect. However, it has been found that small electrolytic lesions to the cerebellum, similar in size to a very large inflammatory lesion but likely far more deleterious, had no impact on mouse rotarod performance (Stroobants *et al*, 2013). Furthermore, that no drop in performance occurred prior to CS onset was surprising as another study in our lab found behavioural changes as early as 9 DPI using the elevated plus maze, finding that EAE mice demonstrated more anxiety like behaviour relative to VO controls (Kocovski *et al*, 2019). Though the exact mechanisms are unclear, this appears to be related to platelet accumulation and increased expression of TNFα and IFNγ in hippocampal GM well before CS onset and, significantly, even CD3+ T cell accumulation in the tissue. More detailed IHC, RNA and protein analysis will be required to determine whether deep GM pathology like that seen in the EAE hippocampus is present in the cerebellar DCN. Lastly, to properly gauge whether MS motor coordination symptoms are replicated in the EAE model behavioural and motor coordination tests such as gait analysis, which Stroobants *et al.* (2013) found to be sensitive to electrolytic lesions in the cerebellum, are required.

In summary, data presented here fails to support the use of rotarod testing for early detection of cerebellar pathology. On the other hand, an accelerating rotarod may offer a more objective measure of disease progression, resulting from combined cerebellar and SC damage. However, there are ethical concerns associated with testing mice that are showing the characteristic ascending paralysis. As mentioned earlier, mice with a moderate CS (CS 1.5+) had immense difficulty remaining on the rod during the idling phase of the test (constant speed of 5 RPM) when the group of mice are being positioned on the rotarod before the rod begins to accelerate. In this lab, mice induced according to our standard EAE protocol typically reach a CS greater than 1.5, past the point the rotarod could provide any

useful information. Furthermore, even with extensive training, daily testing and an accurate measure of peak performance a drop-in time to fall does not occur prior to CS 0.5. Coupled with the greatly increased time required for training and assessment, routine rotarod testing is difficult to justify in this C57Bl/6 variant of EAE. Despite the apparent inability of the accelerating rotarod test to detect pre-clinical disease or cerebellar pathology in EAE, its objective and parametric nature may still make it a useful tool to more accurately quantify smaller improvements in mild EAE models or during therapeutic testing where EAE does not progress beyond CS 1.5, thereby providing more accurate estimates than the standard CS system. Furthermore, alternate rotarod testing protocols have been trialled such that the speed of the rotarod remains static rather than accelerating, where it is argued that this is more sensitive and less prone to confounding effects related to fatigue. However it is unclear how large an impact fatigue may have had on the reduced time to fall of the EAE groups seen in any of the protocols. As this always coincided with CS onset it would be difficult to separate test related fatigue from weakness due to EAE. The significance of cerebellar symptoms as a reflection of wider early pathology, together with the impact of these symptoms on the quality of life of people with MS exhibiting these symptoms warrants further study of cerebellar pathology and its evaluation in the EAE model.

Chapter 5 Discussion

<u>Purpose of project</u>

The EAE model has proven to be a valuable model in understanding inflammatory cascades and contributing to the development of successful treatments, particularly those associated with WM inflammatory lesions. However, with a greater understanding of how important GM disease is in MS, models such as EAE should be used to better understand neurodegenerative processes occurring alongside CNS inflammation. For this to happen either new models or variants must be developed, or current models used more thoughtfully with determine how best to preserved MS GM. To this end, this project sought to:

1) Further characterise cerebellar disease in EAE, focussing particularly on the DCN as a region of high functional significance, but which has received little attention to date.

2) Investigate the feasibility of using an accelerating rotarod test to detect pre-CS disease in EAE as a non-invasive and quantifiable measure of cerebellar functionality.

<u>Summary of findings</u>

Neurodegeneration, atrophy, axonal pathology and demyelination have all been observed in the MS and EAE cerebellum (Albert *et al.*, 2017; MacKenzie-Graham *et al.*, 2012; MacKenzie-Graham *et al.*, 2006; MacKenzie-Graham *et al.*, 2009; Redondo *et al.*, 2015; Wilkins, 2017). In this study mild to severe inflammation was seen in the WM surrounding the DCN, beginning from CS 1.0 - 1.5. Rather strikingly, florid lesions stop abruptly at the perceived border between the WM and DCN, whereby only individual CD3+ cells were observed. However, reactive and amoeboid like macrophages of indeterminate origin (microglia or monocyte derived) were seen throughout the GM and WM. It appears that

these cells are of microglial rather than monocyte origins in early disease, but this distinction could not be confirmed as disease progressed. This was coupled with unidentified TUNEL+ cells in and around the DCN, only a proportion of which could be identified as CD3+ cells and a reduced number of cresyl violet stained cells presumed to be neurons in the DCN. The DCN pathology, specifically the isolated T cells coupled with an abundance macrophage-like cells seen in the C57Bl/6 EAE variant remarkably shows a number of features in common with what is observed in active DGM lesions in MS and may prove to be a valuable region in understanding processes driving neurodegeneration (Haider *et al.*, 2014). This pathology appears to develop independently of the ascending paralysis as a consequence of SC disease, with severe cerebellar inflammation seemingly peaking at CS 2.0 and often appearing less florid at experimental endpoint. It is worth noting that markers of stress and pathology typically used on SC tissue do not appear useful in the cerebellar DCN at a qualitative level due to high levels of αB-crystallin and small calibre NF+ axons in normal controls. However, more rigorous quantitative analysis of the level of expression of these markers may yet show changes between healthy and inflamed tissue.

Rotarod performance did not drop prior to CS onset suggesting that inflammation in the cerebellum, though potentially aggressive/rapid, probably does not precede that of the SC. This is further supported by pre-CS histology on cerebellar sections at DPI 11/12 where no overt inflammation was observed. Recent studies investigating performance on the rotarod test in EAE have found that a drop in rotarod latency is associated with ascending paralysis and SC pathology. That a drop in performance occurs alongside the onset of a CS with no detectable pre-CS drop in performance, while surprising, is also supported here. Unlike other studies however, the extensive pre-induction training and higher maximum RPM improves the rotarod test by limiting learning effects that would otherwise occur post EAE

induction prior to CS onset. This also limits the potential impact on learning capacity that may occur as a result of the aggressive induction procedures. Taken together, the sum of the data supports the conclusion that cerebellar and SC pathology, although coincident, progress independently and therefore tests used to evaluate SC damage are uninformative with respect to cerebellar damage.

Limitations and future directions of this study

In this study we find evidence that the C57Bl/6 and SJL/J EAE variants show deep GM like pathology bearing some semblance to that seen in MS. Future studies should focus on what detrimental impacts the vast swathes of highly reactive macrophage-like cells have on the surrounding GM, the nature of the CD3+ T cell/neuron interactions and how this causes a reduction in of neuronal counts in this region. However, this study is not without limitations. The DCN is composed a diverse array neuron types and sizes, thus the cresyl violet stain was selected due to its broad staining specificity as antibodies routinely used as axonal/neuronal markers in other CNS regions were uninformative in the DCN. Due to the pilot nature of this study, the lower cost associated with cresyl violet staining was also appealing. Cresyl violet does not specifically stain neurons per se however, and other abundant cell types within the CNS (specifically oligodendrocytes, astrocytes and microglia) may also be stained quite strongly, although great care was taken in this study to include only cells with clear neuronal morphology in estimates of neuronal population. Ideally, multiplex sequential staining (Bolognesi *et al*, 2017) would enable a much more accurate estimation of the subtly different neuron subtype population (Uusisaari & Knöpfel, 2013) to determine if: there is indeed a reduction in neuronal numbers; whether this is a sub-population specific effect; said reduction is specifically associated with proximity to WM lesions or some other factor. Determining the underlying processes driving the pathology observed will require a more advanced approach. Application of biopsy punches

to precisely dissect out defined CNS regions for subsequent biochemical and molecular profiling has been successfully used to quantify mRNA/protein in specific deep GM regions of the hippocampus coupled with quantitative IHC for further verification (Kocovski *et al.*, 2019). This may not be possible in the cerebellum. The DCN, particularly the medial and interposed nuclei focussed on in this study are highly convoluted in shape, likely leading to the inclusion of surrounding WM alongside the desired DCN material thus contaminating the analysis. This would be sismilarly infeasible for cortical studies looking to compare responses in the ML and GL. Rather, laser capture microdissection has been used effectively to profile the SC environment of both GM and WM separately as well as that of individual neurons, which could potentially be used to sample large the appropriate of the cerebellum (Orian lab, unpublished data).

In light of recent findings that specific neuronal populations may be more vulnerable to inflammation (Zoupi *et al.*, 2021) and that Purkinje neuron loss has been shown to occur in regions near to meningeal and/or WM lesions alongside the apparent reduction of neuronal numbers seen in the EAE DCN in this study, a similar approach is justified for the DCN where regions proximal to WM lesions may be contrasted with those opposing normal appearing WM. Outside of directly counting neuron population numbers, significant work has been done in investigating cerebellar explants and patterns of excitation/depolarisation patterns seen in healthy neurons in the Purkinje layer and the DCN alongside detailed records of patient balance/gait measures (Uusisaari & Knopfel, 2010; Uusisaari & Knöpfel, 2011; Uusisaari *et al*, 2007; Uusisaari & Knöpfel, 2013). While severe inflammatory lesions will undoubtably have an impact on the axonal conduction (seen most dramatically during relapsing phases of RRMS), it is quite likely that nearby inflammation leading to reactive microglia throughout nearby GM structures will have some impact on neuronal signalling dynamics that could provide insight into manifestation of cerebellar tremor and

ataxia in MS, as well as deep GM pathology in general. Altered expression of channel or receptor proteins such as that which has been observed in Purkinje neurons has been shown to lead to altered firing dynamics (Shields *et al.*, 2015; Shields *et al.*, 2012). A similar phenomenon may also occur from direct intervention from microglia themselves. Synaptic pruning mediated by complement deposition is a regular function of microglia in a healthy CNS, though in an inflammatory setting this potentially could become dysregulated. Furthermore, it has been found that in the case of distal axonal transection, microglia encapsulate dendritic processes of the attached neuron (Chen & Trapp, 2016; Rotterman & Alvarez, 2020). The DCN projects to many regions throughout the brain making it particularly vulnerable to axonal transection. Tract tracing may offer some insight as to whether the extensive Iba1+ reactivity observed is associated with surrounding inflammation, if it is functioning as a preservative measure due to distal DCN axon transection or, in the case of mixed local and peripherally derived macrophages, both.

In all, the rotarod data showed that even at a low CS, a large drop in performance is observed. However the rotarod test does not appear to be useful to detect either localised cerebellar damage or pre-CS disease in EAE. An alternative analysis that has been found to be effective in detecting rotarod silent cerebellar damage is gait analysis (Stroobants *et al.*, 2013). In EAE, gait analysis has been shown to be a more sensitive and statistically powerful method of estimating SC disease than the standard CS system. Likewise, other movement, coordination and balance tests that may be of value include the balance beam (Hoxha *et al*, 2017) or the wire mesh gridwalk test (Barth & Mody, 2014). A similar analysis may be performed the same way the rotarod test was used in this study. Training should be begin prior to induction with testing beginning at 5 DPI prior to the onset of inflammation and continued daily with a time course of cerebellar tissues taken for histology and IHC. However if cerebellar and SC disease develop concurrently the overlap

in the respective structures' control of mobility and balance may mean the movement-oriented tests listed above will be unable to differentiate the relative contributions of cerebellar and SC damage in the same manner as the rotarod test. To address this, rather than begin training prior to EAE induction to avoid the impact of inflammation on learning, this phenomenon could be taken advantage of to compare the rate of improvement mice show between VO and EAE mice, whereby cerebellar inflammation may reduce the rate of improvement in the EAE mice. Alternatively, while the best characterised cerebellar function is associated with coordination, it also plays a crucial role in eye movements and learned blink reflexes. These have been used as a means to detect impaired cerebellar function in the earliest stages of MS (Moroso *et al*, 2017; Moroso *et al*, 2018; Rampello *et al*, 2011). As mice are afoveate, saccadic based studies in the human cannot be easily translated to this model. However cerebellar mutants have been found to have altered eye movements (de Zeeuw *et al*, 1998; van Alphen *et al*, 2010) and using EAE mice focussing on the DPI 7 – onset of CS may reveal changes due to cerebellar damage not influenced by SC disease.

<u>Clinical implications</u>

As pathological changes may occur in almost any region of the brain, the potential array of MS symptoms is staggering. This also makes treatment difficult as an individual symptom may have multiple causes. A number options have been trialled for MS patients suffering from tremor or ataxia, however the cross-sectional nature, at times limited patient numbers/single case reports and studies not specifically focussed on MS associated tremor have made conclusive findings uncommon. As such, many pharmacological/neurochemistry related treatments (isoniazid, levetiracetam, topiramate, ondansetron, primidone) have shown improvements in some studies, with no clear benefit in others (Makhoul *et al*, 2020). It is possible that these varied conclusions regarding an

individual therapeutics' efficacy are associated with the diverse array of pathologies that lead to the development of ataxia and tremor such as disturbances in the proprioceptive, vestibular systems or motor cortices (Ashizawa & Xia, 2016). Less ambiguously, immunomodulatory agents (natalizumab, alemtuzumab) have also been found to lead to an improvement, likely through reduced cerebellar and other ataxia or tremor-related-system lesion burden. To improve the drug assessment process an accurate stratification of MS patients with respect to their individual symptoms and more importantly, underlying pathology, is needed.

Thus far synaptic pathology has been observed in the MS DCN, though sample size in the study was quite limited (Albert *et al.*, 2017). Through the use of post-mortem tissue from early RRMS through to onset of progressive disease a greater understanding of what is driving this synaptic loss and how early this process begins may be obtainable. When coupled with detailed a record of patient balance/gait measures this may offer some insight as to how cerebellar pathology is associated with ataxia/balance disturbances in life, a challenging prospect in human CNS studies. The continual improvements made to both the acquisition and image analysis phases of MRI technologies may assist in this endeavour, where correlation studies are now investigating the contribution of individual cerebellar lobes and the compensatory mechanisms the cerebellum is involved in (Cocozza *et al*, 2018). While some studies noted changes in the dentate nuclei under MRI (later found to be associated with a high retention of contrasting agent from previous examinations; (Roccatagliata *et al.*, 2009; Tedeschi *et al.*, 2016)), few other studies have investigated the dentate or other DCN. A comparison of cerebellar and SC tissue integrity in MS patients exhibiting impaired balance/gait coupled with routine mobility assessment over several years may provide some understanding of the relative contribution of these structures to disability.

While cerebellar disease may be prominent aspect of some MS disease processes, teasing out regional/subsystem specific (i.e. cerebellar) issues from the plethora of disease processes typically seen is a challenging prospect. For this, EAE may be used to provide a valuable proof of concept for how basic pathology leads to complicated disability in MS, and what neuronal populations in the cortical and deep GM structures require the most immediate therapeutic intervention.

Chapter 6 Reference List

Albert M, Barrantes-Freer A, Lohrberg M, Antel JP, Prineas JW, Palkovits M, Wolff JR, Bruck W, Stadelmann C (2017) Synaptic pathology in the cerebellar dentate nucleus in chronic multiple sclerosis. *Brain Pathol* 27: 737-747

Arneth B (2020) Contributions of T cells in multiple sclerosis: what do we currently know? *J Neurol*

Arneth BM (2019) Impact of B cells to the pathophysiology of multiple sclerosis. *J Neuroinflammation* 16: 128

Ashizawa T, Xia G (2016) Ataxia. *Continuum* 22: 1208-1226

Babbe H, Roers A, Waisman A, Lassmann H, Goebels N, Hohlfeld R, Friese M, Schroder R, Deckert M, Schmidt S *et al* (2000) Clonal expansions of CD8(+) T cells dominate the T cell infiltrate in active multiple sclerosis lesions as shown by micromanipulation and single cell polymerase chain reaction. *The Journal of experimental medicine* 192: 393-404

Baker D, Amor S (2014) Experimental autoimmune encephalomyelitis is a good model of multiple sclerosis if used wisely. *Mult Scler Relat Dis* 3: 555-564

Baker D, Gerritsen W, Rundle J, Amor S (2011) Critical appraisal of animal models of multiple sclerosis. *Mutliple Sclerosis* 17: 647-657

Bakshi R, Dmochowski J, Shaikh ZA, Jacobs L (2001) Gray matter T2 hypointensity is related to plaques and atrophy in the brains of multiple sclerosis patients. *J Neurol Sci* 185: 19-26

Barth AM, Mody I (2014) Novel test of motor and other dysfunctions in mouse neurological disease models. *J Neurosci Methods* 221: 151-158

Batoulis H, Recks MS, Addicks K, Kuerten S (2011) Experimental autoimmune encephalomyelitis--achievements and prospective advances. *APMIS* 119: 819-830

Ben-Nun A, Kaushansky N, Kawakami N, Krishnamoorthy G, Berer K, Liblau R, Hohlfeld R, Wekerle H (2014) From classic to spontaneous and humanized models of multiple sclerosis: impact on understanding pathogenesis and drug development. *J Autoimmun* 54: 33-50

Bennett ML, Bennett FC, Liddelow SA, Ajami B, Zamanian JL, Fernhoff NB, Mulinyawe SB, Bohlen CJ, Adil A, Tucker A *et al* (2016) New tools for studying microglia in the mouse and human CNS. *PNAS* 113: E1738-1746

Berard JL, Wolak K, Fournier S, David S (2010) Characterization of relapsing-remitting and chronic forms of experimental autoimmune encephalomyelitis in C57BL/6 mice. *Glia* 58: 434-445

Bernardes D, Oliveira ALR (2017) Comprehensive catwalk gait analysis in a chronic model of multiple sclerosis subjected to treadmill exercise training. *BMC Neur* 17: 160

Bittner S, Afzali AM, Wiendl H, Meuth SG (2014) Myelin oligodendrocyte glycoprotein (MOG35-55) induced experimental autoimmune encephalomyelitis (EAE) in C57BL/6 mice. *J Vis Exp*: 51275

Black JA, Dib-Hajj S, Baker D, Newcombe J, Cuzner ML, Waxman SG (2000) Sensory neuron-specific sodium channel SNS is abnormally expressed in the brains of mice with experimental allergic encephalomyelitis and humans with multiple sclerosis. *Proc Natl Acad Sci U S A* 97: 11598-11602

Blanchette M, Daneman R (2015) Formation and maintenance of the BBB. *Mech Dev* 138 Pt 1: 8-16

Bo L, Vedeler CA, Nyland HI, Trapp BD, Mork SJ (2003) Subpial demyelination in the cerebral cortex of multiple sclerosis patients. *Journal of Neuropathology and Experimental Neurology* 62: 723-732

Bolognesi MM, Manzoni M, Scalia CR, Zannella S, Bosisio FM, Faretta M, Cattoretti G (2017) Multiplex Staining by Sequential Immunostaining and Antibody Removal on Routine Tissue Sections. *J Histochem Cytochem* 65: 431-444

Bross M, Hackett M, Bernitsas E (2020) Approved and Emerging Disease Modifying Therapies on Neurodegeneration in Multiple Sclerosis. *Int J Mol Sci* 21

Calabrese M, De Stefano N, Atzori M, Bernardi V, Mattisi I, Barachino L, Morra A, Rinaldi L, Romualdi C, Perini P *et al* (2007) Detection of cortical inflammatory lesions by double inversion recovery magnetic resonance imaging in patients with multiple sclerosis. *Arch Neurol* 64: 1416-1422

Calabrese M, Filippi M, Gallo P (2010a) Cortical lesions in multiple sclerosis. *Nature Reviews Neurology* 6: 438-444

Calabrese M, Mattisi I, Rinaldi F, Favaretto A, Atzori M, Bernardi V, Barachino L, Romualdi C, Rinaldi L, Perini P *et al* (2010b) Magnetic resonance evidence of cerebellar cortical pathology in multiple sclerosis. *Journal of Neurology, Neurosurgery and Psychiatry* 81: 401-404

Cameron MH, Nilsagard Y (2018) Balance, gait, and falls in multiple sclerosis. *Handb Clin Neurol* 159: 237-250

Cattaneo D, Gervasoni E, Anastasi D, Giovanni RD, Brichetto G, Carpinella I, Cavalla P, Confalonieri P, Groppo E, Prosperini L *et al* (2021) Prevalence and patterns of subclinical motor and cognitive impairments in non-disabled individuals with early multiple sclerosis: a multicenter cross-sectional study. *Ann Phys Rehabil Med*: 101491

Chen Z, Trapp BD (2016) Microglia and neuroprotection. *J Neurochem* 136 Suppl 1: 10-17

Chu F, Shi M, Zheng C, Shen D, Zhu J, Zheng X, Cui L (2018) The roles of macrophages and microglia in multiple sclerosis and experimental autoimmune encephalomyelitis. *J Neuro* 318: 1-7

Cocozza S, Petracca M, Mormina E, Buyukturkoglu K, Podranski K, Heinig MM, Pontillo G, Russo C, Tedeschi E, Russo CV *et al* (2017) Cerebellar lobule atrophy and disability in progressive MS. *Journal of Neurology, Neurosurgery and Psychiatry* 88: 1065-1072

Cocozza S, Pontillo G, Russo C, Russo CV, Costabile T, Pepe A, Tedeschi E, Lanzillo R, Brescia Morra V, Brunetti A *et al* (2018) Cerebellum and cognition in progressive MS patients: functional changes beyond atrophy? *J Neurol* 265: 2260-2266

Compston A, Coles A (2002) Multiple sclerosis. *The Lancet* 359: 1221-1231

Constantinescu CS, Farooqi N, O'Brien K, Gran B (2011) Experimental autoimmune encephalomyelitis (EAE) as a model for multiple sclerosis (MS). *Br J Pharmacol* 164: 1079-1106

Craner MJ, Kataoka Y, Lo AC, Black JA, Baker D, Waxman SG (2003) Temporal course of upregulation of Na(v)1.8 in Purkinje neurons parallels the progression of clinical deficit

in experimental allergic encephalomyelitis. *Journal of Neuropathology and Experimental Neurology* 62: 968-975

Dang PT, Bui Q, D'Souza CS, Orian JM (2015) Modelling MS: Chronic-Relapsing EAE in the NOD/Lt Mouse Strain. *Curr Top Behav Neurosci* 26: 143-177

de Zeeuw CI, van Alphen AM, Koekkoek SK, Buharin E, Coesmans MP, Morpurgo MM, van den Burg J (1998) Recording eye movements in mice: a new approach to investigate the molecular basis of cerebellar control of motor learning and motor timing. *Otolaryngol Head Neck Surg* 119: 193-203

Dendrou CA, Fugger L, Friese MA (2015) Immunopathology of multiple sclerosis. *Nature Reviews Immunology* 15: 545-558

Dhabhar FS (2009) Enhancing versus suppressive effects of stress on immune function: implications for immunoprotection and immunopathology. *Neuroimmunomodulation* 16: 300-317

Dias AT, De Castro SB, Alves CC, Mesquita FP, De Figueiredo NS, Evangelista MG, Castanon MC, Juliano MA, Ferreira AP (2015) Different MOG(35-55) concentrations induce distinguishable inflammation through early regulatory response by IL-10 and TGF-beta in mice CNS despite unchanged clinical course. *Cellular Immunology* 293: 87-94

Diaz C, Zarco LA, Rivera DM (2019) Highly active multiple sclerosis: An update. *Mult Scler Relat Dis* 30: 215-224

Didonna A, Oksenberg JR (2017) *The Genetics of Multiple Sclerosis*. Codon, Brisbane (AU)

Diedrichsen J, Maderwald S, Kuper M, Thurling M, Rabe K, Gizewski ER, Ladd ME, Timmann D (2011) Imaging the deep cerebellar nuclei: a probabilistic atlas and normalization procedure. *NeuroImage* 54: 1786-1794

Dong Y, Yong VW (2019) When encephalitogenic T cells collaborate with microglia in multiple sclerosis. *Nature Reviews Neurology* 15: 704-717

Dum RP, Strick PL (2003) An unfolded map of the cerebellar dentate nucleus and its projections to the cerebral cortex. *J Neurophysiol* 89: 634-639

Dwyer CM, Nguyen LT, Healy LM, Dutta R, Ludwin S, Antel J, Binder MD, Kilpatrick TJ (2020) Multiple Sclerosis as a Syndrome-Implications for Future Management. *Front Neurol* 11: 784

Fazio F, Notartomaso S, Aronica E, Storto M, Battaglia G, Vieira E, Gatti S, Bruno V, Biagioni F, Gradini R *et al* (2008) Switch in the expression of mGlu1 and mGlu5 metabotropic glutamate receptors in the cerebellum of mice developing experimental autoimmune encephalomyelitis and in autoptic cerebellar samples from patients with multiple sclerosis. *Neuropharmacology* 55: 491-499

Fiander MD, Stifani N, Nichols M, Akay T, Robertson GS (2017) Kinematic gait parameters are highly sensitive measures of motor deficits and spinal cord injury in mice subjected to experimental autoimmune encephalomyelitis. *Behav Brain Res* 317: 95-108

Filippi M, Valsasina P, Rocca M (2007) Magnetic resonance imaging of grey matter damage in people with MS. *Int MS J* 14: 12-21

Findling O, Rust H, Yaldizli O, Timmermans DPH, Scheltinga A, Allum JHJ (2018) Balance Changes in Patients With Relapsing-Remitting Multiple Sclerosis: A Pilot Study Comparing the Dynamics of the Relapse and Remitting Phases. *Front Neurol* 9: 686

Franklin K, Paxinos G (2008) *The Mouse Brain in Stereotaxic Coordinates*. Academic Press

Geurts JJ, Barkhof F (2008) Grey matter pathology in multiple sclerosis. *Lancet Neurol* 7: 841-851

Geurts JJ, Bo L, Roosendaal SD, Hazes T, Daniels R, Barkhof F, Witter MP, Huitinga I, van der Valk P (2007) Extensive hippocampal demyelination in multiple sclerosis. *Journal of Neuropathology and Experimental Neurology* 66: 819-827

Gilli F, Royce DB, Pachner AR (2016) Measuring Progressive Neurological Disability in a Mouse Model of Multiple Sclerosis. *JOVE*

Gilmore CP, Bo L, Owens T, Lowe J, Esiri MM, Evangelou N (2006) Spinal cord gray matter demyelination in multiple sclerosis-a novel pattern of residual plaque morphology. *Brain Pathol* 16: 202-208

Gilmore CP, Donaldson I, Bo L, Owens T, Lowe J, Evangelou N (2009) Regional variations in the extent and pattern of grey matter demyelination in multiple sclerosis: a comparison between the cerebral cortex, cerebellar cortex, deep grey matter nuclei and the spinal cord. *Journal of Neurology, Neurosurgery, and Psychiatry* 80: 182-187

Goodin DS (2014) The epidemiology of multiple sclerosis: insights to disease pathogenesis. *Handb Clin Neurol* 122: 231-266

Gruol DL, Koibuchi N, Manto M, Molinari M, Schmahmann JD, Shen Y (2016) *Essentials of Cerebellum and Cerebellar Disorders*. Springer International Publisher, Switzerland

Haider L, Simeonidou C, Steinberger G, Hametner S, Grigoriadis N, Deretzi G, Kovacs GG, Kutzelnigg A, Lassmann H, Frischer JM (2014) Multiple sclerosis deep grey matter: the relation between demyelination, neurodegeneration, inflammation and iron. *J Neurol Neurosurg Psychiatry* 85: 1386-1395

Hamilton AM, Forkert ND, Yang R, Wu Y, Rogers JA, Yong VW, Dunn JF (2019) Central nervous system targeted autoimmunity causes regional atrophy: a 9.4T MRI study of the EAE mouse model of Multiple Sclerosis. *Scientific reports* 9: 8488

Harpaz I, Abutbul S, Nemirovsky A, Gal R, Cohen H, Monsonego A (2013) Chronic exposure to stress predisposes to higher autoimmune susceptibility in C57BL/6 mice: glucocorticoids as a double-edged sword. *Eur J Immunol* 43: 758-769

Hasselmann JPC, Karim H, Khalaj AJ, Ghosh S, Tiwari-Woodruff SK (2017) Consistent induction of chronic experimental autoimmune encephalomyelitis in C57BL/6 mice for the longitudinal study of pathology and repair. *J Neurosci Methods* 284: 71-84

Heppner FL, Greter M, Marino D, Falsig J, Raivich G, Hovelmeyer N, Waisman A, Rulicke T, Prinz M, Priller J *et al* (2005) Experimental autoimmune encephalomyelitis repressed by microglial paralysis. *Nat Med* 11: 146-152

Howell OW, Schulz-Trieglaff EK, Carassiti D, Gentleman SM, Nicholas R, Roncaroli F, Reynolds R (2015) Extensive grey matter pathology in the cerebellum in multiple sclerosis is linked to inflammation in the subarachnoid space. *Neuropathology and Applied Neurobiology* 41: 798-813

Hoxha E, Gabriele RMC, Balbo I, Ravera F, Masante L, Zambelli V, Albergo C, Mitro N, Caruso D, Di Gregorio E *et al* (2017) Motor Deficits and Cerebellar Atrophy in Elovl5 Knock Out Mice. *Frontiers in cellular neuroscience* 11: 343

Jarius S, Konig FB, Metz I, Ruprecht K, Paul F, Bruck W, Wildemann B (2017) Pattern II and pattern III MS are entities distinct from pattern I MS: evidence from cerebrospinal fluid analysis. *J Neuroinflammation* 14: 171

Junker A, Wozniak J, Voigt D, Scheidt U, Antel J, Wegner C, Bruck W, Stadelmann C (2020) Extensive subpial cortical demyelination is specific to multiple sclerosis. *Brain Pathol* 30: 641-652

Kasahara S, Miki Y, Kanagaki M, Yamamoto A, Mori N, Sawada T, Taoka T, Okada T, Togashi K (2011) Hyperintense dentate nucleus on unenhanced T1-weighted MR images is associated with a history of brain irradiation. *Radiology* 258: 222-228

Kemp KC, Dey R, Verhagen J, Scolding NJ, Usowicz MM, Wilkins A (2018) Aberrant cerebellar Purkinje cell function repaired in vivo by fusion with infiltrating bone marrow-derived cells. *Acta Neuropathol* 135: 907-921

Khaleeli Z, Ciccarelli O, Manfredonia F, Barkhof F, Brochet B, Cercignani M, Dousset V, Filippi M, Montalban X, Polman C *et al* (2008) Predicting progression in primary progressive multiple sclerosis: a 10-year multicenter study. *Ann Neurol* 63: 790-793

Kidd D, Barkhof F, McConnell R, Algra PR, Allen IV, Revesz T (1999) Cortical lesions in multiple sclerosis. *Brain: A Journal of Neurology* 122 (Pt 1): 17-26

Kipp M, Nyamoya S, Hochstrasser T, Amor S (2017) Multiple sclerosis animal models: a clinical and histopathological perspective. *Brain Pathol* 27: 123-137

Kipp M, van der Star B, Vogel DY, Puentes F, van der Valk P, Baker D, Amor S (2012) Experimental in vivo and in vitro models of multiple sclerosis: EAE and beyond. *Mult Scler Relat Dis* 1: 15-28

Klineova S, Lublin FD (2018) Clinical Course of Multiple Sclerosis. *Cold Spring Harb Perspect Med* 8

Kocovski P, Jiang X, D'Souza CS, Li Z, Dang PT, Wang X, Chen W, Peter K, Hale MW, Orian JM (2019) Platelet Depletion is Effective in Ameliorating Anxiety-Like Behavior

and Reducing the Pro-Inflammatory Environment in the Hippocampus in Murine Experimental Autoimmune Encephalomyelitis. *J Clin Med* 8

Kuerten S, Javeri S, Tary-Lehmann M, Lehmann PV, Angelov DN (2008) Fundamental differences in the dynamics of CNS lesion development and composition in MP4- and MOG peptide 35-55-induced experimental autoimmune encephalomyelitis. *Clinical Immunology* 129: 256-267

Kuhlmann T, Ludwin S, Prat A, Antel J, Bruck W, Lassmann H (2017) An updated histological classification system for multiple sclerosis lesions. *Acta Neuropathol* 133: 13-24

Kutzelnigg A, Faber-Rod JC, Bauer J, Lucchinetti CF, Sorensen PS, Laursen H, Stadelmann C, Bruck W, Rauschka H, Schmidbauer M *et al* (2007) Widespread demyelination in the cerebellar cortex in multiple sclerosis. *Brain Pathol* 17: 38-44

Kutzelnigg A, Lassmann H (2006) Cortical demyelination in multiple sclerosis: a substrate for cognitive deficits? *J Neurol Sci* 245: 123-126

Kutzelnigg A, Lucchinetti CF, Stadelmann C, Bruck W, Rauschka H, Bergmann M, Schmidbauer M, Parisi JE, Lassmann H (2005) Cortical demyelination and diffuse white matter injury in multiple sclerosis. *Brain : A Journal of Neurology* 128: 2705-2712

Lassmann H (2018) Pathogenic Mechanisms Associated With Different Clinical Courses of Multiple Sclerosis. *Front Immunol* 9: 3116

Lassmann H, Bradl M (2017) Multiple sclerosis: experimental models and reality. *Acta Neuropathol* 133: 223-244

Lassmann H, van Horssen J (2016) Oxidative stress and its impact on neurons and glia in multiple sclerosis lesions. *Biochim Biophys Acta* 1862: 506-510

Lisak RP, Benjamins JA, Nedelkoska L, Barger JL, Ragheb S, Fan B, Ouamara N, Johnson TA, Rajasekharan S, Bar-Or A (2012) Secretory products of multiple sclerosis B cells are cytotoxic to oligodendroglia in vitro. *J Neuro* 246: 85-95

Lucchinetti C, Bruck W, Parisi J, Scheithauer B, Rodriguez M, Lassmann H (2000) Heterogeneity of multiple sclerosis lesions: implications for the pathogenesis of demyelination. *Ann Neurol* 47: 707-717

Lucchinetti CF, Popescu BF, Bunyan RF, Moll NM, Roemer SF, Lassmann H, Bruck W, Parisi JE, Scheithauer BW, Giannini C *et al* (2011) Inflammatory cortical demyelination in early multiple sclerosis. *N Engl J Med* 365: 2188-2197

MacKenzie-Graham A, Rinek GA, Avedisian A, Gold SM, Frew AJ, Aguilar C, Lin DR, Umeda E, Voskuhl RR, Alger JR (2012) Cortical atrophy in experimental autoimmune encephalomyelitis: in vivo imaging. *NeuroImage* 60: 95-104

MacKenzie-Graham A, Tinsley MR, Shah KP, Aguilar C, Strickland LV, Boline J, Martin M, Morales L, Shattuck DW, Jacobs RE *et al* (2006) Cerebellar cortical atrophy in experimental autoimmune encephalomyelitis. *NeuroImage* 32: 1016-1023

MacKenzie-Graham A, Tiwari-Woodruff SK, Sharma G, Aguilar C, Vo KT, Strickland LV, Morales L, Fubara B, Martin M, Jacobs RE *et al* (2009) Purkinje cell loss in experimental autoimmune encephalomyelitis. *NeuroImage* 48: 637-651

Mahad DH, Trapp BD, Lassmann H (2015) Pathological mechanisms in progressive multiple sclerosis. *Lancet Neurol* 14: 183-193

Makhoul K, Ahdab R, Riachi N, Chalah MA, Ayache SS (2020) Tremor in Multiple Sclerosis-An Overview and Future Perspectives. *Brain Sci* 10

Mandolesi G, Grasselli G, Musella A, Gentile A, Musumeci G, Sepman H, Haji N, Fresegna D, Bernardi G, Centonze D (2012) GABAergic signaling and connectivity on Purkinje cells are impaired in experimental autoimmune encephalomyelitis. *Neurobiol Dis* 46: 414-424

Mann MK, Ray A, Basu S, Karp CL, Dittel BN (2012) Pathogenic and regulatory roles for B cells in experimental autoimmune encephalomyelitis. *Autoimmunity* 45: 388-399

Margoni M, Poggiali D, Zywicki S, Rubin M, Lazzarotto A, Franciotta S, Anglani MG, Causin F, Rinaldi F, Perini P *et al* (2021) Early red nucleus atrophy in relapse-onset multiple sclerosis. *Hum Brain Mapp* 42: 154-160

Martin CL, Phillips BA, Kilpatrick TJ, Butzkueven H, Tubridy N, McDonald E, Galea MP (2006) Gait and balance impairment in early multiple sclerosis in the absence of clinical disability. *Mult Scler* 12: 620-628

Maschke M, Weber J, Dimitrova A, Bonnet U, Bohrenkamper J, Sturm S, Kindsvater K, Muller BW, Gastpar M, Diener HC *et al* (2004) Age-related changes of the dentate nuclei in normal adults as revealed by 3D fast low angle shot (FLASH) echo sequence magnetic resonance imaging. *J Neurol* 251: 740-746

Matthews PM, Roncaroli F, Waldman A, Sormani MP, De Stefano N, Giovannoni G, Reynolds R (2016) A practical review of the neuropathology and neuroimaging of multiple sclerosis. *Pract Neurol* 16: 279-287

Mildner A, Huang H, Radke J, Stenzel W, Priller J (2017) P2Y12 receptor is expressed on human microglia under physiological conditions throughout development and is sensitive to neuroinflammatory diseases. *Glia* 65: 375-387

Miller SD, Karpus WJ (2007) Experimental autoimmune encephalomyelitis in the mouse. *Curr Protoc Immunol* Chapter 15: Unit 15 11

Moccia M, Ruggieri S, Ianniello A, Toosy A, Pozzilli C, Ciccarelli O (2019) Advances in spinal cord imaging in multiple sclerosis. *Ther Adv Neurol Disord* 12: 1756286419840593

Montalban X, Hauser SL, Kappos L, Arnold DL, Bar-Or A, Comi G, de Seze J, Giovannoni G, Hartung HP, Hemmer B *et al* (2017) Ocrelizumab versus Placebo in Primary Progressive Multiple Sclerosis. *The New England journal of medicine* 376: 209-220

Moroso A, Ruet A, Deloire M, Lamargue-Hamel D, Cubizolle S, Charre-Morin J, Saubusse A, Brochet B (2017) Cerebellar Assessment in Early Multiple Sclerosis. *Cerebellum (London, England)* 16: 607-611

Moroso A, Ruet A, Lamargue-Hamel D, Munsch F, Deloire M, Ouallet JC, Cubizolle S, Charre-Morin J, Saubusse A, Tourdias T *et al* (2018) Preliminary evidence of the cerebellar role on cognitive performances in clinically isolated syndrome. *J Neurol Sci* 385: 1-6

Muthuraman M, Fleischer V, Kroth J, Ciolac D, Radetz A, Koirala N, Gonzalez-Escamilla G, Wiendl H, Meuth SG, Zipp F *et al* (2020) Covarying patterns of white matter lesions and cortical atrophy predict progression in early MS. *Neurology neuroimmunology & neuroinflammation* 7

Neumann B, Segel M, Chalut KJ, Franklin RJ (2019) Remyelination and ageing: Reversing the ravages of time. *Mult Scler* 25: 1835-1841

Nyul-Toth A, Suciu M, Molnar J, Fazakas C, Hasko J, Herman H, Farkas AE, Kaszaki J, Hermenean A, Wilhelm I *et al* (2016) Differences in the molecular structure of the blood-brain barrier in the cerebral cortex and white matter: an in silico, in vitro, and ex vivo study. *American journal of physiology Heart and circulatory physiology* 310: H1702-1714

Olsson T, Barcellos LF, Alfredsson L (2017) Interactions between genetic, lifestyle and environmental risk factors for multiple sclerosis. *Nature reviews Neurology* 13: 25-36

Ousman SS, Tomooka BH, van Noort JM, Wawrousek EF, O'Connor KC, Hafler DA, Sobel RA, Robinson WH, Steinman L (2007) Protective and therapeutic role for alphaB-crystallin in autoimmune demyelination. *Nature* 448: 474-479

Papadopoulos D, Dukes S, Patel R, Nicholas R, Vora A, Reynolds R (2009) Substantial archaeocortical atrophy and neuronal loss in multiple sclerosis. *Brain Pathol* 19: 238-253

Parmar K, Stadelmann C, Rocca MA, Langdon D, D'Angelo E, D'Souza M, Burggraaff J, Wegner C, Sastre-Garriga J, Barrantes-Freer A *et al* (2018) The role of the cerebellum in multiple sclerosis-150 years after Charcot. *Neurosci Biobehav Rev* 89: 85-98

Parnell GP, Booth DR (2017) The Multiple Sclerosis (MS) Genetic Risk Factors Indicate both Acquired and Innate Immune Cell Subsets Contribute to MS Pathogenesis and Identify Novel Therapeutic Opportunities. *Front Immunol* 8: 425

Peeters LM, Vanheusden M, Somers V, Van Wijmeersch B, Stinissen P, Broux B, Hellings N (2017) Cytotoxic CD4+ T Cells Drive Multiple Sclerosis Progression. *Front Immunol* 8: 1160

Peterson JW, Bo L, Mork S, Chang A, Trapp BD (2001) Transected neurites, apoptotic neurons, and reduced inflammation in cortical multiple sclerosis lesions. *Ann Neurol* 50: 389-400

Pham H, Ramp AA, Klonis N, Ng SW, Klopstein A, Ayers MM, Orian JM (2009) The astrocytic response in early experimental autoimmune encephalomyelitis occurs across both the grey and white matter compartments. *J Neuro* 208: 30-39

Pirko I, Lucchinetti CF, Sriram S, Bakshi R (2007) Gray matter involvement in multiple sclerosis. *Neurology* 68: 634-642

Plastini MJ, Desu HL, Brambilla R (2020) Dynamic Responses of Microglia in Animal Models of Multiple Sclerosis. *Frontiers in cellular neuroscience* 14: 269

Popescu BF, Lucchinetti CF (2012) Pathology of demyelinating diseases. *Annu Rev Pathol* 7: 185-217

Prins M, Schul E, Geurts J, van der Valk P, Drukarch B, van Dam AM (2015) Pathological differences between white and grey matter multiple sclerosis lesions. *Neuroimmunomodulation in Health and Disease* 1351: 99-113

Ramasamy DP, Benedict RH, Cox JL, Fritz D, Abdelrahman N, Hussein S, Minagar A, Dwyer MG, Zivadinov R (2009) Extent of cerebellum, subcortical and cortical atrophy in patients with MS: a case-control study. *J Neurol Sci* 282: 47-54

Rampello L, Casolla B, Rampello L, Pignatelli M, Battaglia G, Gradini R, Orzi F, Nicoletti F (2011) The conditioned eyeblink reflex: a potential tool for the detection of cerebellar dysfunction in multiple sclerosis. *Mult Scler* 17: 1155-1161

Redondo J, Kemp K, Hares K, Rice C, Scolding N, Wilkins A (2015) Purkinje Cell Pathology and Loss in Multiple Sclerosis Cerebellum. *Brain Pathol* 25: 692-700

Reynders T, D'Haeseleer M, De Keyser J, Nagels G, D'Hooghe M B (2017) Definition, prevalence and predictive factors of benign multiple sclerosis. *eNS* 7: 37-43

Reynolds R, Roncaroli F, Nicholas R, Radotra B, Gveric D, Howell O (2011) The neuropathological basis of clinical progression in multiple sclerosis. *Acta Neuropathol* 122: 155-170

Robinson AP, Harp CT, Noronha A, Miller SD (2014) The experimental autoimmune encephalomyelitis (EAE) model of MS: utility for understanding disease pathophysiology and treatment. *Handb Clin Neurol* 122: 173-189

Roccatagliata L, Vuolo L, Bonzano L, Pichiecchio A, Mancardi GL (2009) Multiple sclerosis: hyperintense dentate nucleus on unenhanced T1-weighted MR images is associated with the secondary progressive subtype. *Radiology* 251: 503-510

Rotterman TM, Alvarez FJ (2020) Microglia Dynamics and Interactions with Motoneurons Axotomized After Nerve Injuries Revealed By Two-Photon Imaging. *Scientific reports* 10: 8648

Rzepinski L, Zawadka-Kunikowska M, Maciejek Z, Newton JL, Zalewski P (2019) Early Clinical Features, Time to Secondary Progression, and Disability Milestones in Polish Multiple Sclerosis Patients. *Medicina* 55

Saligrama N, Zhao F, Sikora MJ, Serratelli WS, Fernandes RA, Louis DM, Yao W, Ji X, Idoyaga J, Mahajan VB *et al* (2019) Opposing T cell responses in experimental autoimmune encephalomyelitis. *Nature* 572: 481-487

Satoh J, Kino Y, Asahina N, Takitani M, Miyoshi J, Ishida T, Saito Y (2016) TMEM119 marks a subset of microglia in the human brain. *Neuropathology* 36: 39-49

Schlaeger R, Papinutto N, Panara V, Bevan C, Lobach IV, Bucci M, Caverzasi E, Gelfand JM, Green AJ, Jordan KM *et al* (2014) Spinal cord gray matter atrophy correlates with multiple sclerosis disability. *Ann Neurol* 76: 568-580

Shanahan CJ, Boonstra FMC, Cofre Lizama LE, Strik M, Moffat BA, Khan F, Kilpatrick TJ, van der Walt A, Galea MP, Kolbe SC (2017) Technologies for Advanced Gait and Balance Assessments in People with Multiple Sclerosis. *Front Neurol* 8: 708

Shields SD, Butt RP, Dib-Hajj SD, Waxman SG (2015) Oral administration of PF-01247324, a subtype-selective Nav1.8 blocker, reverses cerebellar deficits in a mouse model of multiple sclerosis. *PloS one* 10: e0119067

Shields SD, Cheng X, Gasser A, Saab CY, Tyrrell L, Eastman EM, Iwata M, Zwinger PJ, Black JA, Dib-Hajj SD *et al* (2012) A channelopathy contributes to cerebellar dysfunction in a model of multiple sclerosis. *Ann Neurol* 71: 186-194

Sloka S, Metz LM, Hader W, Starreveld Y, Yong VW (2013) Reduction of microglial activity in a model of multiple sclerosis by dipyridamole. *J Neuroinflammation* 10: 89

Sonobe Y, Jin S, Wang J, Kawanokuchi J, Takeuchi H, Mizuno T, Suzumura A (2007) Chronological changes of CD4(+) and CD8(+) T cell subsets in the experimental autoimmune encephalomyelitis, a mouse model of multiple sclerosis. *Tohoku J Exp Med* 213: 329-339

Spain RI, Mancini M, Horak FB, Bourdette D (2014) Body-worn sensors capture variability, but not decline, of gait and balance measures in multiple sclerosis over 18 months. *Gait Posture* 39: 958-964

Stroobants S, Gantois I, Pooters T, D'Hooge R (2013) Increased gait variability in mice with small cerebellar cortex lesions and normal rotarod performance. *Behav Brain Res* 241: 32-37

Stys PK, Zamponi GW, van Minnen J, Geurts JJG, 2012. Will the real multiple sclerosis please stand up?, Nature Reviews Neuroscience. pp. 507-514.

Tedeschi E, Palma G, Canna A, Cocozza S, Russo C, Borrelli P, Lanzillo R, Angelini V, Postiglione E, Morra VB *et al* (2016) In vivo dentate nucleus MRI relaxometry correlates with previous administration of Gadolinium-based contrast agents. *Eur Radiol* 26: 4577-4584

Tintore M, Rovira A, Arrambide G, Mitjana R, Rio J, Auger C, Nos C, Edo MC, Castillo J, Horga A *et al* (2010) Brainstem lesions in clinically isolated syndromes. *Neurology* 75: 1933-1938

Tjoa CW, Benedict RH, Weinstock-Guttman B, Fabiano AJ, Bakshi R (2005) MRI T2 hypointensity of the dentate nucleus is related to ambulatory impairment in multiple sclerosis. *J Neurol Sci* 234: 17-24

Trapp BD, Nave KA (2008) Multiple sclerosis: an immune or neurodegenerative disorder? *Annu Rev Neurosci* 31: 247-269

Uusisaari M, Knopfel T (2010) GlyT2+ neurons in the lateral cerebellar nucleus. *Cerebellum (London, England)* 9: 42-55

Uusisaari M, Knöpfel T (2011) Functional Classification of Neurons in the Mouse Lateral Cerebellar Nuclei. *Cerebellum (London, England)* 10: 637-646

Uusisaari M, Obata K, Knopfel T (2007) Morphological and electrophysiological properties of GABAergic and non-GABAergic cells in the deep cerebellar nuclei. *J Neurophysiol* 97: 901-911

Uusisaari MY, Knöpfel T (2013) Neurons of the Deep Cerebellar Nuclei. *Handbook of the Cerebellum and Cerebellar Disorders*: 1101-1110

van Alphen B, Winkelman BH, Frens MA (2010) Three-dimensional optokinetic eye movements in the C57BL/6J mouse. *Investigative ophthalmology & visual science* 51: 623-630

van den Berg R, Laman JD, van Meurs M, Hintzen RQ, Hoogenraad CC (2016) Rotarod motor performance and advanced spinal cord lesion image analysis refine assessment of neurodegeneration in experimental autoimmune encephalomyelitis. *J Neurosci Methods* 262: 66-76

van der Valk P, De Groot CJ (2000) Staging of multiple sclerosis (MS) lesions: pathology of the time frame of MS. *Neuropathology and Applied Neurobiology* 26: 2-10

Vercellino M, Plano F, Votta B, Mutani R, Giordana MT, Cavalla P (2005) Grey matter pathology in multiple sclerosis. *Journal of Neuropathology and Experimental Neurology* 64: 1101-1107

Voskuhl RR, Peterson RS, Song B, Ao Y, Morales LB, Tiwari-Woodruff S, Sofroniew MV (2009) Reactive astrocytes form scar-like perivascular barriers to leukocytes during adaptive immune inflammation of the CNS. *Journal of Neuroscience* 29: 11511-11522

Weier K, Banwell B, Cerasa A, Collins DL, Dogonowski AM, Lassmann H, Quattrone A, Sahraian MA, Siebner HR, Sprenger T (2015) The role of the cerebellum in multiple sclerosis. *Cerebellum (London, England)* 14: 364-374

Weinshenker BG, Rice GP, Noseworthy JH, Carriere W, Baskerville J, Ebers GC (1991) The natural history of multiple sclerosis: a geographically based study. 3. Multivariate analysis of predictive factors and models of outcome. *Brain: a journal of neurology* 114 (Pt 2): 1045-1056

White JJ, Sillitoe RV (2013) Development of the cerebellum: from gene expression patterns to circuit maps. *Dev Biol* 2: 149-164

Wilhelm I, Nyul-Toth A, Suciu M, Hermenean A, Krizbai IA (2016) Heterogeneity of the blood-brain barrier. *Tissue Barriers* 4: e1143544

Wilkins A (2017) Cerebellar Dysfunction in Multiple Sclerosis. *Front Neurol* 8: 312

Yamasaki R, Lu H, Butovsky O, Ohno N, Rietsch AM, Cialic R, Wu PM, Doykan CE, Lin J, Cotleur AC *et al* (2014) Differential roles of microglia and monocytes in the inflamed central nervous system. *The Journal of experimental medicine* 211: 1533-1549

Zhu B, Luo L, Moore GR, Paty DW, Cynader MS (2003) Dendritic and synaptic pathology in experimental autoimmune encephalomyelitis. *Am J Pathol* 162: 1639-1650

Ziehn MO, Avedisian AA, Tiwari-Woodruff S, Voskuhl RR (2010) Hippocampal CA1 atrophy and synaptic loss during experimental autoimmune encephalomyelitis, EAE. *Lab Invest* 90: 774-786

Zoupi L, Booker SA, Eigel D, Werner C, Kind PC, Spires-Jones TL, Newland B, Williams AC (2021) Selective vulnerability of inhibitory networks in multiple sclerosis. *Acta Neuropathol* 141: 415-429

Zrzavy T, Hametner S, Wimmer I, Butovsky O, Weiner HL, Lassmann H (2017) Loss of 'homeostatic' microglia and patterns of their activation in active multiple sclerosis. *Brain: A Journal of Neurology* 140: 1900-1913